

**AN IN-DEPTH STUDY OF NUCLEATION AND
GROWTH PROCESSES DURING STÖBER SILICA
SYNTHESIS**

**A Thesis Submitted to
the Graduate School of Engineering and Sciences of
İzmir Institute of Technology
in Partial Fulfillments of the Requirements for the Degree of**

DOCTOR OF PHILOSOPHY

in Chemical Engineering

**by
Elif Suna SOP**

July 2019

İZMİR

We approve the thesis of **Elif Suna SOP**

Examining Committee Members:

Prof. Dr. Mehmet POLAT

Department of Chemical Engineering, İzmir Institute of Technology

Prof. Dr. Mustafa M. DEMİR

Department of Material Science and Engineering, İzmir Institute of Technology

Assist. Prof. Dr. Ayben TOP

Department of Chemical Engineering, İzmir Institute of Technology

Prof. Dr. Mustafa DEMİRCİOĞLU

Department of Chemical Engineering, Ege University

Assoc.Prof. Dr. Mehmet Faruk EBEOĞLUGİL

Department of Metallurgical and Materials Engineering, Dokuz Eylül University

12 July 2019

Prof. Dr. Mehmet POLAT

Supervisor, Department of Chemical Engineering
İzmir Institute of Technology

Prof. Dr. Erol ŞEKER

Head of Department of Chemical
Engineering

Prof. Dr. Aysun SOFUOĞLU

Dean of Graduate School of Engineering
and Sciences

ACKNOWLEDGMENTS

First and foremost, I would like to express my deepest gratitude to my advisors, *Prof. Dr. Mehmet POLAT* and *Prof. Dr. Hürriyet POLAT*, for their guidance, motivation, caring, patience and confidence. Their way of communication provoked me to improve the scientific communication skills. Their contribution to my PhD and personal life is enormous. I have not only learned a lot about science from them but also how to face the problems in life. Their guidance helped me in all the time of research and writing of this thesis with an excellent atmosphere. I could not have imagined having better mentors.

I wish to thank to thesis committee members *Prof. Dr. Mustafa M. DEMİR*, and *Assist. Prof. Dr. Ayben TOP* for their valuable contributions. Throughout the study, I have benefited a lot from their valuable and most constructive suggestions. I also thank *Prof. Dr. Mustafa Demircioğlu*, *Assoc. Prof. Dr. Mehmet Faruk Ebeoğlugil*, *Prof. Dr. Günseli ÖZDEMİR* and *Prof. Dr. Vedat ARSLAN* for accepting to be in my defense jury.

I would like to thank to *Duygu OĞUZ KILIÇ*, *Mutlu DEVRAN YAMAN* and *Zehra Sinem YILMAZ* for endless diligent hours they spent for me for the SEM analyses carried out in the Material Research and Development Center of IZTECH.

I am really thankful to my friend and labmate *Esin GÖKMEN* for her support and contributions during my experiments. She really became very close to my heart by her love and care. I would like to express my gratitude to my dear friends *Aydın CİHANOĞLU* and *Gizem CİHANOĞLU* for their endless friendship, patience and support during writing of my thesis. It was a nice opportunity to share many ideas with them. I am so glad to know them. I also thank to my nice friends *Ayşe METECAN*, *Önder TEKİNALP* and *Özgün DELİİSMİL*.

Last but not the least; I would like to thank my boyfriend, *Mert KOÇYİĞİT*, for his support during all. Without him, nothing that I have done during this period would be as pleasant. I am really very happy and lucky to continue my life journey with him.

I would also like to send my deepest gratitudes to my parents, *Hüseyin SOP* and *Leyla SOP*, and my sister and her husband, *Tuğba KURT* and *Okan KURT*, for the spiritual support they have given me throughout my life; you are the best. I deeply appreciate the trust of my parents for allowing me to find my own way no matter how far away from home it was.

ABSTRACT

AN IN-DEPTH STUDY OF NUCLEATION AND GROWTH PROCESSES DURING STÖBER SILICA SYNTHESIS

Silica nanoparticles (SNPs) which can be synthesized with high surface area, controllable morphology and desired particle size have gained significant interests in high-end applications such as catalysis, chemical sensors, cosmetics and drug delivery applications. The sol-gel technique is the most commonly applied method for manufacturing these particles owing to its simplicity and suitability for allowing surface modifications to the final product. Though monodisperse amorphous SNPs have been studied extensively, how their formation proceeds through nucleation and growth is still a topic of debate. Over the years, a number of mathematical models have been suggested for the nucleation and growth of SNPs; some suggesting that silica growth occurred through monomer addition while some arguing that aggregation of nuclei/subparticles were the dominant mechanism. Nevertheless, a clear understanding of the nucleation and growth sub-processes is extremely important in control on the size and shape of SNPs for those industrial applications which demand specific morphology and surface properties.

The need for a simple, robust and generalized model, both conceptually and mathematically, to understand formation and growth of Stöber silica particles has been the main driving force for this thesis. In this study, silica synthesis was carried out under a wide variety of experimental conditions while determining the size distributions of the formed particles kinetically during different stages of the synthesis in-situ through SEM analysis using an image analysis software. The outcome of the extensive synthesis work was to obtain a clear understanding of how the formation and growth of the silica particles proceed during synthesis. This conceptual understanding of the nucleation and growth processes was then translated into a mathematical model to predict the size of the particles as a function of synthesis time.

ÖZET

STÖBER SİLİKA SENTEZİ SIRASINDAKİ ÇEKİRDEKLENME VE BÜYÜME PROSESLERİNİN DERİNLEMESİNE İNCELENMESİ

Yüksek yüzey alanları, ayarlanabilir morfolojileri ve istenilen boyutlarda üretilibilmeleri nedeniyle, silika nanotaneler katalizörler, sensörler, kozmetik ürünler ve ilaç taşıyıcılar gibi pek çok yüksek teknoloji uygulamalarında dikkate değer bir ilgi görmektedir. Soljel tekniği, bu tanelerin üretiminde, kolay uygulanabilirliği ve sonuç ürünün niteliklerinin modifikasyonuna olanak vermesi nedeniyle en yaygın kullanılan yöntemdir. Her ne kadar amorf silika taneler sıklıkla çalışılsa da, tanelerin oluşumlarının çekirdeklenme ve büyüme prosesleri ile nasıl ilerlediği sentezin kontrolü ve tekrarlanabilirliği açısından hala bir tartışma konusudur. Yıllar boyunca, sol-jel silika tanelerin çekirdeklenme ve büyüme prosesleri için bir takım matematiksel modeller önerilmiş; kimi silika büyümesinin monomer ilavesi ile olduğunu öne sürmüş kimisi de çekirdek/alt parçacıkların agregasyonun dominant mekanizma olduğunu tartışmıştır. Yine de, çekirdeklenme ve büyüme alt proseslerinin açık bir şekilde anlaşılması, spesifik morfoloji ve yüzey özellikleri gerektiren endüstriyel uygulamalar için silika tanelerin boyut ve morfoloji kontrolü açısından son derece önemlidir.

Stöber silika tanelerin oluşum ve büyüme mekanizmalarının anlaşılması için konsept ve matematik olarak, basit, sağlam ve genel bir modele olan gereksinim bu tezin temel itici gücüdür. Bu çalışmada, silika sentezi geniş deneysel koşulları altında uygulanmış, oluşan tanelerin boyut dağılımları kinetik olarak sentezin farklı basamaklarında, bir görüntü analiz programı kullanılarak SEM analizlerinden elde edilmiştir. Yoğun sentez çalışmalarının neticesi silika tanelerin sentez esnasında oluşum ve büyüme proseslerinin net bir şekilde anlaşılabilirliğinin sağlanmasıdır. Çekirdeklenme ve büyüme proseslerinin konsept olarak anlaşılması ayrıca sentez zamanına karşı tanelerin boyutunun tahmin edilebilmesine olanak sağlayan bir matematiksel modele aktarılmıştır.

*Dedicated wholeheartedly to my beloved family who have been my source of inspiration
and provide moral, spiritual and emotional support...*

TABLE OF CONTENTS

LIST OF FIGURES	x
LIST OF TABLES	xv
LIST OF ABBREVIATIONS.....	xvi
CHAPTER 1. INTRODUCTION	1
CHAPTER 2. SOL-GEL SYNTHESIS OF SILICA (STÖBER METHOD).....	3
2.1. Description of Stöber Method	3
2.2. State of the Art	8
2.2.1. Factors Affecting Characteristic of Silica Particles	10
2.2.1.1. Effect of Process Parameters	10
2.2.1.1.1. Precursors	10
2.2.1.1.2. Solvents	11
2.2.1.1.3. pH	13
2.2.1.1.4. Temperature.....	16
2.2.1.2. Presence of Electrolytes	17
2.2.1.3. Presence of Seed Particles	18
2.2.2. Growth Mechanism of SNPs.....	21
2.2.2.1. Monomer Addition Model.....	21
2.2.2.2. Aggregation Growth Model	23
2.2.2.3. Mixed Growth Mechanism.....	25
CHAPTER 3. EXPERIMENTAL METHODOLOGY	28
3.1. Materials.....	28
3.2. Method	28
3.2.1. Synthesis of SNPs using Stöber Method	29
3.2.2. Electrolyte Addition.....	30

3.2.3. Seed Addition (Seeded Growth)	31
3.2.3.1. Effect of NH ₃ Concentrations in Growth Solution	31
3.2.3.2. Effect of Seed/TEOS Amounts and TEOS Addition Rates	32
3.2.3.3. Effect of Electrolytes in Growth Solution.....	34
3.3. Characterization Studies.....	34
CHAPTER 4. EFFECT OF PROCESS PARAMETERS AND ELECTROLYTES ON NUCLEATION AND GROWTH	36
4.1. Characterization of Stöber Silica SNPs	36
4.1.1. Effect of Process Parameters on Size of SNPs	43
4.1.1.1. H ₂ O Amount.....	43
4.1.1.2. NH ₃ Concentration	45
4.1.1.3. TEOS Concentration	47
4.1.1.4. Mode of TEOS Addition	48
4.1.1.5. Agitation Intensity.....	53
4.1.2. Electrolyte Addition.....	57
CHAPTER 5.USING SEED PARTICLES TO DISTINGUISH NUCLEATION AND GROWTH	62
5.1. NH ₃ Concentrations on Growth Solution.....	62
5.2. Effect of Seed Amounts and TEOS Feeding Rates.....	66
5.3. Seed Addition in the Presence of Electrolytes	77
CHAPTER 6. DEVELOPMENT OF A MODEL FOR PARTICLE GROWTH.....	80
6.1. Concept of the Model.....	80
6.2. Rate of Collision and Aggregation under Diffusion	84
6.3. Hydrolysis of TEOS with No Condensation and No Aggregation	89
6.4. Hydrolysis of TEOS with Condensation to Form Oligomers and No Aggregation of Oligomers	95
6.5. Hydrolysis of TEOS with Condensation to Form Oligomers and Aggregation of Oligomers to Form Final Particles	100

CHAPTER 7. SUMMARY AND CONCLUSIONS.....	106
REFERENCES	108
APPENDICES	
APPENDIX A: Electrostatic Interactions.....	121
APPENDIX B: Hydrolysis of TEOS with No Condensation and No Aggregation	123
APPENDIX C: Hydrolysis of TEOS with Condensation to Form Oligomers and No Aggregation of Oligomers	126
APPENDIX D: Hydrolysis of TEOS with Condensation to Form Oligomers and Aggregation of Oligomers to Form Final Particles	127

LIST OF FIGURES

<u>Figure</u>	<u>Page</u>
Figure 2.1. Silica network production through the hydrolysis and condensation reactions of TEOS	6
Figure 2.2. Polymerization pathway of silicates according to Iler	6
Figure 2.3. Formation of cyclic species during hydrolysis and condensation reactions.	7
Figure 2.4. Schematic representation of the nucleation and growth process of	9
Figure 2.5. Schematic illustrations of the formation of silica structures under different values of pH	14
Figure 2.6. Hydrolysis and condensation rates with respect to pH.....	15
Figure 2.7. Schematic graph of the formation and consumption of intermediate ($[\text{Si}(\text{OC}_2\text{H}_5)_{4-\chi}(\text{OH})_\chi]$) for seed growth.	20
Figure 2.8. Schematic of proposed model by LaMer	22
Figure 3.1. Flowsheet for the electrolyte addition to the silica synthesis medium.	30
Figure 3.2. Flowsheet of the procedure for seeding experiments in changing NH_3 solution.	32
Figure 3.3. Flowsheet of the procedure for seeding experiments using different amount of seed particles with different TEOS addition rate.	33
Figure 4.1. a) A representative SEM image of the SNPs after 24 hours of synthesis; b) number frequency size distribution obtained from the SEM image.	37
Figure 4.2. Zeta potential distribution of SNPs synthesized by Stöber method.	37
Figure 4.3. TGA (top) and DrTGA (bottom) curves belong to the SNPs obtained from Classical Stöber method.	38
Figure 4.4. FTIR spectrum of SNPs obtained from Classical Stöber method	39
Figure 4.5. IR spectra with respect to time of silica particles obtained from Classical Stöber method.	40
Figure 4.6. Conductivity and pH monitoring of the Stöber reaction for 0.250 M TEOS concentration.	42
Figure 4.7. Conductivity and pH monitoring of the Stöber reaction for 0.125 M TEOS concentration.	42

<u>Figure</u>	<u>Page</u>
Figure 4.8. SEM images of silica particles synthesized with different H ₂ O amounts (M).....	44
Figure 4.9. Effect of H ₂ O amounts (M) on final size of SNPs	44
Figure 4.10. SEM images of the silica particles with different NH ₃ concentrations.....	45
Figure 4.11. Final mean sizes of silica particles with different NH ₃ concentrations.....	46
Figure 4.12. Representative SEM images of silica particles with different TEOS concentrations.	47
Figure 4.13. Final mean sizes of silica particles with time for different TEOS concentrations.	48
Figure 4.14. Comparison of pulse vs continuous TEOS addition rate on final size of SNPs as a function of time	49
Figure 4.15. SEM images of continuous TEOS addition (in 1 h) as a function of time	49
Figure 4.169. SEM images of the SNPs after 24 hours of synthesis for different TEOS addition rates for 0.125 M and 0.250 M TEOS	50
Figure 4.17. Number frequency distributions of the SNPs obtained from the SEM images in Figure 4.16 for different TEOS addition rates for a) 0.125 M and b) 0.250 M TEOS c) Number of particles for all TEOS addition rates.	51
Figure 4.18. Size distribution of silica particles synthesized without agitation applying.....	53
Figure 4.19. SEM images of the size distribution of silica particles with different agitation modes.	54
Figure 4.20. Size distribution of silica particles with different agitation modes.	55
Figure 4.21. Peclet numbers calculated for possible sizes of the diffusing species in the cell for the two mixing speed (0.250 M TEOS Pulse addition).....	56
Figure 4.22. Effect of the presence of electrolyte on the potential energy of interaction, a) No electrolyte, b) 0.04 mol/L electrolyte concentration (Note that valence of electrolyte was taken as 2).....	58

<u>Figure</u>	<u>Page</u>
Figure 4.23. Effect of electrolyte concentration on the potential energy of interaction, a) 10^{-4} mol/L, b) 0.04 mol/L (Note that valence of electrolyte was taken as 2).	58
Figure 4.24. SEM images of silica particles in the presence of ionic compounds at 0.04 M concentrations.	59
Figure 4.25. SEM images of silica particles in the presence of ionic compounds at 10^{-4} M and 0.04 M concentrations (after 24 h of production).	60
Figure 4.26. SEM images of silica particles synthesized with Mode B in the presence of ionic compounds at 10^{-4} M concentration (after 24 h of production).....	61
Figure 5.1. SEM images and size distributions for seed particles obtained by Stöber method after; a) 4 min, SP1 and b) 24 h, SP2	63
Figure 5.2. SEM images of GP particles in 1.09 M NH_3	64
Figure 5.3. SEM images of GP particles in the absence of NH_3 (0 M) in growth solution.....	65
Figure 5.4. a) A representative SEM image of the seeds after 24 h of synthesis; b) number frequency size distribution obtained from the SEM image. $d_{-2\sigma}$ and $d_{+2\sigma}$ represent the nominal lower and upper size bounds of the distribution which contain 95.4% of the population.....	67
Figure 5.5. SEM images of the SNPs after 24 hours of synthesis in the presence of selected seed amounts for 0.125 M and 0.250 M total TEOS amounts for pulse addition case	68
Figure 5.6. Sizes of the SNPs after 24 hours of synthesis carried out in the presence of different amounts of seeds for the case of 0.125 and 0.250 M total TEOS additions for 0.02 mL/min, 0.10 mL/min and pulse TEOS additions.	69
Figure 5.7. Amount of TEOS condensed on seed SNPs and the number of secondary SNPs formed for (a) 0.125 M and (b) for 0.250 M pulse TEOS addition in the presence of different seed amounts. The dashed line represents the total TEOS in the system.	71

<u>Figure</u>	<u>Page</u>
Figure 5.8. Amount of TEOS condensed on seed SNPs and the number of secondary SNPs formed for (a) 0.125 M and (b) for 0.250 M pulse TEOS addition in the presence of different seed amounts .The dashed line represents the total TEOS in the system	72
Figure 5.9. Representative SEM images of the SNPs sampled at different synthesis times in the presence of different amount of seeds for continuous TEOS addition case (0.1 mL/min) (the scale is the same in all photos).....	74
Figure 5.10. SEM images of seeded growth method agitation conditions vs solute size.....	75
Figure 5.11. SEM images of the size distribution of silica particles with different modalities obtained from seeding studies	76
Figure 5.12. SEM images of the silica particles with seed particles in the presence of 4×10^{-2} M NaCl in growth solution.	77
Figure 5.13. SEM images of the silica particles with seed particles in the presence of 4×10^{-2} M CaCl ₂ in growth solution.....	78
Figure 5.14. SEM images of the silica particles with seed particles in the presence of 4×10^{-2} M AlCl ₃ in growth solution	78
Figure 6.1. Schematics of the idea under the particle growth process.....	82
Figure 6.2. Aggregation of two particles apart from each other with a distance r.	85
Figure 6.3. Diffusion of particle 1 towards particle 2.....	87
Figure 6.4. Approximation of $\frac{(R_1+R_2)^2}{R_1R_2}$ ($f_1(R_2)$) and $\left(2 + \frac{R_2}{R_1}\right)$ ($f_2(R_2)$) for different radii.	89
Figure 6.5. Changes in the number of monomers as a function of time.....	94
Figure 6.6. Condensation of monomers to form oligomers	96
Figure 6.7. Change in the number of monomeric species with considering condensation into oligomers.	98
Figure 6.8. Change in the oligomer radius as a function of time when oligomers do not interact with each other.....	99

<u>Figure</u>	<u>Page</u>
Figure 6.9. Change in the mass of monomers and oligomers with respect to time.	99
Figure 6.10. Change in the mass of monomers, oligomers and aggregated particles with time.	102
Figure 6.11. Change in the final particle radius with time	103
Figure 6.12. Comparison of experimental data with the model.....	103
Figure 6.13. TEM images of SNPs after 2 mins of the synthesis	104
Figure 6.314. Zeta potential of particles as a function of size.	105
Figure B.1. Numerical solution of the model belongs to hydrolysis of TEOS with no condensation and no aggregation.....	124
Figure B.2. Analytical solution of the model belongs to hydrolysis of TEOS with no condensation and no aggregation.....	125
Figure B.3. $-dn_{0a}(t)/n_{0a}(t)$ vs time	125
Figure D.1. Change in the number of monomers divided by total TEOS number as a function of time.....	128

LIST OF TABLES

<u>Table</u>	<u>Page</u>
Table 2.1. Solvating power of several solvents	12
Table 2.2. Summary of the suggested models for silica particle formation	26
Table 3.1. Experimental parameters for preparation of SNPs	29
Table 4.1. Calculated diffusion coefficients and Pe numbers.....	56
Table 5.1. Critical seed surface areas for changing TEOS addition rates and concentrations.....	71

LIST OF ABBREVIATIONS

AlCl ₃	Aluminum chloride
BET	Brunauer–Emmett–Teller
CaCl ₂	Calcium chloride
CMC	Critical micelle concentration
CTAB	Hexadecyl trimethyl ammonium bromide
DLS	Dynamic light scattering
DLVO	Derjaguin-Landau-Verwey-Overbeek
EDL	Electrical double layer
EtOH	Ethanol
FTIR	Fourier transform infrared spectroscopy
KBr	Potassium bromide
NaCl	Sodium chloride
MW	Molecular weight
NH ₄ OH	Ammonium hydroxide
NP	Nanoparticle
PSD	Particle size distribution
SDS	Sodium dodecyl sulphate
SEM	Scanning electron microscopy
SNPs	Silica nanoparticles
TEM	Transmission electron microscopy
TEOS	Tetraethyl orthosilicate
TGA	Thermogravimetric analysis
TX-100	Triton X-100

CHAPTER 1

INTRODUCTION

Silicon oxides or known as silicates (silica) are by far the most abundant constituent of the Earth's crust which have general chemical formula of SiO_2 . It has been used widely for manufacturing of glass, ceramics and silicones as well as the in the construction of buildings and roadways as a basis for concrete, mortar and sandstone owing to its availability and ease of recovery for years. Colloidal silica has been investigated extensively in nano and microparticle research because of its superior properties such as relatively large surface area, low toxicity, and optical transparency, relative chemical and thermal and high colloidal stability in many conditions. Considering these large number of usage areas, it is not a surprising that colloidal silica production has gained a serious research interest (Hyde et al., 2016).

Although naturally formed silica mineral(s) are abundant in nature, their use requires comminution processes which are expensive and detrimental to health. Also, the size, shape and impurity control is near impossible when the particles are manufactured by crushing and grinding processes. Therefore, silica particles with special and specific morphologies (spherical, solid, hollow, mesoporous, etc.) are generally produced via synthetic (chemical) pathways. Sol-gel method is mostly used synthetic method to synthesize solid silica particles with well-defined and uniform morphologies as well as preferable purity and homogeneity on a molecular level. It includes the transformation of the precursor species into the final product through the simultaneous hydrolysis and condensation reactions. Reactant concentrations, solvent type, pH, temperature and reactant feeding rates are some of the parameters that have to be studied to control the morphology and size distribution. Use of seed particles, addition of electrolytes and/or surfactants will also influence the rates of hydrolysis and condensation reaction, hence, the particle size distribution and morphology.

Though fine-tuning of the properties of manufactured nanoparticles is highly desired, the amount of work for providing a basis for systematic relationship between the reaction conditions of hydrolysis, condensation and particle growth is limited and the

available results are confounding. Commonly-held paradigm is that hydrolysis and condensation reactions provides the precursor species (silanol monomers, dimers, trimers, oligomers, etc.) and supersaturation allows for the formation of primary particles (also known as nuclei). These primary particles will then grow to a final size by direct monomer addition to the particle surface or aggregation of these primary particles to the nuclei. Although suggested mechanisms exist in the literature for enabling one to make an informed decision, the need for generalized robust models still exists to predict and simulate synthesis reactions (Norazmi et al., 2018; Schubert and Hüsing, 2012; Rahman et al., 2007; Kim et al., 2002; Brinker, 1988).

In this study, silica particles were synthesized using Stöber method under well-controlled conditions using a standard cell. Hydrolysis and condensation reaction kinetics of TEOS were investigated for different synthesis conditions to understand and distinguish the sub-processes of synthesis: hydrolysis, nuclei formation and particle growth to provide a better conceptual understanding of the Stöber process. The conceptual model developed was then expressed in mathematical form for predicting the time-dependent particle growth. The advantage of the model is that it distinguishes the hydrolysis and condensation rates in predicting how particles achieve their final size (through hydrolysis, nucleation and growth). The role of different synthesis modes and processing parameters onto the formation process were also presented and their influence on the structural and morphological properties was discussed.

CHAPTER 2

SOL-GEL SYNTHESIS OF SILICA (STÖBER METHOD)

This chapter starts with the description of Stöber method which is most common and easy method to synthesize SNPs. Following that state of the art will be given including detailed information about parameters affecting characteristics and growth mechanism of SNPs.

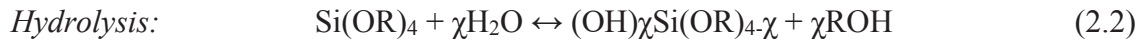
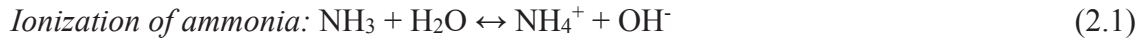
2.1. Description of Stöber Method

Use of nano-sized silica particles has been gaining momentum as an high added-value material in applications including chemical sensors (Krutovtsev et al., 2013; Bonacchi et al., 2011; Yang et al., 2011; Roca and Haes, 2008; Tao et al., 2004), drug delivery (Buyukserin et al., 2014; Hakeem et al., 2014; Ma et al., 2013; He and Shi, 2011; He et al., 2011; Liu et al., 2011; Jin et al., 2009), energy storage media (Chieruzzi et al., 2015; Zhang et al., 2015; Membreno et al., 2014; Zhao et al., 2012) and catalysis (Pahlevanneshan et al., 2016; Zare et al., 2016; Sun et al., 2016; Dam et al., 2016; Habibi and Vakili, 2015; Nogueira et al., 2014) owing to their low density, good thermal and mechanical stability, chemical inertia and controllable morphologies. Their unique properties are linked to their size and different from bulk materials (Membrano et al., 2014; Thanh et al., 2014; Gorji et al., 2012). The majority share of commercially produced specialty silicas are provided from the colloidal silica that its economic advantages predicted to keep growing in the future market (Hyde et al., 2016). The universal specialty silica market size was valued at 5.61 billion USD in 2018 and is expected to grow at a CAGR (compound annual growth rate) of 9.4% over the forecast period (Specialty Silica

Market Size, Share & Trends Analysis Report, Accessed Date:19 March, 2019, <https://www.grandviewresearch.com/industry-analysis/specialty-silica-market/toc>).

It is possible to obtain SNPs with distinctive morphologies as solid, porous and hollow. In recent years, hollow silica nanoparticles (HSNs) have been receiving increased attention because of their low density, large specific surface area, high storage capacity, good thermal and chemical stability (Chen et al., 2013). Amorphous silica has been synthesized by various methods including the sol-gel technique (Greasley et al., 2016), soft-template process (Zhang et al., 2007), hydrothermal reaction (Abdelaal et al., 2014), chemical vapor deposition (Leach et al., 2002) and flame synthesis (Yue et al., 2013). Among these methods, sol-gel method has numerous benefits including moderate temperature synthesis and control of reaction pathways on a molecular level during the transformation of the precursor species to the final product. Moderate temperature synthesis is succeeded through solution-mediated formation of strong covalent bonds between elements; otherwise extremely high temperatures (~1000°C) are required to create network formation. It can be shape products in bulk, powder, fiber or thin-film form with high purity and homogeneity, so it can be used to obtain products of different sizes, shapes and eventually applications (Bergna et al., 2003). For alkoxides, the process involves simultaneous hydrolysis and condensation reactions (Owens et al., 2016; Dubey et al., 2015; Cho et al., 2009; Tabatabaei et al., 2006). Due to the large number of reaction parameters that have to be rigorously controlled (hydrolysis and condensation rate of the metal oxide precursors, pH, temperature, method of mixing etc.), sol-gel chemistry is also a quite complex process in order to provide reproducibility of the synthesis procedure (Toygun et al., 2013).

Of particular interest, the Stöber process, which allows production of spherical, monodisperse silica particles with final mean particle sizes ranging between 0.05 and 2 μm , is one of the most extensively studied sol-gel synthesis route (Stöber et al., 1968). The method is based on reacting a silica source (mainly tetraethyl orthosilicate, TEOS) with a water-solvent mixture in the presence of a base catalyst (ammonia, NH_4OH) and alcohol as the solvent. According to Stöber's study, 1968, the changing in the reactant mixture color from transparent to opaque was observed within the first 1–5 min after alkoxide supplementation, evidencing silica formation, nonetheless, a total reaction time of 120 min was selected as base for experiments. The reactions that underlying Stöber method are described as follows (Green et al., 2003-a):



Where R is C_2H_5 for TEOS.

It has been brilliantly known that TEOS hydrolyzes to form hydrolyzed monomers which then condense to form the first nanostructures. The hydrolysis and condensation reactions provide initial particles called nuclei and the formation period of this nuclei known as “induction period” and this is the less controllable stage of the synthesis. The hydrolysis of alkoxy silanes substantiates by nucleophilic mechanism, such that under basic conditions, water dissociates to produce nucleophilic hydroxyl anions (OH^-) in a rapid first step (Equation 2.1). Then the hydroxyl anion attacks the silicon atom on TEOS molecules during the reaction, the ethoxy group of TEOS reacts with the water molecule to form the intermediate $[\text{Si}(\text{OC}_2\text{H}_5)_{4-x}(\text{OH})_x]$ with hydroxyl group substituting ethoxy groups (Equation 2.2). Ammonia works as a basic catalyst in this reaction. Since the TEOS–water system exhibits an immiscibility condition, a homogenizing medium, as alcohol, is frequently used in the synthesis. Following the hydrolysis reaction, the condensation reaction occurs instantaneously where the hydroxyl group of intermediate $[\text{Si}(\text{OC}_2\text{H}_5)_{4-x}(\text{OH})_x]$ reacts with either the ethoxy group of other TEOS molecules “alcohol condensation (alcoxolation)” (Equation 2.3) or the hydroxyl group of another hydrolysis intermediate “water condensation (oxolation)” (Equation 2.4) to form Si-O-Si bridges which lead to the silica network formation. Alcoxolation should be favored condensation reaction between partially hydrolyzed titanate precursors. On the other hand, for silicates oxolation rather than alcoxolation is favored reaction between partially hydrolyzed monomers according to the Si-NMR results (Brinker, 1990). Figure 2.1 illustrates the steps involved in the development of a silica network from TEOS through simultaneous hydrolysis and condensation reactions and typical condensation pathways involved in the evolution of monomer, dimer, trimer, and tetramer for the pH is smaller than 7 and pH is bigger than 7 in the absence and presence of salts are illustrated in Figure 2.2 (Iler, 1980).

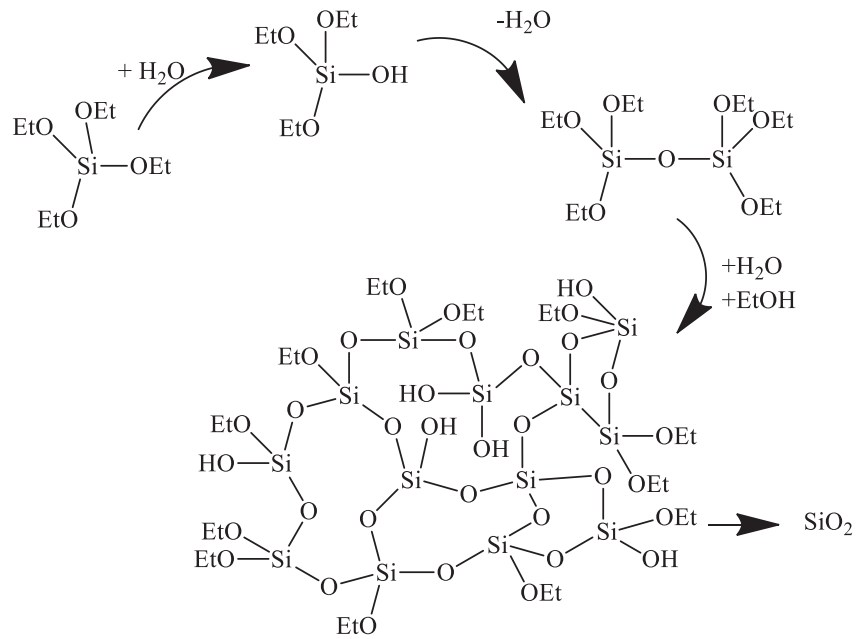


Figure 2.1. Silica network production through the hydrolysis and condensation reactions of TEOS.

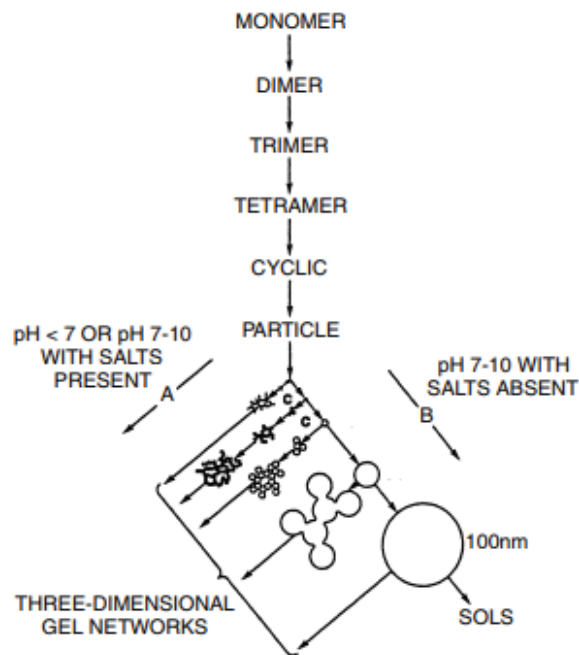


Figure 2.2. Polymerization pathway of silicates according to Iler (Source: Iler, 1980).

Reactive monomers (the hydrolyzed form of alkoxide) such as dimers, trimers, linear and cyclic species (silica rings and cages) can be developed in the array during the

reactions. Dimers, trimers, linear and cyclic species are shown in Figure 2.3. Rings with 2-fold to 6-fold can grow up, however in general, only the structures with at least 4 silicon tetrahedra liable to be stable. The rings behave as a nucleation center and three dimensional particles can finally be obtained by the addition of monomers and other species. Condensation of reactive species can occur within the same molecule or more likely intermolecular resulted in forming a closed loop which refers intramolecular cyclization. Although the chain silica structures are more stable than cyclic one and very likely to form at the very initial stages of reactions, structures with 3 or 4 tetrahedra created the cyclic structures and initial particles of 1–2 nm are formed (Innocenzi, 2016).

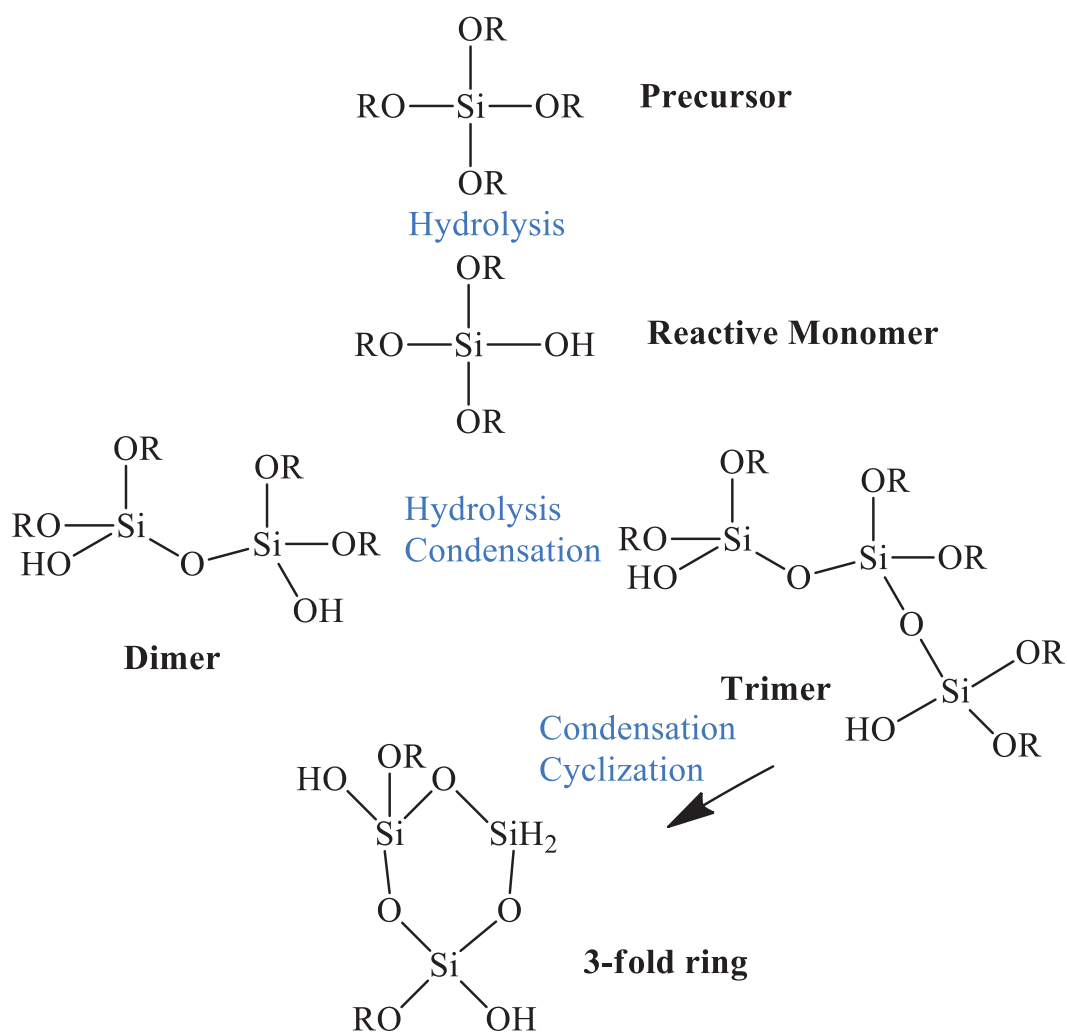


Figure 2.3. Formation of cyclic species during hydrolysis and condensation reactions.

2.2. State of the Art

It is well accepted in the literature that intermediate silica species (hydrolyzed monomers) built up and condense to form the initial colloidal structures (nuclei) during an induction period. The respective concentrations of TEOS, ammonia, water and alcohol control the reaction rate which governs the induction period; hence the balance between the hydrolysis of TEOS to hydrolyzed monomers and condensation of the hydrolyzed species to the first nanostructures (Green et al., 2003-b). Also, the feed rate of silica source, mixing conditions, temperature and other reaction conditions have been reported as important parameters on the rate of hydrolysis and condensation reactions since final particle size depends on the ionic strength of the reaction medium (Carcöuet et al., 2014; Zainal et al., 2013; Rahman and Padavettan, 2012; Yoo and Stein, 2011; Teng et al., 2010; Zhang et al., 2007; Zhang et al., 2003; Giesche, 1994). Since Stöber's study, a large number of researches have been conducted to elucidate the mechanism of hydrolysis, condensation and subsequential growth of these particles (Park et al., 2006). Nevertheless, there seems to be a lack of agreement in terms of how these parameters have effect on the hydrolysis and condensation reactions (Zeng et al., 2015; Carcöuet et al., 2014, Zainal et al., 2013; Li et al., 2012; Singh et al., 2011; Ibrahim et al., 2010; Branda et al., 2007; Tsai et al., 2005; Liu et al., 2004; Buining et al., 1996; Giesche, 1994).

It is demonstrated that the hydrolysis of TEOS is slower than the following condensation reaction rate for base-catalyzed silica synthesis in general. The conductivity results strongly suggests that hydrolysis of TEOS is faster at the early stage of reaction process and the anionic silanol monomers is accumulating in the reaction solution. Following this, condensation of the anionic silanol monomers takes place forming the siloxane networks. The hydrolysis-dominant initial reaction stage is specified as the induction period (T_i). After this period, the condensation of anionic silanol monomers starts to happen dominant and depletes more anionic silanol monomers than those freshly formed by hydrolysis of the remaining TEOS molecules. Here, as an important and reasonable hypothesis, condensation of the silanol monomers with TEOS (Equation 2.3) is not taken into account since the same amount of TEOS was consumed when the hydrolysis and condensation of TEOS reached equilibrium (Han et al., 2017).

According to the study conducted by Han et al., 2017, regardless of the ammonia concentration, only about 15% of the TEOS molecules in the reaction medium are spent during T_i , while the most of the TEOS molecules (about 85%) are consumed later. Owing to the consumption of TEOS during T_i , it is concluded that hydrolysis of one ethoxyl group of TEOS molecules to form monovalent anionic silanol monomers, $\text{Si}(\text{OEt})_3(\text{O}^-)_1$, is the rate-limiting step for TEOS hydrolysis. This means that hydrolysis can be facilitated when the more ethoxy groups are eliminated from TEOS molecule. It is also imparted that the anionic silanol monomers obtained thereafter tend to react with each other (see Equation 2.2) rather than to combine with TEOS molecules (see Equation 2.3). Otherwise, the latter might make the fraction of TEOS consumed in T_i dependent on the ammonia concentration, as the silanol monomers obtained at higher ammonia concentration have more ethoxyl groups displaced by hydroxyl groups and become more active. Their results also explain that the entire of the Stöber process can be handled considering two following steps as shown in Figure 2.4. The first is specified as the induction period, where nucleation and growth of silica particles is specified mainly by TEOS hydrolysis (pathway I) where the conductivity of the reaction medium reaches the maximum. The second stage is the responsible from the size enlargement (growth) of silica particles obtained at the first stage where particle grows occur due to addition of newly formed silanol monomers through condensation (pathway II). With regard to the underlying growth mechanism, pathway I is evocative of the growth by aggregation model, while pathway II is evocative of the growth by the monomer addition model. These models are going to explain in next sections.

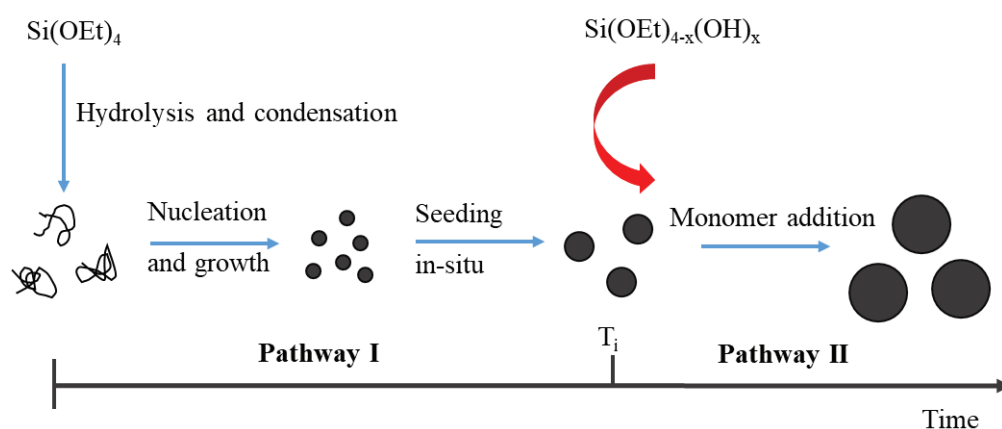


Figure 2.94. Schematic representation of the nucleation and growth process of SNPs (Han et al., 2017).

2.2.1. Factors Affecting Characteristic of SNPs

This part can be come up including effect of process parameters on final characteristic of SNPs (size, shape, morphology, etc.) and other factors such as addition of electrolytes and seed particles.

2.2.1.1. Effect of Process Parameters

The parameters discussed here are precursors (source of silica), solvents, pH and synthesis temperature. These parameters are related to requirements of the Stöber synthesis itself, and hence they are named as “process parameters”.

2.2.1.1.1. Precursors

The most popular precursors for sol-gel silica synthesis are silicon alkoxides (alkoxisilanes). They are recognized by the strong covalent Si-O bonding, hydrophobicity and immiscibility with water. The reactivity of alkoxides related to the steric hindrance of organic groups and hence largest alkoxide organic groups increase the boiling point and the reactivity of silicon alkoxide decreases with the increase of the size of the alkoxy as,



Tetraethylorthosilicate (TEOS), Si(OEt)_4 , is the first alkoxide of the series and commonly used one, followed by tetramethyl orthosilicate (TMOS), Si(OMe)_4 , which is however insecure to work and hydrolyzes more than four times faster than TEOS because of the retarding effect of the bulkier ethoxide group (Innocenzi, 2016; Lim et al., 2012). According to the findings of Finnie et al., 2007, TMOS is preferred for drug encapsulation because of enhanced hydrolysis rates under both acidic and basic conditions. Stöber, 1968

noted that by increasing the alkyl-chain length of the alkoxy silane, the condensation reaction rate got slower and the final silica mean size was decreased. Lim et al., 2012 emphasized that when silica sources with long alkoxy groups were used, large particles were obtained due to the steric effects that decrease the rate of hydrolysis.

Additionally, when TEOS is the case, Jiang et al., 2019 pointed that size of the SNPs increased with increasing concentration of TEOS. Ibrahim et al., 2010 observed that when TEOS concentration was increased, nucleation period become shorter (faster) and growth rate was increased, resulting in larger silica particles which is consistent with the observations reported by Li et al., 2012; Wang et al., 2010b; Kim et al., 2004.

2.2.1.1.2. Solvents

Alcohol does not play the negligible role as solvent, it has an active part in the process. If the alkoxy silane is chosen as TEOS, the best solvent choice should be ethanol. For any specific reason such as different boiling point, if another alcohol is chosen, the possibility of alcohol exchange reactions will change the kinetics of the reactions which demonstrates that alcohol has an important part in the synthesis. On the other hand, alcohol is needed to homogenize the solution because water and alkoxy silanes are immiscible (Innocenzi, 2016).

The selection of alcohol type is also important from the point of solubility of intermediates since the solvents may change the electrostatic and hydrogen bonding interactions and stability. Ionization degree of silanol groups which depended on dielectric constant of solvent might control the zeta potential of silica particles. Solvating power of solvents could be balanced by polarity, degree of hydrogen bond and viscosity and the values of these for some of the alcohols are given in Table 2.1. Solvent polarity is generally denoted by the dielectric constant, ϵ . The size of SNPs increases and PSD becomes narrower with increasing MW and decreasing dielectric constant of the alcohol. Hydrogen bonding ability, δ , and miscibility increase as the alcohol MW decreases. The solvent that have low polarity, low hydrogen bonding ability and high viscosity could increase the size of SNPs (Malay et al., 2013; Lim et al., 2012; Mine et al., 2005).

Table 2.1. Solvating power of several solvents

Solvent	ϵ	δ (at 25°C)	μ ,cP (at 25°C)
Water	80.1	47.8	0.89
Methanol	32.7	29.6	0.54
Ethanol	24.5	26.5	1.07
n-propanol	20.1	24.5	1.95
n-butanol	17.7	23.1	2.54

According to the Stöber's study, 1968, when methanol as a short chained alcohol with faster reacting capability was used, particle size distributions become wider compared to the longer chain length alcohol, such as butanol. Matsoukas and Gulari, 1988 also reported that reactions rates are faster in methanol that resulted in a smallest particle size. Since the ethanol viscosity is twice than methanol, particles grow to a bigger size in ethanol. Harris et al., 1990, studied hydrolysis rate in aqueous solution of alcohols including methanol, ethanol, 1- propanol, 2-propanol and 1-butanol and concluded that the hydrolysis rate was affected by water-alcohol hydrogen bonding and that was strongly depended on steric effects of the alcohols. Mine et al., 2005, concluded that the average sizes of resultant particles in the reaction systems containing different alcohols were in the order of 1-butanol > 1-propanol > ethanol and the interparticle repulsion in the reactions was the strongest for ethanol and the weakest for 1-butanol. Park et al., 2006 emphasized that long chain alcohols are expected to have less polarity and viscosity compared to short chain alcohols and expected to overcome the van der Waals attraction between particles that the results are in accordance with the others. Dabbaghian et al., 2010 emphasized that the size of SNPs increases dramatically by increasing ethanol content because increased amount of hydrolyzed TEOS increases the probability of collision and then decreases gradually as a result of enlarging reaction medium that is resulting higher spacing between reacting agent and decreasing rate of condensation. Similarly Lim et al., 2012 said that when long alkyl chain alcohols were used, the size of SNPs was increased. It was included that different sizes for methanol (4 nm) and ethanol (8 nm) were result of the supersaturation ratio of the hydrolyzed silica sources which was higher in methanol. In short, smaller seeds in huge number were generated in fast reaction condition in methanol and could induce smaller SNPs.

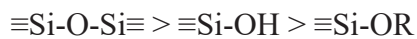
2.2.1.1.3. pH

Water is not adequate alone to initiate the hydrolysis and condensation reactions so a catalyst is required. This is an important selection because the final particle structure is mainly based on the choice of the catalyst and hence pH. Therefore the choice should be between an acidic or basic conditions for sol-gel reactions (Innocenzi 2016). To say why the selection of the catalyst is so important, one need to understand the mechanism involved in the hydrolysis and condensation reactions.

The silicon alkoxides fall into a transition states during hydrolysis and condensation reactions and the electronic density of the silicon atom decreases (silicon electrophilicity increases) with the progress of the process in the following order. For acid catalyzed systems, increasing electronic density increases hydrolysis reaction rate in the order as:



Whereas, vice versa is obtained for base catalyzed systems (silicon electrophilicity decreases):



It is known that, in acidic conditions, because of the higher reactivity of the electrophilic silicon atom with the growth of Si-O-Si bonds, more chain like structures are come to the forefront because of the reactions at central silicon atom. Additionally, produced silica has little or no surface charge and thus flocculation/connectivity between silica particles are facilitated. Differently from this, in basic conditions, branched and more connected silica structures are obtained because reaction proceed at terminal silicon atom. Basic conditions stabilize the suspension allowing the production of individual particles with a highly negative surface charge. The reactivity of hydrolyzed or partially hydrolyzed species is higher than the monomeric alkoxide for basic conditions, the opposite for what we have observed for acid catalyst (Hyde et al., 2016; Innocenzi, 2016; Lim et al., 2012).

Figure 2.5 shows the schematic representation of the formation of silica gels and particles under different values of pH.

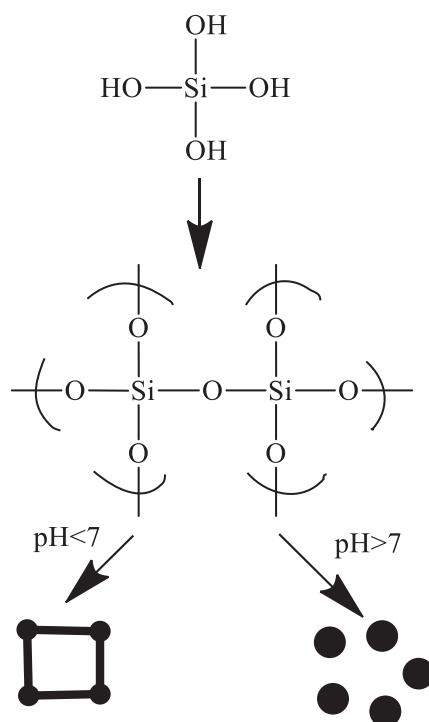


Figure 2.5. Schematic illustrations of the formation of silica structures under different values of pH.

It was also known that, in acid catalyzed systems, the hydrolysis rate of TEOS was relatively fast but the condensation rate was relatively slow because of the aforesaid reasons, and the changes in the hydrolysis and condensation reaction rates with respect to pH is shown in Figure 2.6. When pH value is lower than around 5, dominant reaction is the hydrolysis reaction and its rate starts to decrease with the increasing pH and reaches a minimum around 7. After this point, the hydrolysis rate facilitates a bit quickly when pH is increased. On the other hand, the condensation rate ensues a similar trend and is lowered with the increases of pH up to the value of around 5. After this point, the condensation rate rapidly escalate to around 10, then slows down again. Also knowing that Point of Zero Charge (PZC) of silica is about 2.1 and surface is negatively charged above this pH and positively charged below this pH (Innocenzi, 2016); growth above about pH 7 is different than below pH 7 by at least two factors:

- When $\text{pH} > 7$, particle surfaces are considerably charged and thanks to electrostatic interactions, particle aggregation is improbable; whereas around the isoelectric point ($\text{pH} \sim 2$) there is no electrostatic particle repulsion, so the growth and aggregation processes are related to each other and may be indistinguishable.

- Silica solubility and size dependence of solubility are greater when pH is higher than 7, so growth of initial particles progresses by Ostwald ripening, that is smaller and more soluble particles dissolve and reprecipitate on larger and less soluble particles. Growth stops when the variation in solubility between the largest and smallest particles becomes negligible. Above pH 7, growth continues by Ostwald ripening until the particles reach 5–10 nm in diameter, however at lower pH growth stops when the size of particles achieve after a size of only 2–4 nm. Because of improved silica solubility at higher temperatures, growth continues to larger sizes, especially above pH 7 (Iler, 1980). There have been numerous studies to understand and predict how these sub-processes act at various stages of the particle formation and growth processes leading to particles of specific size, shape and morphology (Lin et al., 2015; Carcöuet et al., 2014; Sato-Berru et al., 2013; Rahman and Padavettan, 2012; Ibrahim et al., 2010; Brinker and Scherer 1990). According to scattering experiments, primary particles of about 2 nm in diameter produced at the initial stages of formation, but no agreement has been reached on the steps that lead to enlargement the particles (Carcöuet et al., 2014).

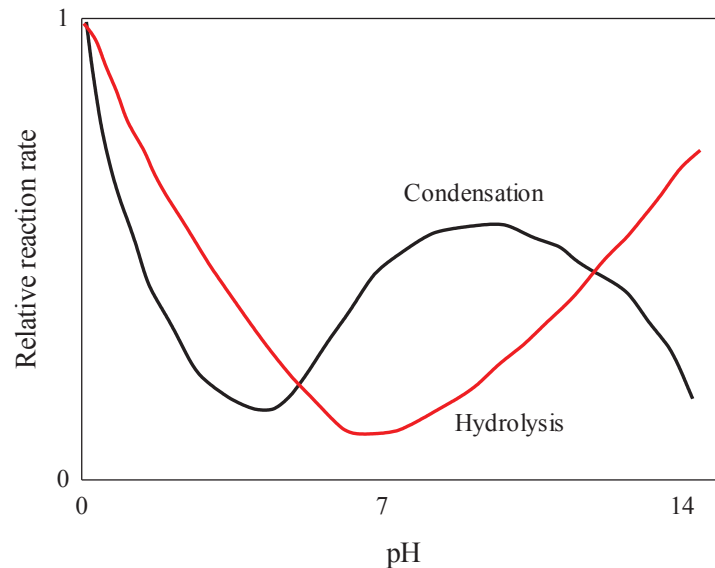


Figure 2.6. Hydrolysis and condensation rates with respect to pH.

Beganskiene et al., 2004 reported that with increasing concentration of ammonia, water dissociated faster producing higher amount of OH^- ions and increase the rate of hydrolysis. Matsoukas and Gulari, 1988 emphasized factor that inhibit hydrolysis and

nucleation produces bigger particles. With increasing ammonia concentration, it was observed that rate of hydrolysis was increased. Ammonia as a basic catalyst promotes hydrolysis reaction but also promotes the polymerization rate to an ever higher degree that results in the formation of larger particles. Dabagghian et al., 2010 showed that the particle size initially increases and then decreases by increasing ammonia amount. When ammonia concentration is low, its effect on hydrolysis predominant, by keeping in mind that higher hydrolysis rate results in larger particles, but when its concentration exceeds a certain amount, condensation rate is more influenced results in sudden condensation and thus smaller particles will be obtained. On the other hand, Li et al., 2012 reported that when ammonia concentration was increased, the diameter of silica particles decreased slightly. Han et al., 2017 stated that the hydrolysis rate increased from 2.4×10^{-3} to $21.6 \times 10^{-3} \text{ min}^{-1}$ and condensation rate increased from 16.2×10^{-3} to $86.4 \times 10^{-3} \text{ min}^{-1}$ by increasing ammonia amount from 0.25 to 1.17 M. It was concluded that with an agreement with literature, the hydrolysis of TEOS was more slowly than the following condensation.

2.2.1.1.4. Temperature

Temperature is one of the other main parameter that have to be controlled during synthesis. According to the researchers, increasing temperature creates smaller particles compared to the lower temperature synthesis. It may be because of two reasons. Firstly, increasing temperature increases equilibrium solubility (C_s) of an intermediate product obtained by the hydrolysis of TEOS, $\text{Si}(\text{OH})_4$. Consequently, time for growing particles is shorten by the increase of equilibrium solubility, which decreases particle size because the growth of particles proceed until the reaction stops due to equilibrium solubility. Consequently, the growth period is shorter compared to the low temperature synthesis. Secondly, if reaction temperature rises, nucleation rate increases. High nucleation rate prohibits nuclei from growing into larger particles, and small particles are obtained at high reaction temperature (Dabagghian et al., 2010; Kim and Kim, 2002). Bogush et al., 1988 conducted the Stöber method to explore the effect of temperature among the range of 9–55°C and reported a distinct decrease in mean particle size with increased

monodispersity when temperature was increased. Fouilloux et al., 2012 reported that increasing temperature increases solubility and reduces the critical supersaturation at which the nucleation takes place resulting in fewer and bigger nuclei.

2.2.1.2. Presence of Electrolytes

The potential of electrolyte additives are highly efficient for controlling particle growth, however has not yet gained significant concern in the synthesis of SNPs. The concentrations of electrolytes can also effect the morphology of the SNPs. Supposedly the surface potential of the SNPs and the ionic strength of the reaction medium could be reduced by the addition of electrolytes which probably influences the growth of silica particles (Giesche, 1994). Bogush and Zukoski, 1991a reported that addition of NaCl to Stöber solutions increased particle sizes, verifying aggregative growth model. They summarized that final particle size can be modified through changes in ionic strength of the solution while keeping the particle growth rates and rates of loss of TEOS as constant. According to the study of Nagao et al., 2000b particle size is increased by the addition of electrolytes (KCl and LiCl) due to an increase in ionic strength and decrease in surface potential. In their study, the concentration dependence of mean diameter for KCl was superior than for LiCl. The effect of electrolytes was also examined in seed growth experiments and the results showed that the presence of KCl depressed the formation of secondary particles (Nagao et al., 2000a). Kim et al., 2004 have fabricated monodispersed SNPs with a mean diameter about 35 nm to hundreds of nm depending on the TEOS, water, and ammonia concentrations in the absence of additives. They have reported if a small amount of mono-valent electrolyte additives such as NaI was introduced to the system, the size of SNPs decreased up to 17.5 nm due to an enhanced particle surface electric charge, thereby inhibiting particle growth. A further increase in the electrolyte concentration (above the optimal concentration) significantly increased the particle size, because of the particle charge neutralization, thereby promoting particle growth. Rahman et al., 2006 stated that ammonium salts were reduced the particle size of SNPs due to hindered growth arise from electrostatic repulsion. It was also found that the effectiveness in reducing silica particles sizes can be related to the size of anions as Br⁻ and I⁻ had the

highest effect while Cl^- had the least. Accordingly, in this study, addition of ions with different valences at specific concentration were investigated in silica production by sol-gel. Nakabayashi et al., 2010 reported that the addition of 3 mol/m^3 potassium ion (alkali metal ion) to the reaction system containing 5 kmol/m^3 water effectively increased the silica particle sizes to $6.6 \mu\text{m}$.

In principle, it is possible to adjust the properties of SNPs in the desired manner by controlling one of the above listed parameters which essentially requires the understanding of the formation processes.

2.2.1.3. Presence of Seed Particles

In order to control the growth process, some researchers also used seed growth method which uses smaller particles as seeds for the production of bigger particles which have different size distributions by the multi-step hydrolysis and condensation of TEOS (Huang and Pemberton, 2010; Buining et al., 1996; Chen et al., 1996-a; 1996-b;). Large particles ($>1 \mu\text{m}$) can also be obtained by condensing all TEOS in the system directly on the seeds which is highly attractive as spacers of liquid crystal display (LCD) polarized films and dental fillers (Chang et al., 2005). It is observed that seed addition has a more direct effect on the final size distribution compared to the chemical composition of the reacting solution and the operational conditions. Clearly, the surface nucleation sites provided by the seeds suppress the formation of fresh nuclei in solution, which would otherwise grow into new (secondary) SNPs and lead to broad or multimodal size distributions. The amount of secondary SNPs generated could be controlled by adjusting the size and amount of the seeds, which suggests that critical seed surface area may be the key for obtaining a desired size distribution. It was also shown that controlled addition of TEOS into the reaction system at a rate slower than the hydrolysis and condensation rates in the reactor was also able to generate monodisperse size distributions of varying sizes at a given seed concentration (Han et al., 2017; Jarzebski et al., 2015; Chou et al., 2008; Chang et al., 2005; Chen et al., 1996a).

Matsoukas and Gulari, 1988; 1989; 1991 stated that, if an enough number of stable particles are produced in the initial stage of the synthesis, further particle formation would

depressed which is resulted with a monosized particles. Otherwise, secondary particles would appear because of the exceeded supersaturation. A similar argument was proposed by Chen and his co-workers, 1996 that they prepared large monodisperse silica particles using seed particles. They also recommended that secondary particle formation is a function of the generation rate of supersaturation by the reaction and the consumption rate by particle growth. Their results indicated that under a given set of reaction conditions, the larger the total surface area of the seed particles, the fewer the newly formed particles during growth of the seed particles. They argued that the early stages of growth of silica particles are controlled by diffusion of electrically charged condensed species onto the surface of the silica seeds against the electrostatic repulsion. They argued that this was demonstrated by the dramatically decreased number of newly formed particles by the addition of an electrolyte to the seed-growth system which decreased the energy barrier and promoted aggregation between the condensed species and the seed particles on the expense of new particle formation. According to the study done by Chang et al., 2005 summarized that production of monodispersed particles would be possible under certain conditions, on the other hand it could hardly be say that the particles would exceed a certain size due to the challenge of control on the formation and growth of particles. In another words, monodispersed and small particles will be formed if enormous number of stable silica particles formed under initial high supersaturation meaning that secondary particle formation will inhibited. Conversely, multidispersity will occur if small number of particles are formed under low initial supersaturation. Wang et al., 2010a who grew and fixated spherical or anisotropic SNPs by TEOS addition through controlled self-assembly of 22 nm spherical silica seeds on various substrates. They reported that the growth and fixation of the seeds were controlled by the suppression of the electrostatic interaction through the adjustment of the dielectric constant and ionic strength of the reaction media.

Interestingly, the study performed by Chang et al., 2005 remarked that turbulent fluid motion advocates the growth of particles due to the lowering hydrodynamic barrier against the transport of materials required for growth. Hence, it is not suprising that secondary particle formation inhibited and seed particle growth promoted by agitation. At a mild agitation regime, a tiny secondary particles (smaller than 100 nm) with large population were formed, which were gradually reduced as agitation speed increased. This population eventually disappeared at an agitation speed of 1500 rpm.

In another point of view, Chou and Chen, 2008 related secondary nucleation with the distance between seed particles. When this distance exceeded a critical value, secondary nucleation would be emerged. When the distance between seed particles was below this critical value simple growth was observed. Higher generation rate corresponded to shorter distance. In other words, the reaction intermediates would have only a certain limited time of diffusion to find a seed surface for precipitate. Otherwise, these species will aggregate to form new nuclei which destroy monodispersity. It is a competition between the diffusing time for growth against the time for secondary nucleation. The schematic related to this discussion is given in Figure 2.7. Their results also indicated that when the seed size is large, more specific seed surface area (i.e. higher seed concentration) is needed to inhibit the production of new particles. Zhao et al., 2012 expressed that the evolution of secondary particles, which created multimodal distribution of particle size, was also overcome by varying the TEOS concentration and reaction temperature.

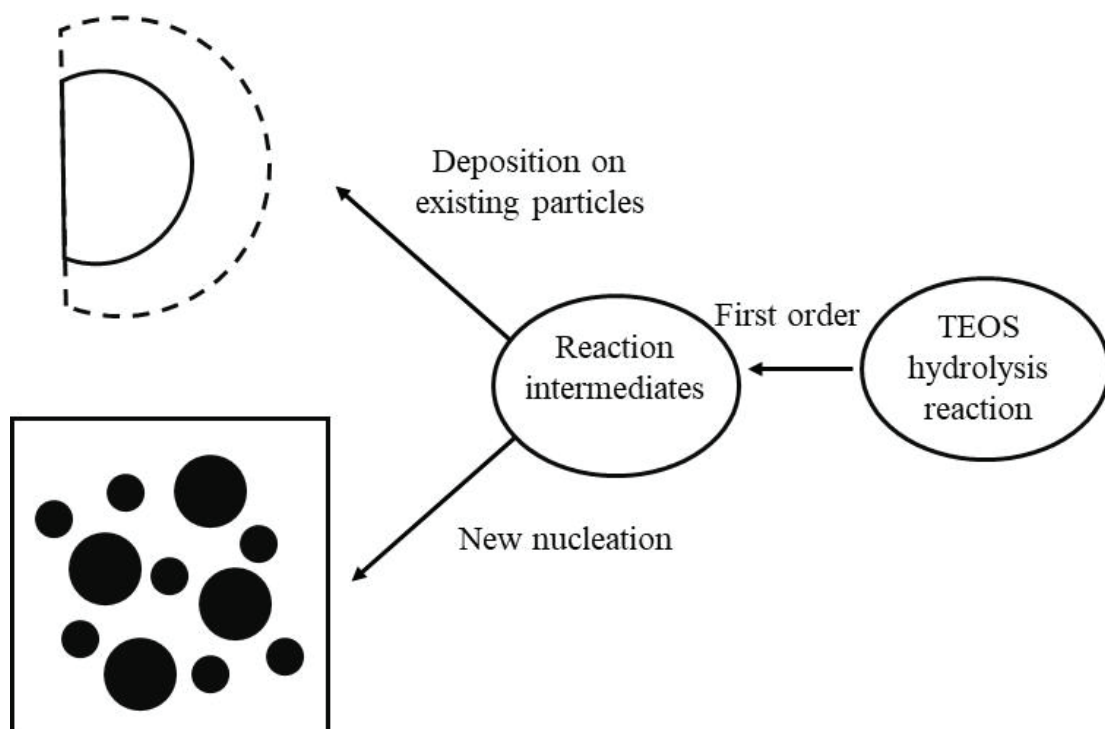


Figure 2.7. Schematic graph of the formation and consumption of intermediate $[\text{Si}(\text{OC}_2\text{H}_5)_{4-\chi}(\text{OH})_\chi]$ for seed growth.

2.2.2. Growth Mechanism of SNPs

The controversy in the literature comes into prominence when considering the question of how the initial colloidal structures formed by the hydrolysis and condensation processes grow to form the final particles. According to the literature surveys, the mechanism is validated by two extremes: “*monomer addition*” and “*controlled aggregation*” model. Researches have indicated that both models are helpful to demonstrate particle formation and growth for various conditions. All of the proposed particle formation models be in similarity that the reaction starts with the generation of nuclei (initial particles) and maintains increasing in size with time. However, the important distinctness between the models are related to the definition of nuclei and the growth mechanism. Here these differences are put forward in detail and summarized in Table 2.2.

2.2.2.1. Monomer Addition Model

The spearheading model of particle growth through monomer addition was provided by LaMer and Dinegar, 1950 and the model was built on the formation of monodispersed sulfur hydrosols. They were suggested monomer addition model, that nucleation is limited to the early stages of the reaction (all of the particles are formed at this period) after that nucleation does not occur and the growth is based on the solution transfer from the bulk to the already formed particles and deposition on the particle surface without additional nucleation. Conventionally, nucleation is identified as homogeneous, which is, as soon as supersaturation is obtained the precipitable material concentration decreases in the solution in a quick outburst. Particle growth takes place by the condensation of monomers on the surface of the freshly formed nuclei or already formed particles. In their model solid cyclooctasulfur (S^8) rings were denoted as nuclei. The number of nuclei determined the number of final particles, which means each particle formed individually and grew only via the addition of monomers proportional to the amount of total diffusible sulfur, which was a function of time solely, with negligible

aggregation. Through applying of the Fick's first law of diffusion they expressed the molecular concentration profile of sulfur precursor as a function of time only. The schematic representation of proposed model by LaMer is shown in Figure 2.8.

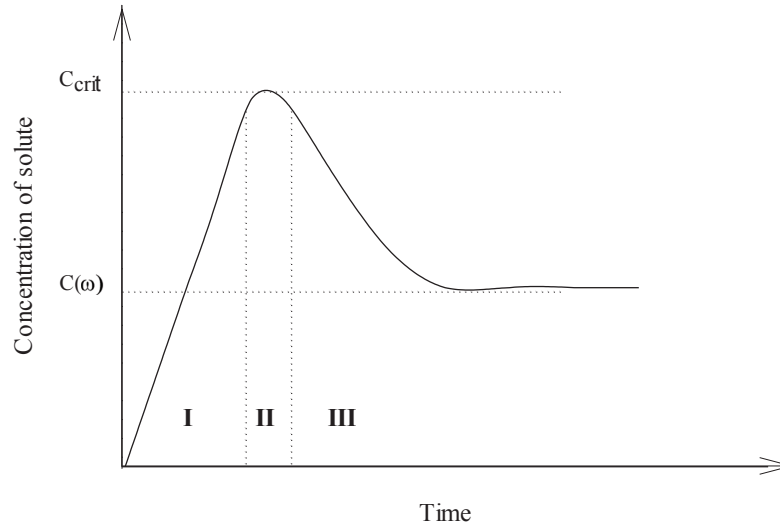


Figure 2.8. Schematic of proposed model by LaMer (Thanh et al., 2014).

According to the proposed model by LaMer; the nucleation and growth mechanism can be divided into three sections (Thanh et al., 2014):

- I) A speedy rise in the concentrations of free monomers in the solution,
- II) Reduce in the concentration of free monomers as a result of “burst nucleation”, where further nucleation is improbable,
- III) Succeeding nucleation, growth continues on existing nuclei by diffusion of monomers through the solution.

Matsoukas and Gulari, 1988 also recommended a monomer addition model for silica formation and growth similar to the model proposed by LaMer and Dinegar. In their model (1989) when two hydrolyzed TEOS molecules were combined, nuclei formation occurred. The narrow particle size distribution of silica particles signified that nucleation was likely restricted at the initial stages of the reaction. They assumed hydrolysis is the rate limiting step through the reactions and hence the change in mass of particles with time was proportional to the hydrolysis constant. Also, three irreversible chemical reactions were dealt in their model that all of them were first order rate equations (1988).

First reaction was the hydrolysis of alkoxy groups with hydroxyl groups. The second reaction was a nucleation reaction in which polymerization of two hydrolyzed reaction to form nucleus or dimer. The third reaction was the growth reaction where a hydrolyzed monomer was added to an oligomer of “i” monomers (denoted as “i”-mer), thus producing “i+1”-mer. By solving these three rate equations, it was found that hydrolysis was the rate limiting step and the progress of particle mass was independent of whether the reaction was diffusion or reaction limited. On the other hand, final mean size of particles was related to the growth kernel and hence which of the mechanism was limiting.

Bailey and Mecartney, 1992 conducted Si NMR to elucidate reaction mechanism and their results showed that the dominant species in the solution were TEOS monomer and its first and second hydrolyzed intermediates (one or two hydrolyzed groups). According to their results, silica atoms appeared in a random expanded polymeric ring, denoted as low density or microgel particle. These particles were assumed to grow by the monomer addition pathway, while simultaneously intramolecular condensation bonds formed within the gel resulting densification. The densifying particles grew till the precipitation occurred. The colloiddally stable particles continued to grow by monomer addition while aggregation was inhibited due to existing double layer repulsion. This model which was later broadened further by others (Lee et al., 1997; 1998) discounted aggregation and proposed that the narrow size distributions observed develop by a “single burst” of nucleation followed by diffusion limited growth.

In the study of Jiang et al., 2019, it was indicated that the smooth surface of particles are because of the monomer addition model. They found that while $\text{Si}(\text{OH})_4$ behaved as the nucleus of nanoparticles and the size of particles increased via the addition hydrolyzed monomer ($\text{Si}(\text{OH})_4$).

2.2.2.2. Aggregation Growth Model

In contrast to above works, this models depend on aggregation mechanism that consider binary collision of fine particles (primary particles or subparticles). Bogush and Zukoski, 1991-a, 1991-b proposed a model that did not obey the criteria of the classic nucleation and growth model. According to their model, the initial primary particles are

very small in size (<10 nm), unstable and they tend to aggregate. The larger and stable aggregates then spread in the solution, collecting freshly formed primary particles and smaller aggregates. They argued that uniform particle size was achieved because of the size-dependent aggregation rate; with the help of the aggregation rate for large/large pairs was slower than the small/small or small/large pairs, aggregation process ended up with a narrow final size distribution (Bergna et al., 2003; Green et al., 2003-a). Assuming a solely aggregative mechanism, Bogush and Zukoski, 1991 carried out the Smoluchowski equation to characterize the growth of SNPs. The development of the particle number density function according to time was considered to be equal to the net summation of an aggregative birth, an aggregative death and a nucleation terms. The kernels for both birth and death terms were assumed to be a function of van der Waals, electrostatic and solvation interactions to include particle–particle interactions in their model. By comparing the model and experimental data, they said that particle diameter and size distribution could be predicted correctly using aggregation mechanism. The model proposed by Bogush and Zukoski is still one of the most common model to investigate particle formation and growth.

If the final SNPs characteristics are influenced by some of the experimental parameters including ionic strength, pH and solvent properties (the dielectric constant and viscosity), aggregation is feasibly the dominant growth mechanism (Hyde et al., 2016). The same view is supported by Lee et al., 1998 who argue that the observed particle size development during Stöber synthesis can be satisfactorily presented by aggregation of the nucleated silica structures and that the respective rates of nucleation and aggregation controls the final particle size. The work by Okudera and Hozumi, 2003 demonstrated that the silica films were formed by aggregations of primary particles and then grew by the adhesion of primary particles forming continuously in the solution; supporting simultaneously both the continuous nuclei formation and the growth by aggregation. Branda et al., 2007 also argued in favor of aggregation and state that dominant aggregation mechanism could be between the freshly generated nuclei and large aggregates and pointed out to the importance of mixing conditions. Also, Zeng et al., 2015 showed that their results which were obtained in a range of ammonia concentrations were very consistent with prediction of aggregation model.

2.2.2.3. Mixed Growth Mechanism

This growth mechanism takes into account that particle growth is a result of the combination of both aggregation (generally at the early stages of growth) and monomer addition (at the later stages of growth) processes. These models are more complicated than the monomer addition only or aggregative growth models.

Harris et al., 1990 declared that nucleation continued through the most of the synthesis and new particles were still forming during the reaction by looking at the concentration of silicic acid that is more than three times larger than its equilibrium concentration. The unstable nuclei (size of 1-5 nm) were proposed to either aggregate with each other very quickly to form larger, more stable particles or deposit on to the surface of existing particles during the first half of the reaction period. However, during the other half of the reaction, particles grew by the dominant monomer addition mechanism. This change in the growth mechanism between aggregation to monomer addition occurred when particle diameter reached nearly 135 nm with constant particle number density. Similarly, Harris, 1990 and Van Blaaderen et al., 1992 stated that two of the mechanisms were responsible for growth and they suggested that controlled aggregation occurred for much of the reaction, followed by monomer addition for smoothing of the particle surface. Giesche, 1994 reported that the critical size of primary nuclei that were formed at the very first reaction stages was about 1 to 2 nm and they aggregated to form larger particles through a surface reaction limited condensation. The number and size of the particles could be determined from the colloidal stability and aggregation rate of the primary nuclei. Later on the reaction, the growth mechanism changed to monomeric or dimeric addition of silicic acid to already existing particle surfaces. A relatively recent work by Wang et al., 2010b also recommended a combination of monomer addition and aggregation models for the formation mechanism of silica particles.

As can be seen from the above discussions, particle formation through nucleation and growth processes are complicated phenomena. Mathematical modelling of the system is helpful to be able to achieve a general framework of how nuclei are formed and grow to final particles. It is obvious that, about the modeling the formation of silica particles through nucleation and growth, numerous studies exist in literature. However, the models

show a change related to the synthesis conditions and so are the matter of future work as different silica production procedures are employed. As a conclusion, there is a need to understand how the initial colloidal structures are able to grow to create the final monodisperse Stöber particles. In this study, we aim to investigate several sub-processes in the synthesis of silica particles for the purpose of provide a better understanding how various sub-processes (nucleation through hydrolysis/condensation and particle growth) develop and interact during Stöber synthesis. Understanding these processes in detail does not only have significant scientific relevance, but will also carry important consequences in controlling and manipulating product particle size, shape and morphology for the industrial applications mentioned above.

The differences in the particle growth models suggested in literature and in the definition of nuclei are summarized and showed in detail in Table 2.2.

Table 2.2. Summary of the suggested models for silica particle formation (Hyde et al., 2016)

Authors	Nuclei definition/ suggested model for nuclei formation	Particle growth mechanism	Growth limiting phenomenon
LaMer and Dinegar, 1950	Sulfur rings/ monomer addition	Monomer addition	Monomer diffusion
Matsoukas and Gulari, 1988, 1989	Dimer of hydrolyzed silica species/ monomer addition	Monomer addition	Surface reaction
Harris et al., 1990	Stable particle/aggregation of unstable subparticles	Aggregation at early stages and monomer addition at final stages	Monomer diffusion
Bogush and Zukoski, 1991a, 1991b	Densification/ monomer addition	Aggregation	Primary particle production
Bailey and Mecartney, 1992	Densification/ monomer addition	Monomer addition	Monomer diffusion

(cont. on next page)

Table 2.2. (continued)

Van Blaaderen et al., 1992	Stable particles/aggregation of small silica moieties	Monomer addition	Surface reaction
Giesche, 1994	Nanosized subunits/aggregation	Aggregation at early stages and monomer addition at final stages	Surface reaction
Nagao et al., 2000	Nanosized subunits/no mechanism proposed	Aggregation	Reaction limited at early stage and diffusion limited at final stage
Nozawa et al., 2005	Seed particle/ no mechanism proposed	Monomer addition	Surface reaction limited at early stages and diffusion limited at later stages
Zhao et al., 2012	Stable particles/Monomer addition	Monomer addition	Monomer diffusion

CHAPTER 3

EXPERIMENTAL METHODOLOGY

This chapter gives information about the experimental methodology of the silica nanoparticle synthesis. For this, used materials in the synthesis are given and methods of synthesis is expressed in detail.

3.1. Materials

Tetraethyl orthosilicate (TEOS) (Merck, 98%) as silica source, ethanol (Tekkim, 96%) as solvent and ammonium hydroxide (NH₄OH) (Sigma-Aldrich, 26%) as basic catalyst were used in the synthesis of SNPs. Ultrapure water (18.2 MΩ) was used in all the experiments. Sodium chloride (NaCl) (Sigma-Aldrich), Calcium chloride (CaCl₂) (Sigma-Aldrich) and Aluminum chloride (AlCl₃) (Fluka) were used as ionic compounds. All chemicals were used as received.

3.2. Methods

SNPs were synthesized using base-catalyzed classical Stöber method that includes hydrolysis and condensation of tetraethyl orthosilicate in alcoholic medium in the presence of base catalyst (ammonia) and the experimental details are given in the following sections. Besides this, addition of some of the external parameters including addition of seed particles which were also produced through Stöber method and electrolytes to the classical Stöber method were also conducted.

3.2.1. Synthesis of SNPs using Stöber Method

Stöber method that includes base-catalyzed hydrolysis and condensation of TEOS gives particles with spherical morphology and monosized distribution. In the classical Stöber method, the solution of ammonium hydroxide (1.09 M) and water (11.67 M) were mixed with ethanol (12.14 M) under mild stirring. By the pulse addition of TEOS (0.25 M) to the prepared solution silica synthesis was started. The experimental parameters studied for preparation of silica particles are tabulated in Table 3.1. All the experiments were conducted at room temperature ($\sim 20^\circ\text{C}$) and the reactions were allowed to continue for 24 h for completion. Then, particles were separated from the solution using centrifugation and collected final particles were washed with water and ethanol to remove unreacted reagents. Finally particles were dried at room temperature for further characterization studies.

Table 3.1. Experimental parameters for preparation of SNPs

<i>Parameters</i>	<i>Value</i>
^a TEOS, mol/L	0.05, 0.1, 0.18, 0.25, 0.35, 0.5, 0.75
^b NH ₃ , mol/L	0.27, 0.55, 1.09, 2.18, 3.27
^c H ₂ O, mol/L	5.67, 11.67, 17.67
TEOS addition rate, mL/min	0.02, 0.04, 0.1, <i>pulse</i>
Stirring rate, rpm	0, 250, 810
Reaction time, h	24

^a While keeping EtOH/NH₃/H₂O ratios constant

^b While keeping EtOH/H₂O/TEOS ratios constant

^c While keeping EtOH/NH₃/TEOS ratios constant.

Solid silica particles having different mean sizes can also be obtained by the addition of seed particles of known characteristics, electrolytes and surfactants to the Classical Stöber recipe that are described above in detail.

3.2.2. Electrolyte Addition

Solid silica particles using Classical Stöber recipe were also produced in the presence of electrolytes to understand the mechanism of silica growth. For this purpose, mono, di, multi-valent aqueous solution of electrolytes, NaCl, CaCl₂ and AlCl₃, were initially loaded in the reactor while keeping the concentrations of TEOS (0.25 M), NH₃ (1.09 M) and ethanol (12.14 M) constant. The flowsheet of the study is given in Figure 3.1. For the first synthesis condition (named as Mode A), ethanol, ammonium hydroxide and electrolyte solution were loaded in the reactor initially and TEOS was added to this solution as a pulse. In the second condition (named as Mode B), TEOS, ethanol and electrolyte solution were loaded in the reactor and ammonium hydroxide was added to this solution. The reactions were allowed to continue for 24 hours. The concentration of electrolytes was varied between 4×10^{-2} and 1×10^{-4} M at fixed TEOS and EtOH concentrations to depress the surface charge of silica particles. The concentration values given above should be considered according to the final mixture volume in the reactor.

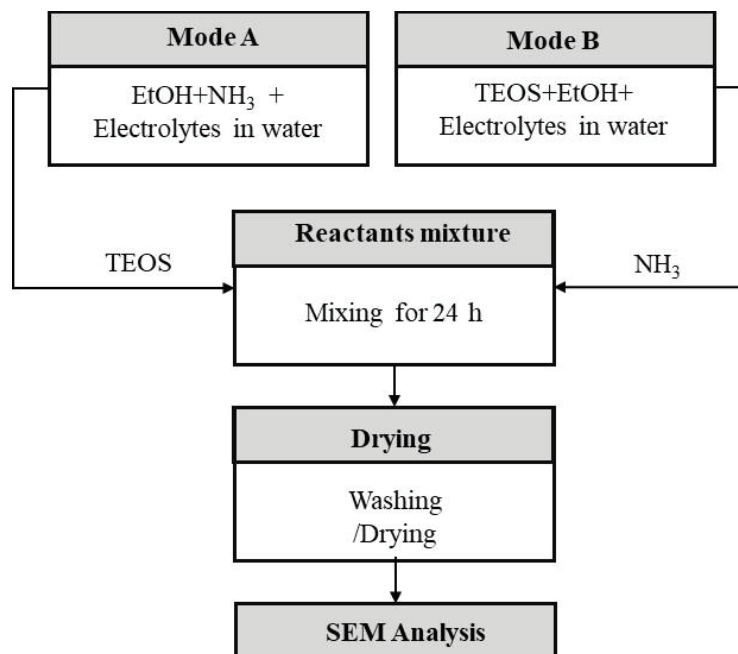


Figure 3.1. Flowsheet for the electrolyte addition to the silica synthesis medium.

3.2.3. Seed Addition (Seeded Growth)

The synthesis of silica nanoparticles was performed in the presence of seed particles with known characteristics to obtain silica nanoparticles with different modalities under control. In the seeded growth experiments, a pre-determined amount of monodispersed silica particles were seeded into the growth solution containing ammonium, water and ethanol solution before the TEOS was added to the reactor and allowed to grow. The study includes first the synthesis of seed particles and then growth of these seed particles. These studies with seed particles were performed to investigate the effects of the followings:

- i) NH_3 concentrations,
- ii) Seed amounts,
- iii) TEOS amounts and addition rates,
- iv) Addition of electrolytes on final size and distribution of SNPs were investigated.

3.2.3.1. Effect of NH_3 Concentrations in Growth Solution

For the demonstration of the effect of NH_3 in silica growth solution, classical Stöber method was performed and a little amount of silica solution (18.5 mL), that is equal to the amount of TEOS in the classical Stöber solution for total volume of 330 mL, was withdrawn after 4 mins of production and replaced in two other fresh Stöber solutions (containing water and ethanol with the same amount of the Stöber solution in the presence and absence of NH_3), one with standard NH_3 concentration (1.09 M) and the other one with the absence of NH_3 and the solution was mixed for 24 hours (GP1). After that, additional TEOS at different amounts (0, 1.85 and 18.5 mL which correspond to 0, 0.025, 0.25 M, respectively) were introduced to the system as pulse and stirred another 2 hours and new particles were generated (GP2, GP3). Then representative samples were taken from the suspensions and sizes of particles were determined by Scanning Electron

Microscopy (SEM) coupled with an image analysis software (ImageJ). The flowsheet of the experimental procedure for this seeding experiment is given in the Figure 3.2.

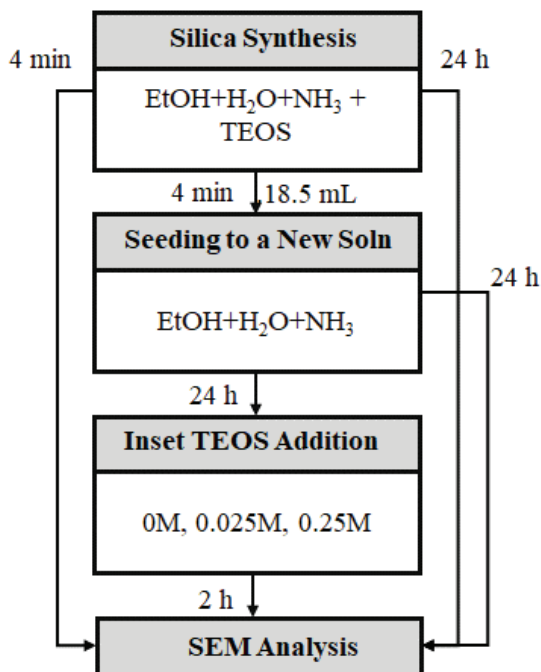


Figure 3.2. Flowsheet of the procedure for seeding experiments in changing NH_3 solution.

3.2.3.2. Effect of Seed/TEOS Amounts and TEOS Addition Rates

Stöber procedure (EtOH: 12.14 M, NH_3 :1.09 M, H_2O :11.67 M, TEOS: 0.25 M in 330 mL total solution volume) which described in Section 3.2.1 was applied. TEOS was added to the solution at once (pulse addition) during seed preparation. The reaction lasted for 24 hours for complete conversion of TEOS into seed SNPs. The seeds formed were collected by centrifuging (Eppendorf Centrifuge 5804, Hamburg), washed and diluted with deionized water to stop residual reactions and stored as a stock solution of 15 g/L solid concentration assuming complete conversion of TEOS into silica. Known aliquots from the seed stock solution which correspond to seed amounts of 25, 50, 75, 100, 150, 200 and 300 mg (equivalent to seed surface areas of 0.137, 0.273, 0.410, 0.547, 0.820, 1.094 and 1.641 m^2 which are calculated using mean diameters and number of seed

particles) were transferred into TEOS free Stöber solutions containing EtOH/H₂O/NH₃. After proper dispersion of the seeds, 0.125 M and 0.250 M TEOS was added with an addition rate of 0.1 mL/min, 0.04 mL/min, 0.02 mL/min and as a pulse (direct addition) such that to initiate synthesis which lasted for 24 hours. Representative samples were taken from the suspensions and size of particles were determined by SEM coupled by an image analysis software. The flowsheet of the procedure for seeding experiments is given in the Figure 3.3.

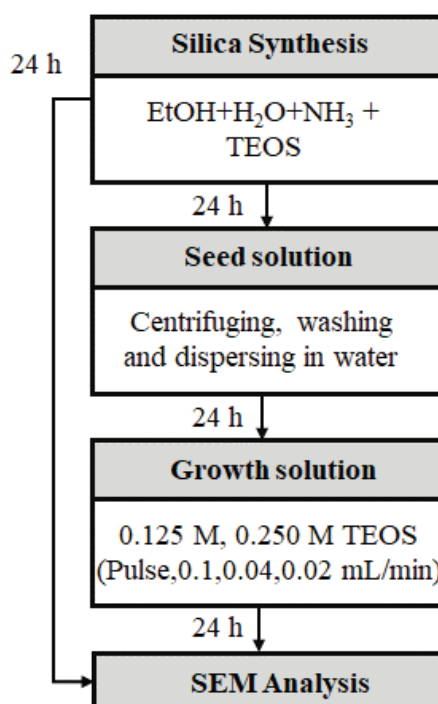


Figure 3.3. Flowsheet of the procedure for seeding experiments using different amount of seed particles with different TEOS addition rate.

Seeded growth studies were also tested with the whole system used as seed particles directly after washing the particles or unwashed particles. For this, Stöber synthesis were conducted (EtOH: 12.14 M, NH₃:1.09 M, H₂O:11.67 M, TEOS: 0.25 M) for 24 h to ensure that all TEOS was consumed in the system. In one of the condition, final particles were separated from unreacted reagents by washing 3 times with water. Then the particles were redispersed in fresh TEOS-free Stöber solution (NH₃/H₂O/EtOH), in other words growth solution, so as to use as seed solution. In another condition, the

final particles were not washed and whole system was used as seeds as it is. Then additional TEOS (same amount as the Stöber solution) was added both of these systems and stirred for another 4 h. SEM images were used to characterize the systems by counting 100 particles diameters.

3.2.3.3. Effect of Electrolytes in Growth Solution

The seed preparation procedure was same as Section 3.2.3.2. A proper amount of seed particles were taken from this solution and putted into a TEOS free Stöber solution (growth solution). Electrolytes (NaCl, CaCl₂ and AlCl₃) that have different valences at 4×10^{-2} M concentration were included in the growth solution and TEOS was added to this solution as a pulse.

Classical Stöber method was conducted that explained detailed in Section 3.2.1 and particles were separated from the solution by centrifugation and redispersed in water again. A proper amount of seed particles were taken from this solution and putted into a TEOS free Stöber solution (growth solution). Electrolytes (NaCl, CaCl₂ and AlCl₃) that have different valences at 4×10^{-2} M concentration were included in the growth solution and TEOS was added to this solution as a pulse.

3.3. Characterization Studies

The in-situ size and morphology of the particles were measured by SEM Scanning Electron Microscopy (SEM) (Quanta 250 FEG) at preset time intervals. A drop of colloidal suspension from the reaction solution was placed on an aluminum foil and dried in air; the sample was then coated by gold (Au) film before analysis. Mean particle diameters were estimated at different magnifications by measuring and counting ~100 particles from SEM images using image analysis software of ImageJ. Transmission Electron Microscopy (TEM) (Jeol 2100F HRTEM) was used to determine the interior structure of particles. Brunauer–Emmett–Teller (BET) analysis was used to obtain the

surface area of particles. The zeta (ζ) potentials were determined by Malvern Zetasizer NanoZS. The chemical structures of the samples were determined using Fourier Transform Infrared Spectroscopy (FTIR) (Shimadzu FTIR-8400S) in the wavenumber range of 4000-400 cm^{-1} . The pellets for samples were prepared for the analysis. First, certain amount of silica particle was mixed with potassium bromide (KBr) (3 mg sample in 150 mg KBr-silica sample). Then, the samples were grounded in a mortar and pressing. Thermogravimetric analysis (TGA) (Setaram Scientific&Industrial Equipment) was conducted to study the amount of weight change of samples up to 1000° C.

CHAPTER 4

EFFECT OF PROCESS PARAMETERS AND ELECTROLYTES ON NUCLEATION AND GROWTH

Since there is a need to understand how the initial colloidal structures grow to create the final monodisperse Stöber particles, we aimed to investigate several sub-processes that may happen during the synthesis of silica particles for accomplishing desired morphology.

In the Stöber synthesis, the hydrolysis and condensation reactions provide initial particles (nuclei) and the final particle size, size distribution and morphology are in a good agreement with initial particles and controlled by the relative contribution from nucleation and growth mechanisms. The overall reaction is like (Ibrahim et al., 2010);



As one of the pioneering work in this field, Bogush and Zukoski, 1988 summarized that primary parameters influence the size and distribution of SNPs. These are: concentrations of TEOS, ammonia, water, alcohol and reaction temperature. Hence, systematical experimental findings on the concept of the nucleation and growth through the hydrolysis and condensation reactions will hopefully help to clear up the idea behind the formation of monodisperse silica particles synthesized by Stöber method.

4.1. Characterization of Stöber Silica SNPs

In a typical synthesis, Classical Stöber method (0.25 M TEOS, 1.09 M NH₃, 12.14 M EtOH and 11.67 M H₂O) resulted in perfectly spherical and monodisperse solid silica particles and the size and size distributions of these particles after 24 h of the

synthesis are given in Figure 4.1. It can be seen that, particles have mean sized of 500 nm with a monosized distribution. Particles have surface area of 9.5 m²/g. The zeta potential of these particles distribution graph is shown in Figure 4.2.

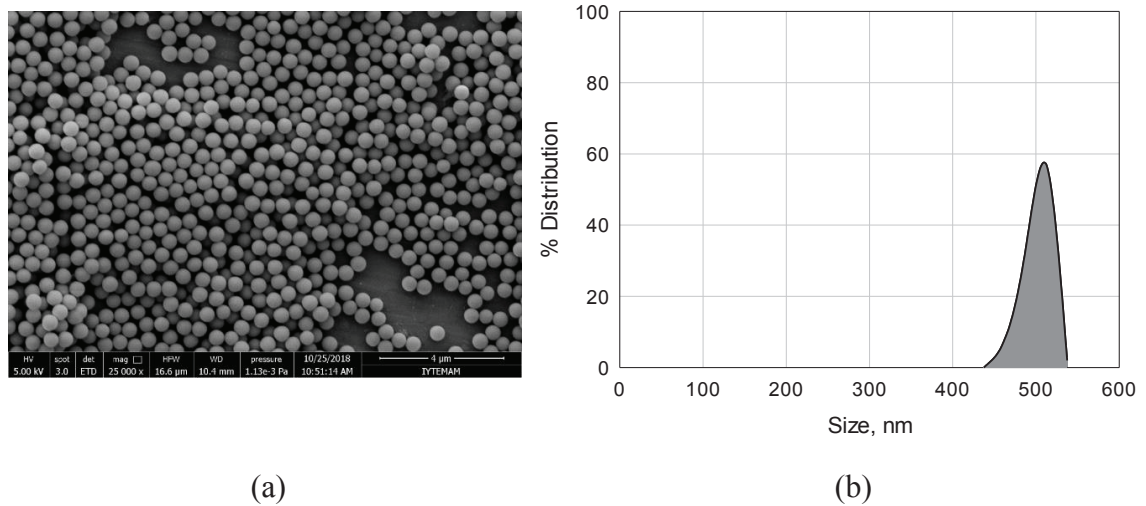


Figure 4.1. a) A representative SEM image of the SNPs after 24 hours of synthesis; b) number frequency size distribution obtained from the SEM image.

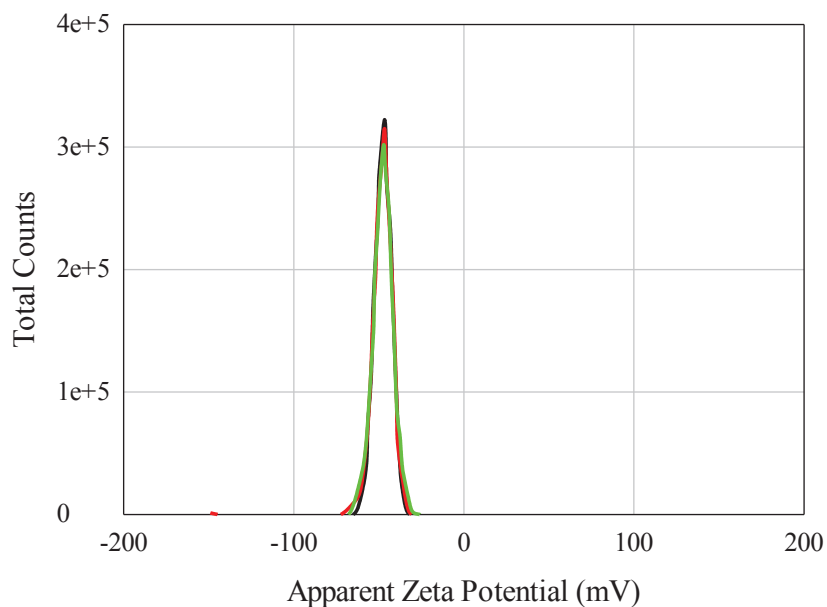


Figure 4.2. Zeta potential distribution of SNPs synthesized by Stöber method.

Silica nanoparticles were washed with water and then distributed in water again for zeta potential measurements at a pH value of around 7. Particles have a zeta potential value of -50 mV which is consistent with literature (Samuel et al., 2010).

The typical TGA curve and FTIR spectra of the SNPs are given Figure 4.3 and Figure 4.4, respectively.

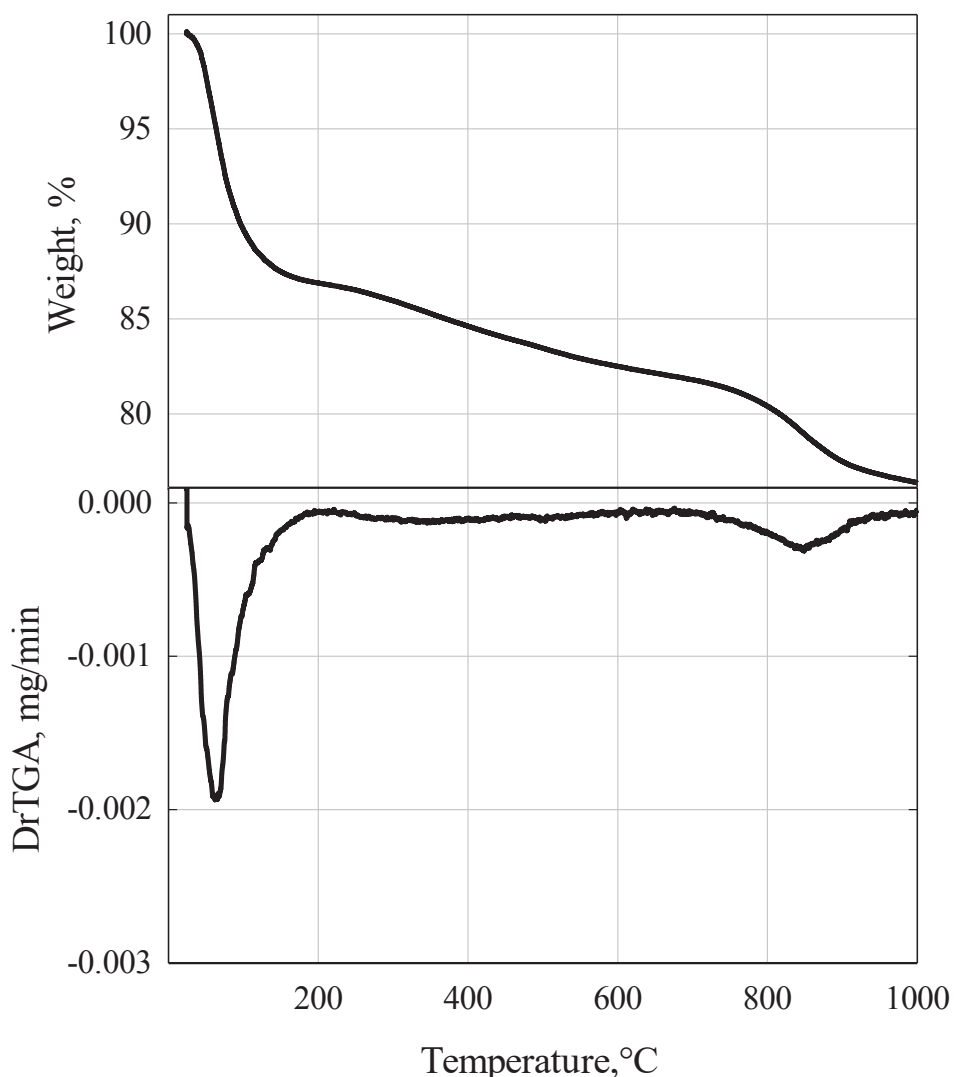


Figure 4.3. TGA (top) and DrTGA (bottom) curves belong to the SNPs obtained from Classical Stöber method.

As can be seen from Figure 4.3, the first observed weight loss below 150° C was due to the evaporation of physically adsorbed water. The second loss between 200° C and 400° C appears to be comprised of strongly held (probably hydrogen bonded) water and ammonia. The third and last loss came from the condensation of the silanol groups into

siloxane bonds with the elimination of water. As a result, TGA curve shows a three-step decrease, the weight loss was determined in two regions: 0-150° C , 200-400° C and 800-1000° C: the former corresponds to desorption of physically adsorbed water, strongly held water and the latter to silanol condensation. This result is similar with the other researchers (Somasundaran, 2004, Shin et al., 2008).

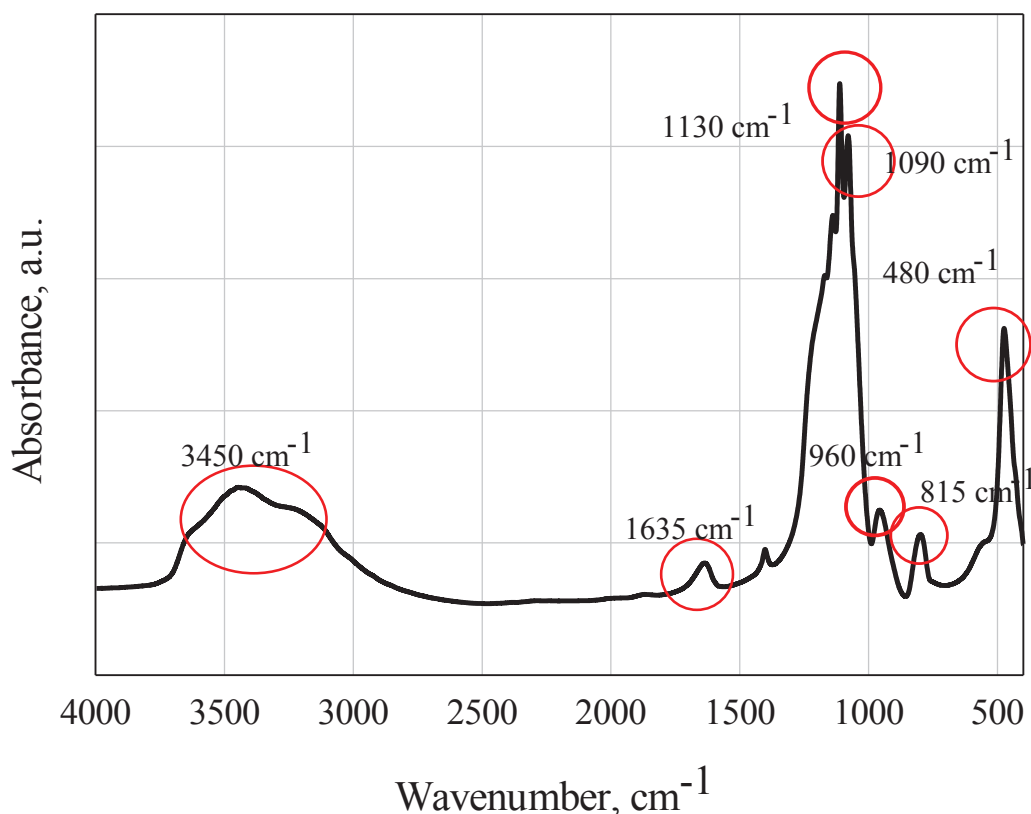


Figure 4.4. FTIR spectrum of SNPs obtained from Classical Stöber method.

From the FTIR spectrum shown in Figure 4.4, the absorption bands between 800 and 1200 cm⁻¹ have been described as a superimposition of several SiO₂ peaks, Si-OH bonding and peaks due to residual organic groups. Silica particles show absorption bands originated from asymmetric vibration of Si-O (1090 cm⁻¹), asymmetric vibration of Si-OH (960 cm⁻¹), and symmetric vibration of Si-O (815 cm⁻¹). Water shows a common absorption peak between 3300 cm⁻¹ and 3500 cm⁻¹ due to O-H stretching in hydrogen bonded water. Also this band can be controlled from the 1635 cm⁻¹ band due to scissor

bending vibration of molecular water. The lack of peaks at 2980 cm^{-1} (CH_3) and 2930 cm^{-1} (CH_2) identify that TEOS was consumed during the synthesis in the silica particles.

FTIR studies were also conducted with time through the synthesis of silica particles for 24 h to monitor the peaks increasing/decreasing with time and the results are given in Figure 4.5. Asymmetric vibration of Si–O (1086 cm^{-1}) and symmetric vibration of Si–O (815 cm^{-1}) appeared at the beginning of the reaction (4 min) and increased as time proceed. On the other hand, asymmetric vibration of Si–OH (960 cm^{-1}) appeared at 4 min of the reaction and decreased as time increased. This result means that first particles were formed within 4 min that was also known from the color change of solution from transparent to opaque at 4 min of the reaction.

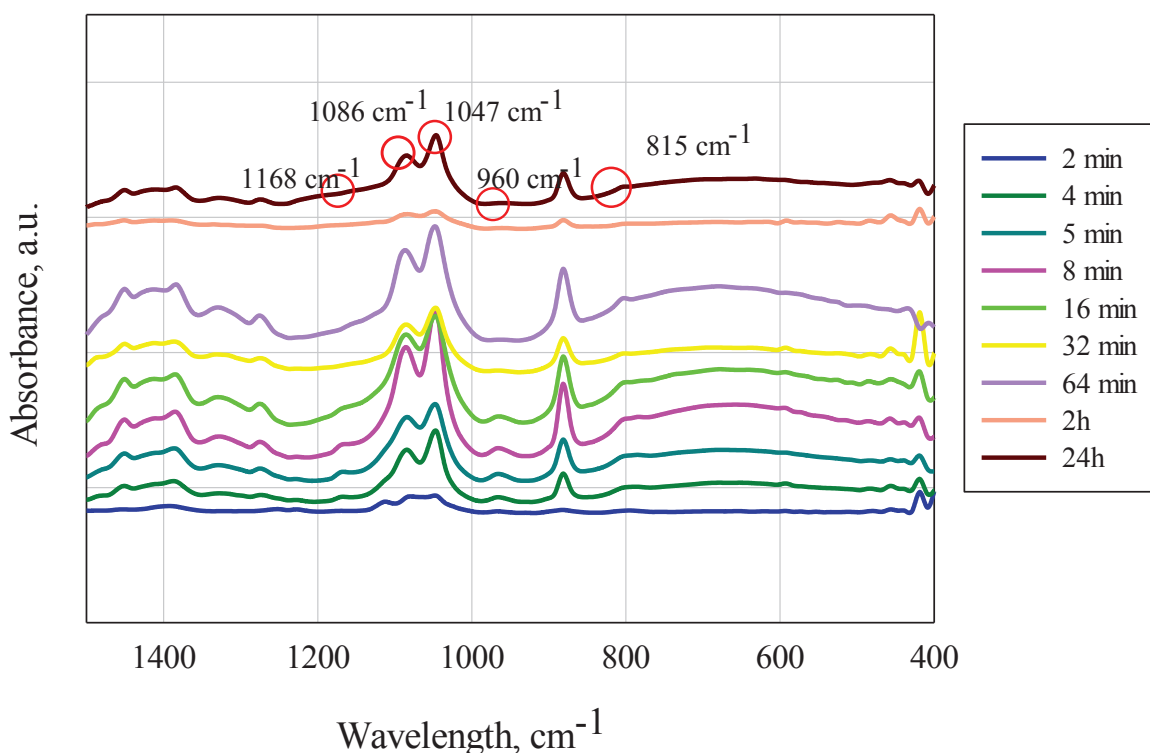


Figure 4.5. IR spectra with respect to time of silica particles obtained from Classical Stöber method.

The progress of the reaction was also monitored by measuring the pH and conductivity of the solution for two different TEOS concentrations (0.250 M and 0.125 M) while keeping the other reactants concentrations constant (EtOH: 12.14 M, NH_3 : 1.09

M, H₂O:11.67 M) and the results are displayed in Figure 4.6 and Figure 4.7 for 0.250 M and 0.125 M TEOS concentrations, respectively. The initial pH measured before the addition of TEOS as 12.21 and after the directly addition of TEOS it rapidly dropped to 11.43 due to its conversion into silicic acid and decreased during 4 min and then remained stable. After 30 min, the pH suddenly increased and over the course of 15 min reached pH of 11.46 after which it slowly decreased and stabilized at pH ~ 10.21 at the end of the reaction. The behavior of this pH change was similar with the other researchers (Carcouët et al., 2014).

We also monitored the reaction kinetics of classical Stöber synthesis through conductivity profiles of the system for 0.250 M and 0.125 M TEOS, which is simple and effective. Under basic conditions, the hydrolyzed monomers as shown in Eq. 4.2 to Eq. 4.4 will be ionized to form monomeric ionic species which will then react with hydrolyzed monomers to form siloxane bonds, as illustrated below:

Ionization of ammonia:



Ionization of hydrolyzed monomers:



Consumption of ionic monomeric species:



Since the system contains ionic species which will be produced and consumed during the silica synthesis as shown in Eq 4.2 to 4.4, conductivity measurement can clear up the reaction kinetics. The increasing part of the graphs in Figure 4.6 and Figure 4.7 (during first 4 min) shows the net formation of the ionic monomeric species through Eq 4.3, while the decreasing part shows the net consumption of these species, indicating the silica growth (Eq 4.4). Increasing TEOS concentrations (shown in Figure 4.6) increased the conductivity value which implies increasing in the hydrolysis and condensation reaction rates with increasing TEOS concentration while trend of change in the pH and conductivity is same compared to the case of low TEOS concentration (0.125 M) (shown in Figure 4.7).

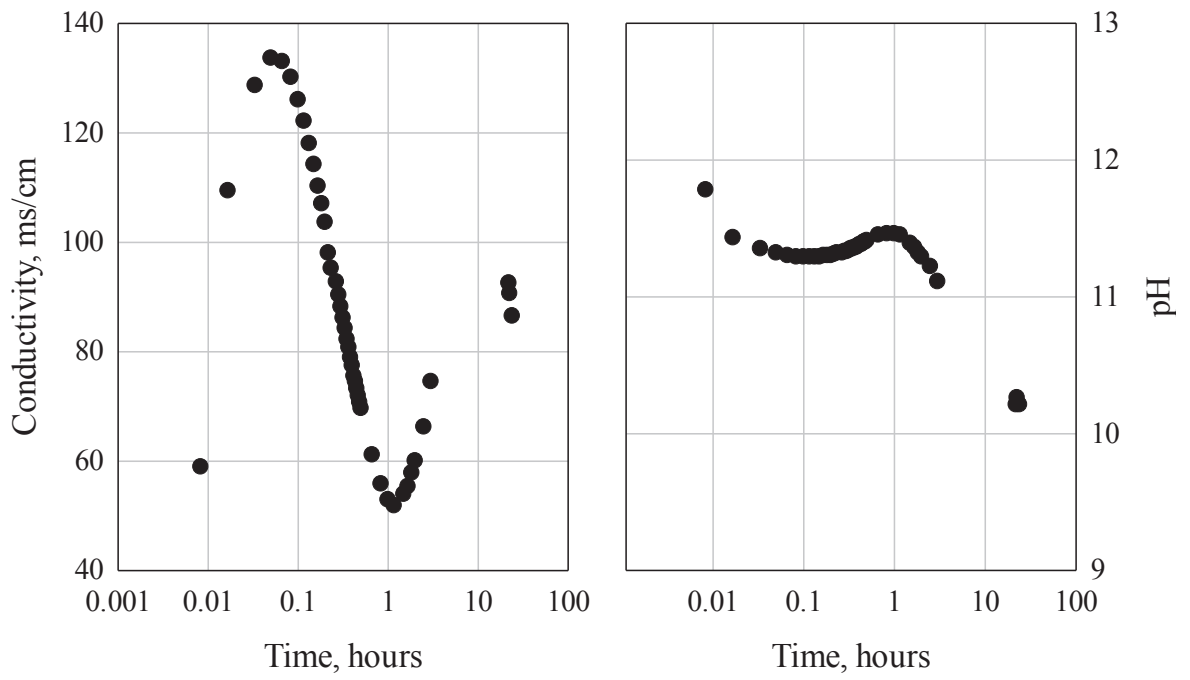


Figure 4.6. Conductivity and pH monitoring of the Stober reaction for 0.250 M TEOS concentration.

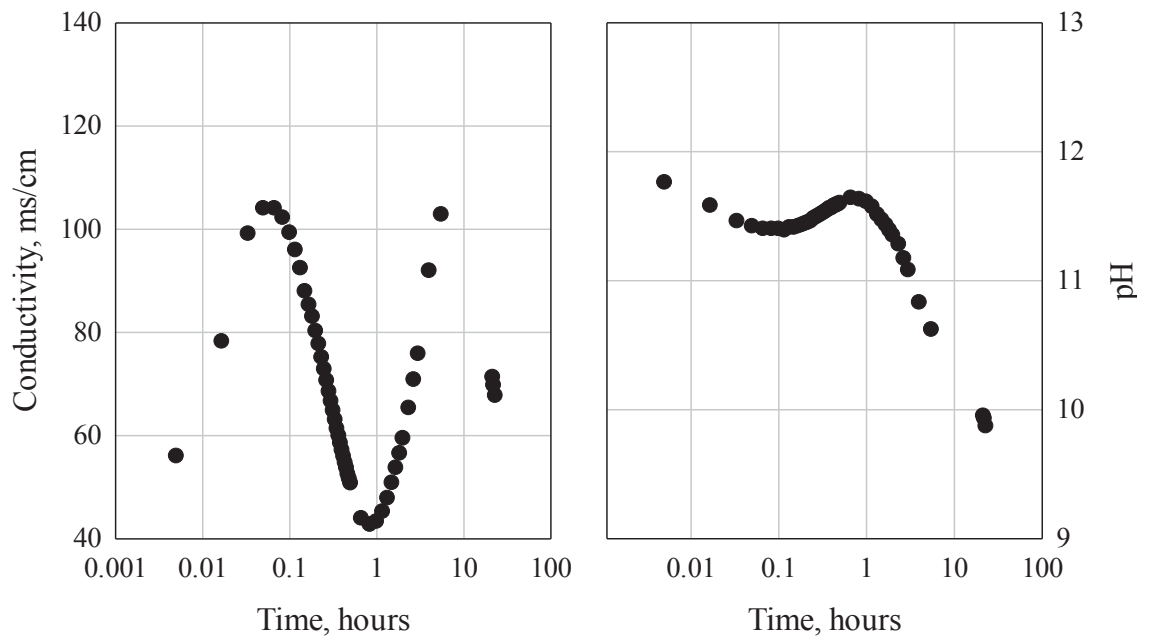


Figure 4.7. Conductivity and pH monitoring of the Stober reaction for 0.125 M TEOS concentration.

4.1.1. Effect of Process Parameters on Size of SNPs

In the Stöber synthesis, concentrations of water, ammonium hydroxide, TEOS were changed and additionally different mode of TEOS addition and agitation intensity were studied and the results are given in following sections.

4.1.1.1. H₂O Amount

It has been expressed that water is a key element in the sol-gel synthesis and one of the major parameter to be controlled in the process. Amount of water will affect the kinetics of the hydrolysis and condensation reactions. By taking into account the structure of silicon tetravalent alkoxide Si(OR)₄, four molecules of water are necessary for a complete hydrolysis, while a ratio of 2 is enough for conversion of Si(OR)₄ into an oxide, stoichiometrically. Figure 4.8 shows the SEM images of silica particles synthesized using different H₂O amounts while keeping other reactant concentrations constant (EtOH/NH₃: 11.14, EtOH /TEOS:48.6) as a function of time. Final mean sizes were calculated from SEM images by counting almost 100 particles diameters and shown in Figure 4.9. As can be seen from Figure 4.8, particles show spherical morphology for all water concentrations and particle sizes increase with increasing time. For water concentrations of 5.67 and 11.67 M, final mean sizes were close to each other, however further increase in the water amount decreased particle size. This effect can be clearly seen in Figure 4.9.

It is expected that if the amount of water available in the solution is increased, rate of hydrolysis and condensation should increase. It is true but, on the other hand, if water amount is increased while keeping the amount of solvent as constant, the silicate concentration are going to be reduced. This dilution effect will change the hydrolysis and condensation reactions rate with an increase of the gel time also. Within the range studied, it can be said that the dilution effect is more effective. Also, when water amount is increased, dilution effect caused the number of final particles growing by collecting the surrounding monomers or oligomers should increase. In another words, distance between these particles is increased and each particles grow on their own and creates large number

of final particles. The increase in the number of growing particles decreased the mean size of the particles due to the less amount of residual TEOS.

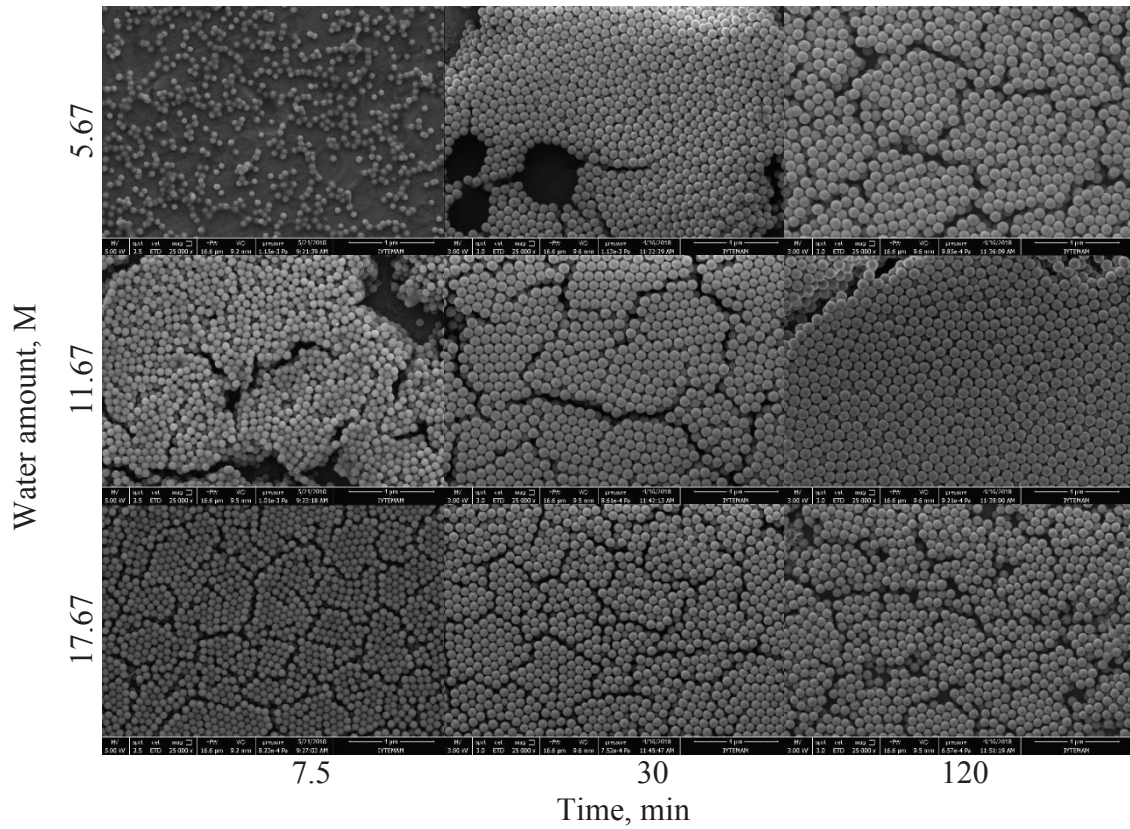


Figure 4.8. SEM images of silica particles synthesized with different H₂O amounts (M).

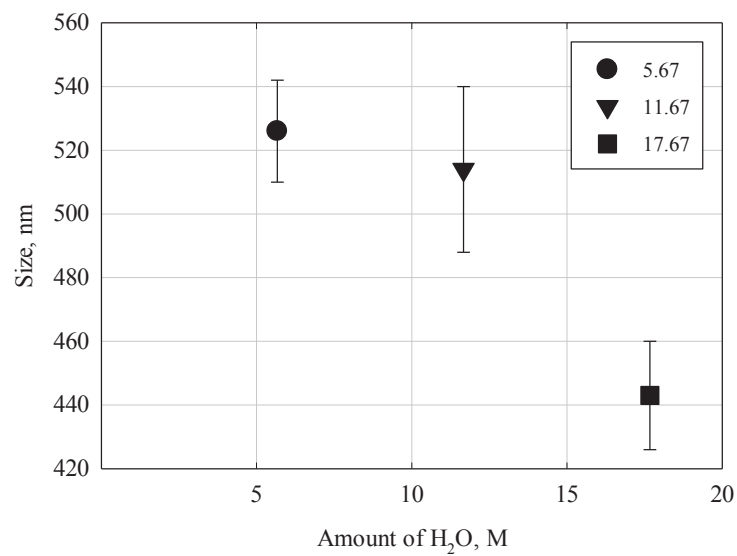


Figure 4.9. Effect of H₂O amounts (M) on final size of SNPs.

4.1.1.2. NH₃ Concentration

Ammonia is used as a catalyst to synthesize spherical silica particles by Stöber process. Hydrolysis and condensation reaction rates and colloidal stability of particles depend on the solution pH and hence ammonia concentration, such that concentration of ionic species in solution vary with ammonia concentration. An increase in pH causes an increase in the hydrolysis rate while a decrease in pH causes an increase in NH₄⁺ concentration which change in ionic strength and colloidal stability (Zeng et al., 2015). In the absence of ammonia, the silica flocculated in irregular shape and spherical particles could not be observed. Thus, ammonia apparently has a major influence on the morphology of particles (Stöber et al., 1968). In this study, we changed the concentrations of NH₃ while keeping other reagents concentrations constant (EtOH/TEOS: 48.6) and the representative SEM images for three different ammonia concentrations are given in Figure 4.10. The scale is same in all SEM images in Figure 4.10.

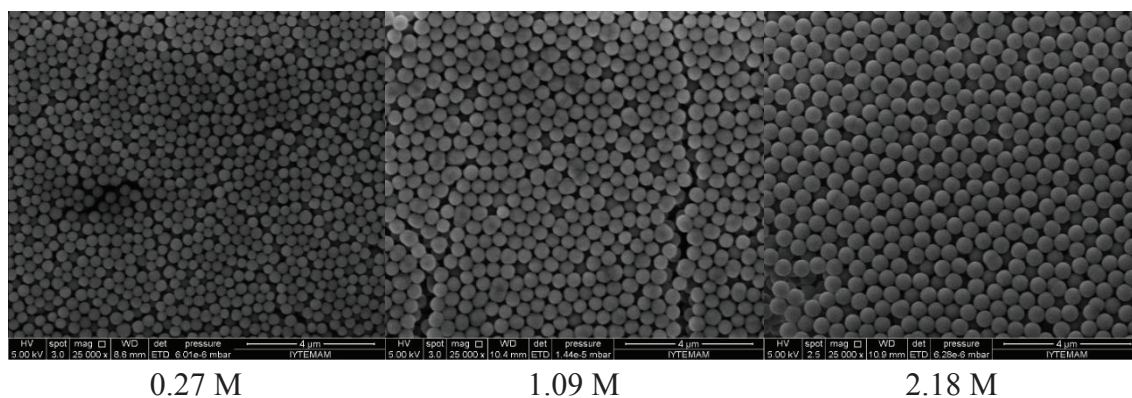


Figure 4.10. SEM images of the silica particles with different NH₃ concentrations.

The particles reached their equilibrium size nearly after 2h. The size distributions are self-preserving, so mean sizes can be used. Silica particles show spherical morphology for all NH₃ concentrations.

Figure 4.11 shows the size distribution of silica particles synthesized with different NH₃ concentrations.

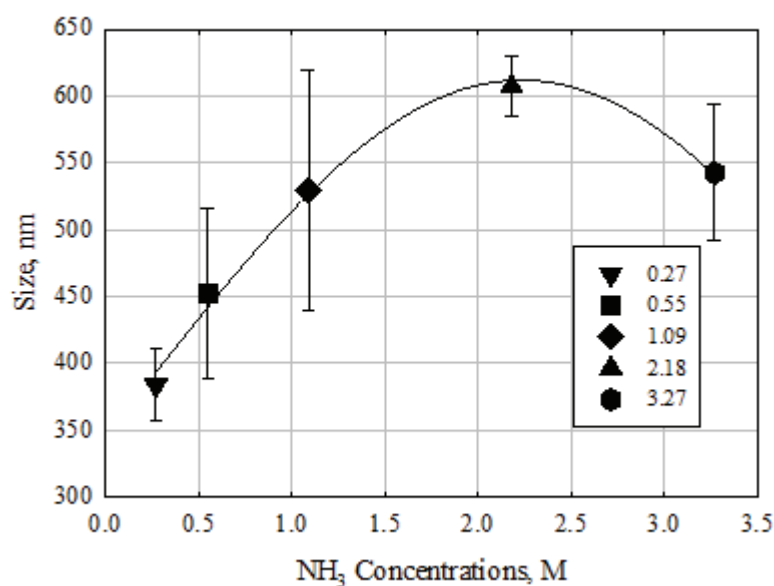


Figure 4.11. Final mean sizes of silica particles with different NH₃ concentrations.

From previous studies, it is known that hydrolysis reaction was the controlling step because of its lower reaction rate than condensation. Alkoxy groups (OC₂H₅) of TEOS were substituted by hydroxyl groups (OH) in hydrolysis reaction which then condensed with each other to form final particles. So, hydroxyl concentration played a critical role to control hydrolyzed species and ammonia can tune the concentration of hydroxyl in reaction system. With increase of ammonia concentration, hydroxyl concentration was increased (according to equation 4.2) and larger number of hydroxyl groups substituted alkoxy groups of TEOS. Hence, the hydrolysis of TEOS was accelerated. It is seen that the size of particles goes through a maximum as ammonia concentration is raised because of the large number of particles developed at the early stages of the reaction and then tends to decrease. Keeping in mind that increased rate of hydrolysis reaction produces larger particles, the concentration of ammonia can be assumed to be directly proportional to the final particle size in lower levels of ammonia. Nevertheless, when its concentration exceeds a critical amount, kinetics of condensation reaction is more influenced, resulting to the sudden condensation of the particles and thus the formation of smaller particles. Similar results were reported by Dabbaghian et al., 2010.

4.1.1.3. TEOS Concentration

TEOS is the source of the monomers that forms the primary particles in the sol-gel system which will grow further to form the final particles. Hence it is important to take the TEOS concentration into account. Figure 4.12 and Figure 4.13 show the representative SEM images and final mean size of silica particles for different TEOS concentrations, respectively. The concentration of other reactants was kept constant for these experiments (EtOH/NH₃: 11.14, EtOH /H₂O:1.04).

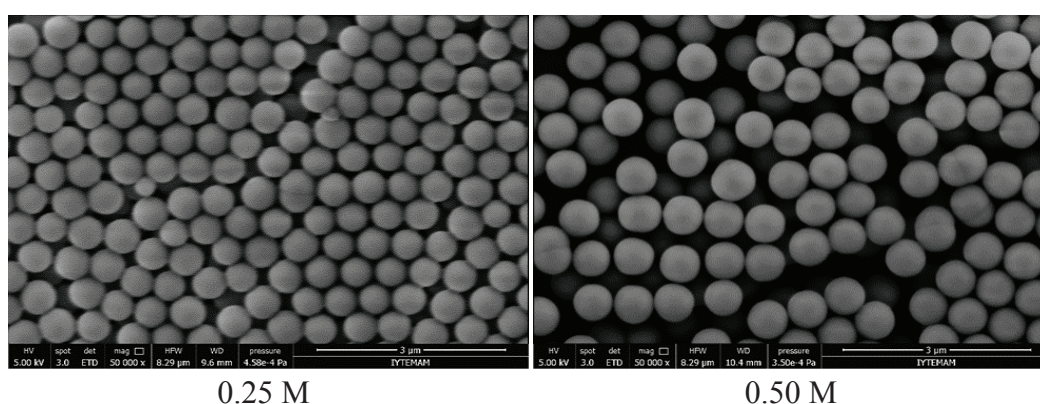


Figure 4.12. Representative SEM images of silica particles with different TEOS concentrations.

The particles reached their equilibrium size nearly after 2h, and the size distributions are self-preserving, so after 24 h, final mean sizes were shown in Figure 4.13.

It can be seen that there is an initial stage where mean size increases much faster with TEOS concentration (up to ~0.25 M, the Stöber concentration), after this point mean size linearly increases with TEOS concentration at a much lower rate. With the increasing TEOS concentration, both hydrolysis and condensation reactions will become faster, correspondingly the intermediate $(\text{Si}(\text{OC}_2\text{H}_5)_{4-x}(\text{OH})_x)$ will be increased due to the high hydrolysis rate and when it reaches supersaturation, the consumption rate of intermediate through condensation reaction is also relatively fast, which probably shortens the nucleation period. So, the total number of nuclei will be less in numbers and the residual TEOS will lead to a larger size of particles.

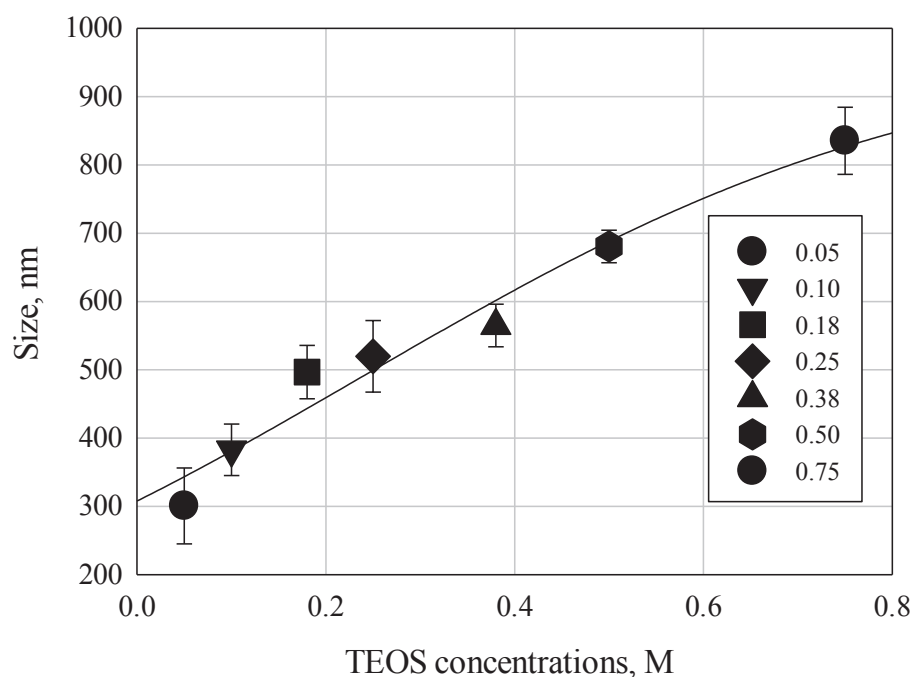


Figure 4.13. Final mean sizes of silica particles with time for different TEOS concentrations.

4.1.1.4. Mode of TEOS Addition

TEOS addition rate will be a factor that influences the nucleation and growth processes. In this study, the same amount of TEOS (0.25 M) was introduced to the mixture (cell) at different feed rates, the direct-quick addition (pulse) and the long time addition (in 1 h) by syringe pump when the system included 12.14 M EtOH, 11.67 M H₂O, 1.09 M NH₃, and the final particle size with respect to time results are shown in Figure 4.14.

It was observed that the pulse addition created smaller particles with narrow size distribution after 1 hour whereas, the long time or drop wise addition of TEOS created larger particles with wide size distribution. This is most probably due to the number of nucleation sites created. Which is expected to be more in the case of direct addition and the residual TEOS will be less to hydrolyze and condense around these nuclei (growth) and the size of particles will be smaller. This result is parallel to the study of Nozawa et al., 2005, showed that the particle size decreased with an increase in the rate of addition

of the TEOS. The deviation from monosized distribution for the case of long time addition of TEOS was also shown in SEM images given in Figure 4.15 for 0.1 mL/min TEOS addition rate.

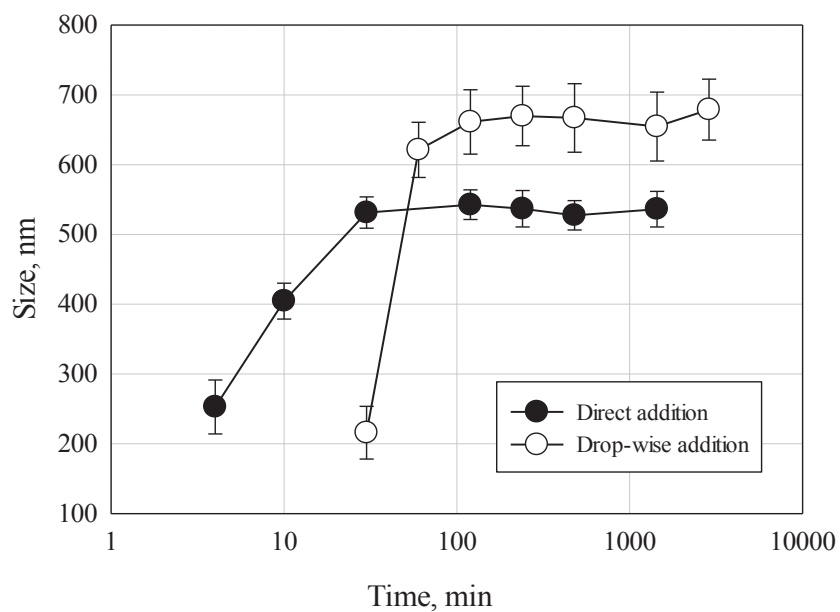


Figure 4.14. Comparison of pulse vs continuous TEOS addition rate on final size of SNPs as a function of time.

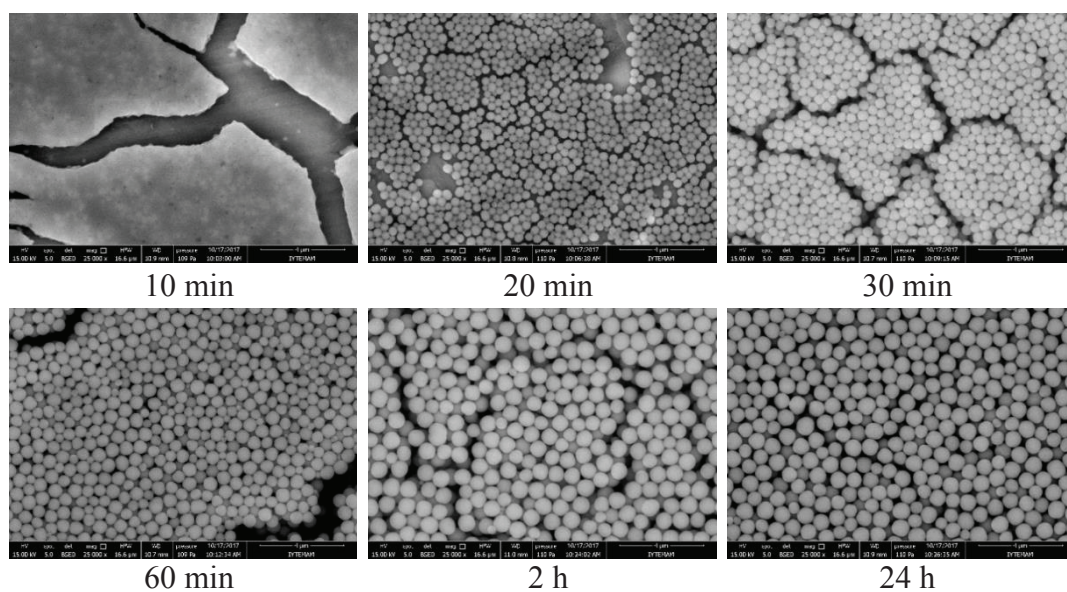


Figure 4.15. SEM images of continuous TEOS addition (in 1 h) as a function of time.

Additionally, for continuous addition, different TEOS feeding rates (0.02, 0.04, 0.1 mL/min and direct addition) were also studied for 0.125 M and 0.250 M TEOS concentrations and the SEM pictures are displayed in Figure 4.16.

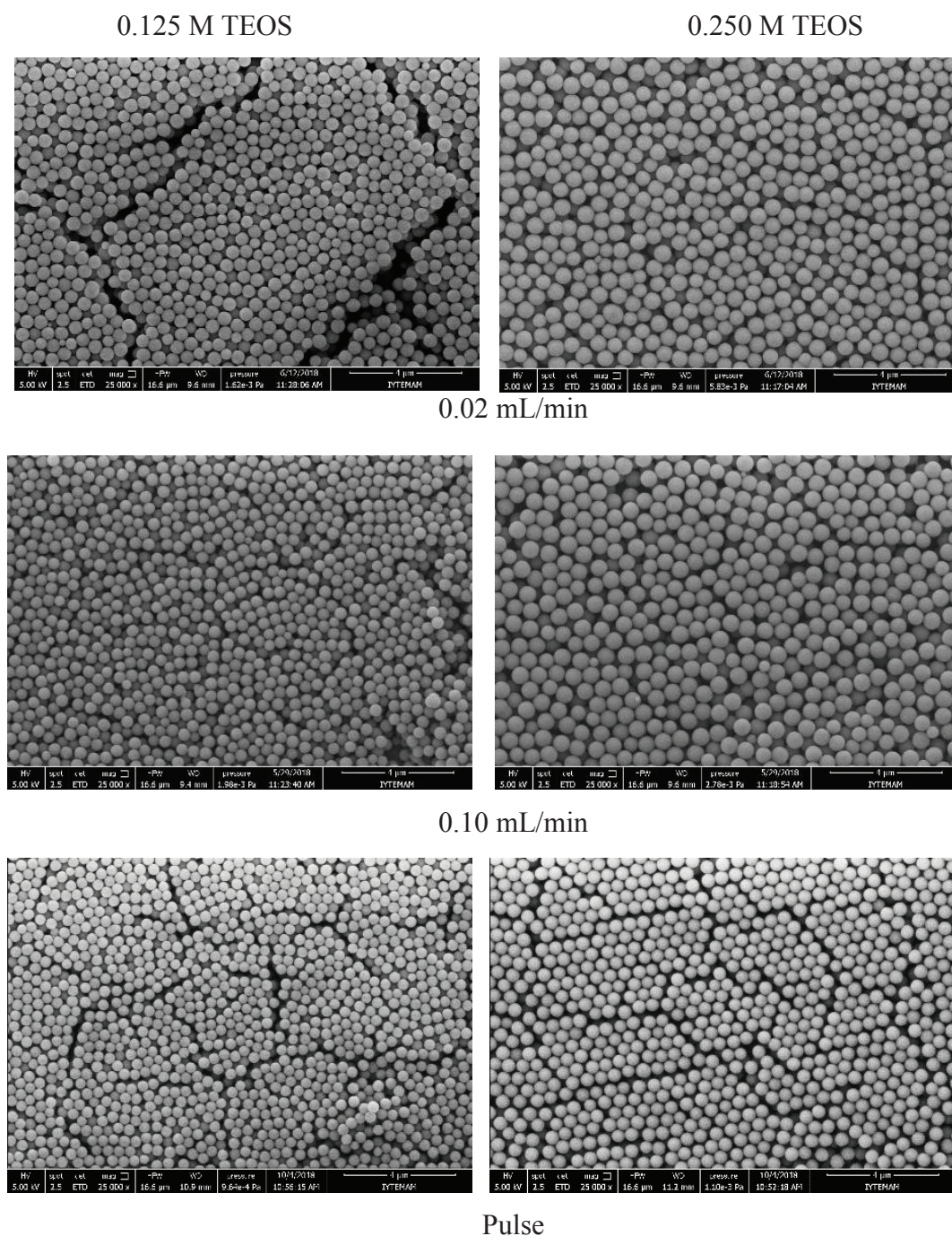


Figure 4.16. SEM images of the SNPs after 24 hours of synthesis for different TEOS addition rates for 0.125 M and 0.250 M TEOS.

The number distributions of the same particles are presented in Figure 4.17-a and Figure 4.17-b as normal distribution graphs. Number of particles were also given in Figure 4.17-c.

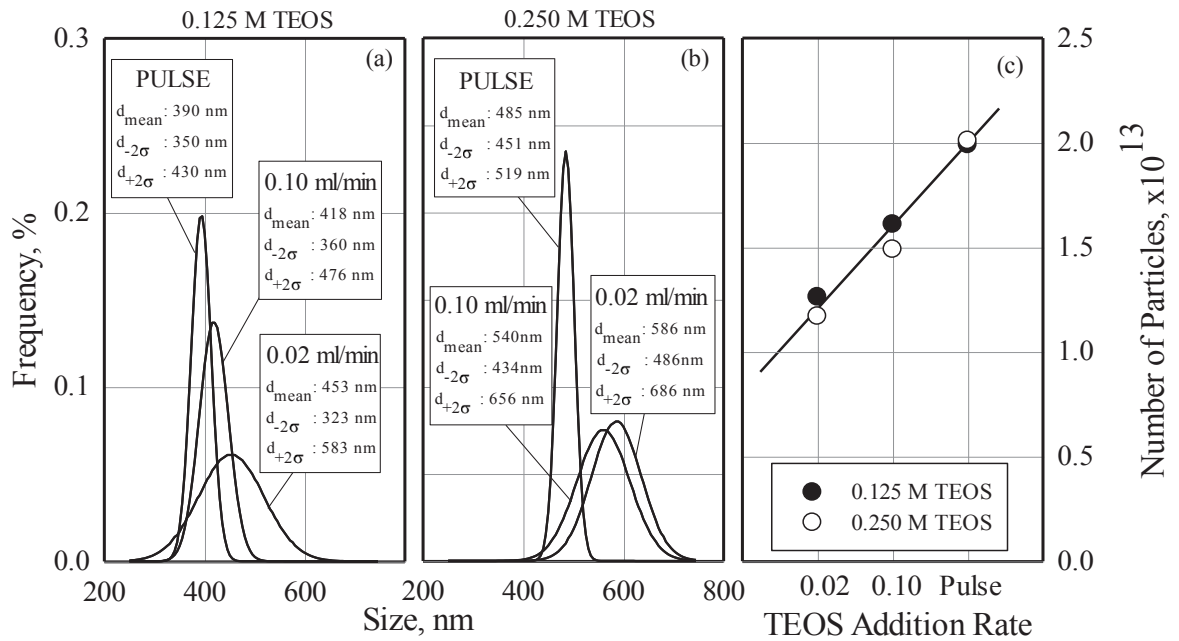


Figure 4.17. Number frequency distributions of the SNPs obtained from the SEM images in Figure 4.16 for different TEOS addition rates for a) 0.125 M and b) 0.250 M TEOS c) Number of particles for all TEOS addition rates.

Both the SEM photographs and the distributions show that the particles have very narrow size distributions and smaller mean sizes for pulse addition case for both TEOS amounts, suggesting simultaneous (burst) formation of a larger number of nuclei early in the of the synthesis. The SNPs develop progressively wider distributions and larger mean sizes as the TEOS addition rate is decreased, indicating continuous creation of a smaller number of nuclei for extended durations during synthesis.

The numbers of SNPs formed for 0.125 and 0.250 M TEOS addition for different addition rates (calculated from mean sizes in Figure 4.17-a and Figure 4.17-b) are presented in Figure 4.17-c. The graph displays that the number of SNPs is nearly the same for 0.125 and 0.250 M TEOS amounts for all addition rates. This behavior can be explained providing the concept of model developed in this study and the model is

expressed in detail in Chapter 5. As summary, hydrolysis of TEOS into hydrolyzed monomers, condensation of hydrolyzed monomers into oligomers or oligomers into early nuclei is expected to take place homogeneously in the whole synthesis volume. However, forming a final particle through condensation or aggregation of these species can be assumed to occur in isolated micro volumes, which can be likened to batch micro reactors, each of which generating a single final particle. This can also be viewed as if a random nucleus within each micro volume acts as a “collector” nucleus onto which all the monomers, oligomers or early nuclei diffuse and coalesce, eventually forming a final particle. Then, the number of these micro volumes will be equal to the number of final particles. The results given in Figure 4.17-c imply that the number of micro volumes should be the same for TEOS concentrations of 0.125 and 0.250 M for all TEOS addition rates. For the synthesis volume employed, the size of these micro volumes is same for 0.125 and 0.250 M TEOS amounts and comes out to be around $8.1 \mu\text{m}^3$ for the pulse addition case. The larger final mean particle size of 485 nm observed for the 0.250 M TEOS amount can be explained conveniently due to having more TEOS species within the micro volumes to be devoured by the “collector” nuclei compared to the 0.125 M TEOS case which yields a smaller final mean particle size of 390 nm.

The results in Figure 4.17-c display that decreasing the addition rate of TEOS causes a decrease in the number of the final SNPs formed while leading to a broader size distribution. The increase in the breadth of the distribution can be explained as follows: An extremely small TEOS amount in solution during the first moments of gradual addition creates a respectively smaller number of collector nuclei separated by large distances. As more TEOS is gradually added to the system, new generations of collector nuclei can form and fill these voids among the earlier generations which are steadily growing. Once reaching a critical number, TEOS added to the system is now devoured by these different generations of collector nuclei of different sizes rather than forming new ones, causing the wider size distributions observed. The decrease in the number of collector nuclei, hence, the number of final SNPs, can be explained by the fact that a smaller critical number of collector nuclei is sufficient to collect the slowly added TEOS, which leads to increased micro volumes of 10.6 and $13.6 \mu\text{m}^3$ for 0.1 and 0.02 mL/min addition rates, respectively. The volumes correspond to cells with a unit length of 2.0, 2.2 and 2.4 μm , respectively.

4.1.1.5. Agitation Intensity

It is important to ensure efficient and optimum operation of stirred vessel to get particles with monosized distribution. There is also a need to create process conditions that are optimum at the lab-scale. The mixing characteristic will influence the product quality and efficiency of the process to a great degree (Pordal and Matice, 2003). Hence, it is checked that whether the agitation mode (with agitation/without agitation) and speed could play a role for the synthesis of silica particles while fixing reagents concentrations constant (EtOH: 12.14 M, H₂O: 11.67 M, NH₃: 1.09 M, TEOS: 0.25 M). Figure 4.18 shows the size distribution after 2 h of silica synthesis where agitation were not applied.

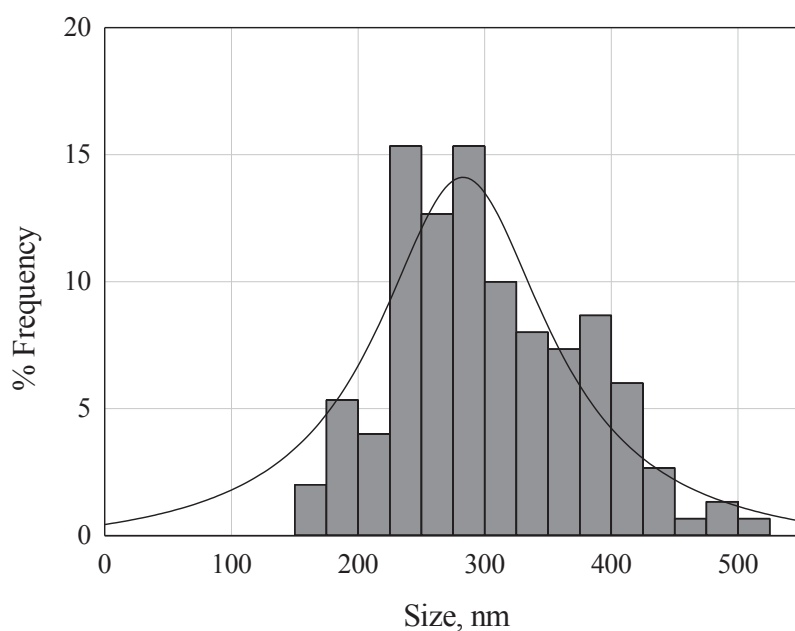


Figure 4.18. Size distribution of silica particles synthesized without agitation applying.

When EtOH, NH₃ and water were put into a beaker and by the direct addition of TEOS to this solution without applying any agitation, the phase separation was observed within a few minutes and transition between transparent to opaque phase was occurred relatively later than the case of agitation was applied. This could be because of the non-homogenous distribution of TEOS throughout the system. It causes particles to have wider size distribution, and deviation from monosized distribution was observed as shown

in Figure 4.19-a. Hence, to see the effect of agitation mode, TEOS distributed to the system firstly by agitation (only first 1 min) then the agitation stopped (Figure 4.19-b). Also, effect of agitation speed on final size of silica particles were tested with lower (Figure 4.19-c) and higher speed (Figure 4.19-d) (250 and 810 rpm, respectively) were clarified and the results are shown in Figure 4.20.

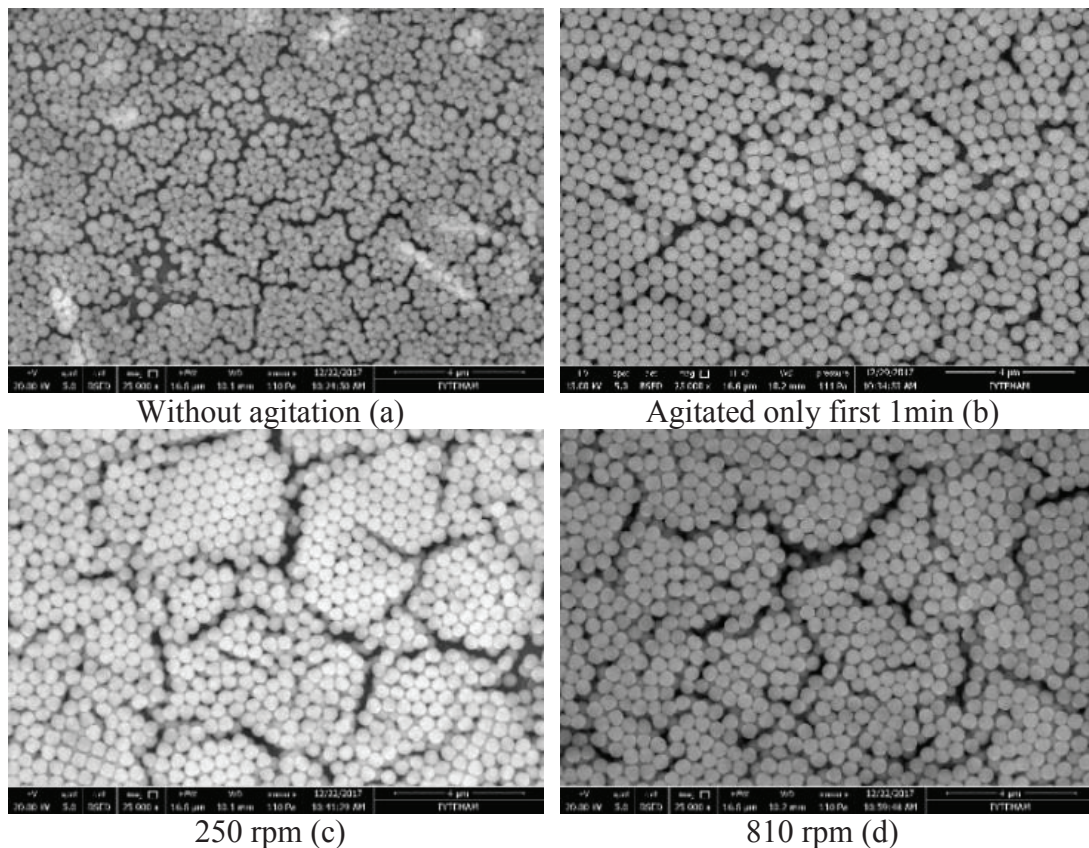


Figure 4.19. SEM images of the size distribution of silica particles with different agitation modes.

When the system was not agitated, nucleation may occur non-homogeneously during the process, hence particles were grown at different rates. This means that, when TEOS contacts with water/ethanol/ammonia media, because of the phase separation, nucleation occurred only in the contact volume during its diffusion to another phase. Because of the nucleation occurred in different times, final particle size distribution become widen. However, in case of stirring was applied, different stirring rates have no significant impact on the average size of silica particles as shown in Figure 4.20.

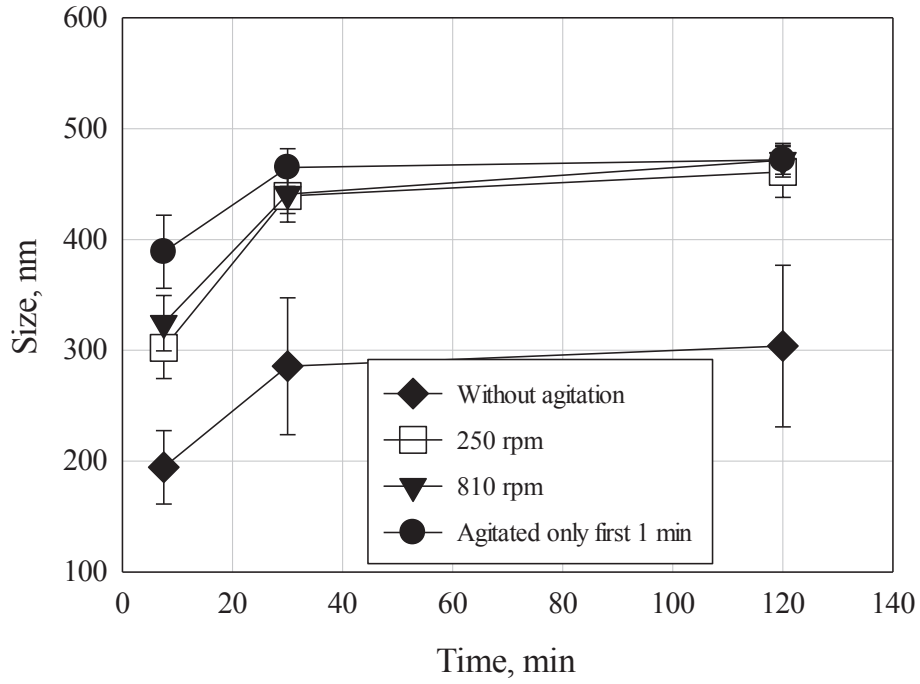


Figure 4.20. Size distribution of silica particles with different agitation modes.

The reproducibility of the result is not surprising since the associated hydrodynamic Peclet number, Pe , which compares the effect of shear (known as the convective effect, when Pe number is bigger than 1) with the effect of diffusion of the particles in a reactor (when Pe number is smaller than 1), is much smaller than unity in both cases. Pe number can be calculated from the equation shown below (Hiemenz, 1986);

$$Pe = \frac{\Omega r^2}{D_m} \quad (4.5)$$

where Ω , r , and D_m are the angular velocity associated to the stirring, the particle radius, and the molecular diffusion coefficient of the solute within the mixture, respectively. Diffusion coefficient can be calculated using Einstein-Stokes equation as:

$$D = \frac{k_B T}{6\pi\eta r_a} \quad (4.6)$$

where k_B is the Boltzmann constant (1.38×10^{-23} J/K) and r_a is the solute radius. Using the ethanol (as it is the major part of the solvent phase) viscosity $\eta = 1.2 \times 10^{-3}$ Pa.s (at $T = 20$ °C), molecular diffusion coefficients were calculated starting from the typical

solute size range from 2 Å to 200 nm. For the angular velocities of 4.16 Hz (250 rpm/60) and 13.50 Hz (810 rpm/60) with a final particle size of 450 nm, Peclet numbers were calculated for every solute size and angular velocities and the results are given in Table 4.1 and Figure 4.21. For mild agitation condition, Pe numbers are smaller than 1 in all sizes. At high agitation up to ~100 nm, the distribution of particles is only slightly altered by the flow and the growth is totally dominated by diffusional relaxation of particles. This result is consistent with the study of Nozawa et al., 2005. Liang et al., 2016 also demonstrated that stirring rates has no significant impact on the average size of silica particles.

Table 4.1. Calculated diffusion coefficients and Pe numbers

$r_a \cdot 10^9$, solute size, m	$D_m \cdot 10^{10}$, m ² /s	Pe ($\Omega=4.16$ Hz)	Pe ($\Omega=13.5$ Hz)
0.2	8.94	0.0002	0.0008
2	0.89	0.0024	0.0076
20	0.089	0.0236	0.0764
200	0.0089	0.2355	0.7643
400	0.0044	0.4710	1.5285

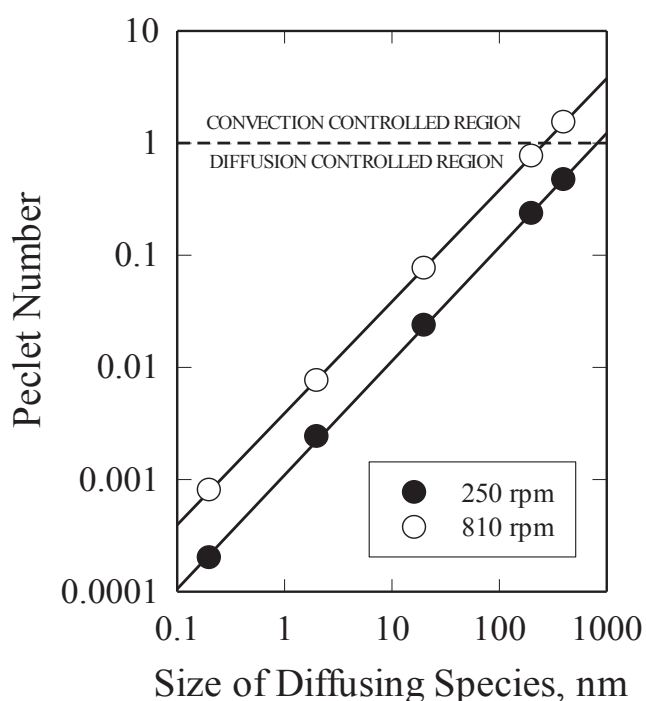


Figure 4.21. Peclet numbers calculated for possible sizes of the diffusing species in the cell for the two mixing speed (0.250 M TEOS Pulse addition).

4.1.2. Electrolyte Addition

To better comprehend the mechanism of particle formation through nucleation and growth, ionic compounds, which have different valences (z) as NaCl ($z=1$), CaCl₂ ($z=2$) and AlCl₃ ($z=3$), were added to the system. The electrolytes were fed into the reaction mixture together with the water with or without the NH₃ solution (Mode A and Mode B explained in Section 3.2.2). The reagents concentrations were as fixed at 12.14 M EtOH, 1.09 M NH₃ and 0.25 M TEOS, while electrolyte concentrations were changed between 10^{-4} M and 4×10^{-2} M. Figure 4.22 shows the potential energy curves in the absence or presence of electrolytes (electrolyte valance of 2 and electrolyte concentration of 4×10^{-2} M) and Figure 4.23 shows the effect of electrolyte concentration on the potential energy of interaction. The curves of van der Waals (vdW), electrostatic (el) and total interaction energy for two spherical silica particles (average size of 500 nm) in ethanol medium can be seen as a function of the separation distance between the particles. The potential energy associated with repulsion is defined as positive, while the attraction is negative and the useful relations are given in Appendix A.

It should be noted that, particles are under the influence of repulsive forces in the absence of electrolytes, however when 4×10^{-2} M electrolytes were presence in the system, vdW attraction dominates the particles. To compare electrolyte concentration on the potential energy of interaction, From Figure 4.23, it can be seen that at 10^{-4} M electrolyte concentration particles were under the electrostatic repulsion. Figure 4.24 and Figure 4.25 show the SEM images of silica particles synthesized in the presence of 4×10^{-2} M electrolytes related to Mode A (Electrolyte solution/NH₃/EtOH fed to the reactor initially, then TEOS added) and 10^{-4} M and 0.04 M electrolyte concentrations comparison, respectively.

Particle aggregation was enhanced in the presence of electrolytes at 4×10^{-2} M concentrations because of the depression of particle charge due to according to the DLVO theory explained above. The system has certain amount of cations (Al³⁺, Ca²⁺, Na⁺), which is believed to give attraction effect and covers the surface of silica particles that can inhibit particle growth. The primary particles were not stable and started to associate immediately; aggregates with lower particle size compared to no-electrolyte case resulted, demonstrating the importance of the surface charge of the primary particles.

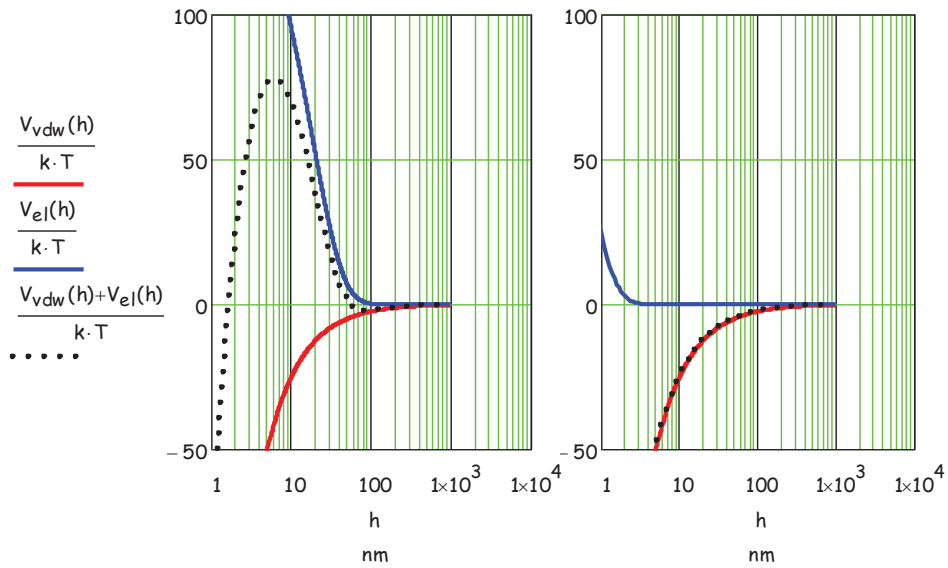


Figure 4.22. Effect of the presence of electrolyte on the potential energy of interaction, a) No electrolyte, b) 0.04 mol/L electrolyte concentration (Note that valence of electrolyte was taken as 2).

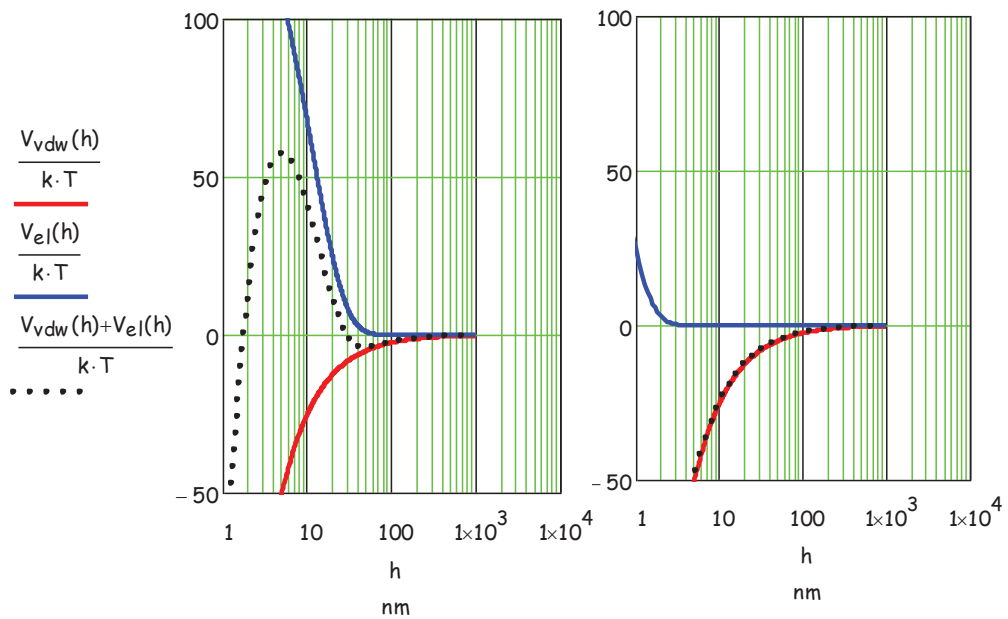


Figure 4.23. Effect of electrolyte concentration on the potential energy of interaction, a) 10^{-4} mol/L, b) 0.04 mol/L (Note that valence of electrolyte was taken as 2).

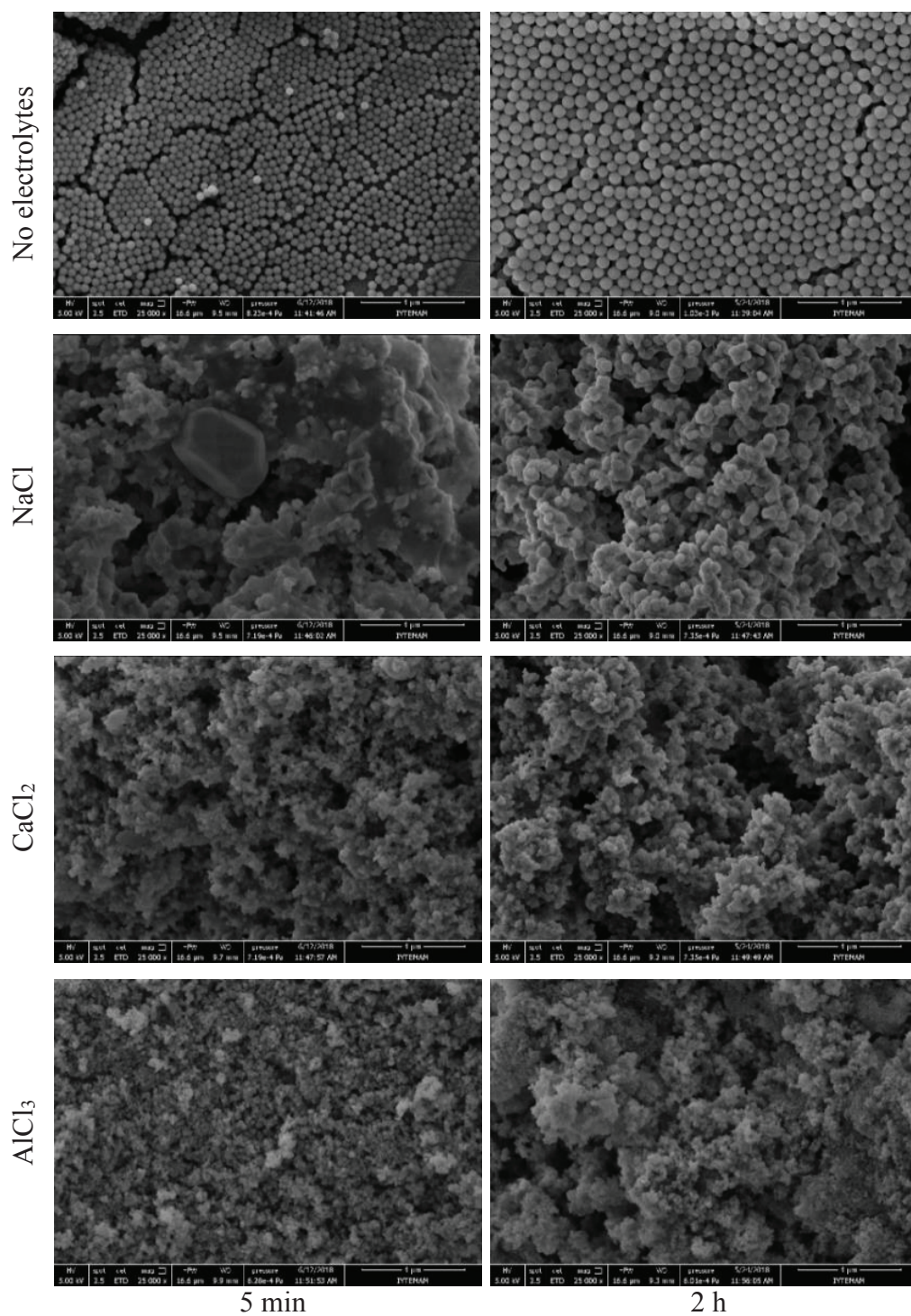


Figure 4.24. SEM images of silica particles in the presence of ionic compounds at 0.04 M concentrations.

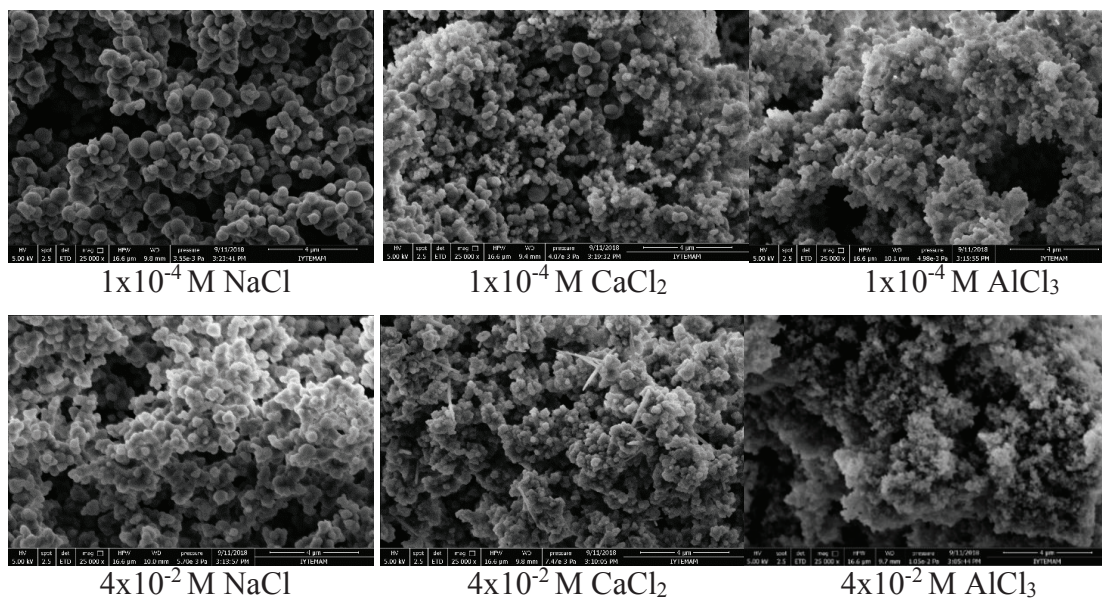
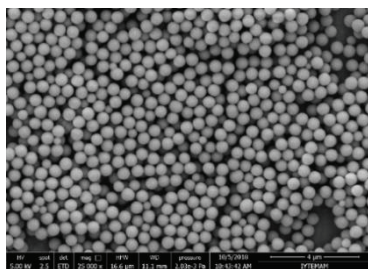


Figure 4.25. SEM images of silica particles in the presence of ionic compounds at 10^{-4} M and 0.04 M concentrations (after 24 h of production).

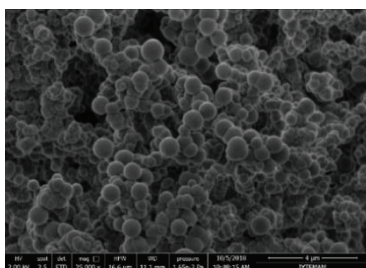
It has been suggested that for silica particles with a size of a few nanometers to be stable, a high surface charge is required (Carcöuet et al., 2014). In the case of 10^{-4} M electrolyte concentration, by using the interaction curves that were given in Figure 4.23, particles were under the electrostatic repulsion and comparatively bigger size was obtained.

When the electrolyte solutions were fed to the system with NH_3 , precipitation occurred immediately. Hence, NH_3 were planned to add separately to the mixture of TEOS/EtOH/Electrolyte solution. SEM images related to Mode B (Electrolyte solution/EtOH/TEOS were fed to the reactor initially than NH_3 was added to the solution) were given in Figure 4.26. The post addition of NH_3 to the classical Stöber solution (without electrolyte) is also shown in Figure 4.26.

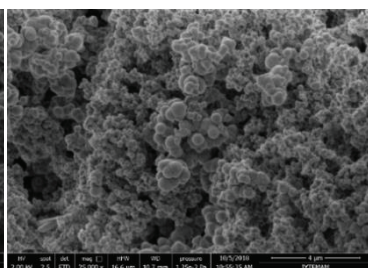
In the absence of electrolytes in the system, particles have spherical morphology with a mean size of 544 nm. As can be seen from the Figure 4.26, in the presence of electrolytes, particles showed more spherical morphology compared to the synthesis of Mode A.



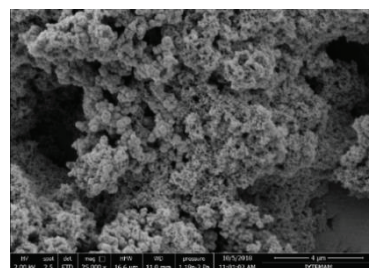
Without electrolyte



1×10^{-4} M NaCl



1×10^{-4} M CaCl₂



1×10^{-4} M AlCl₃

Figure 4.26. SEM images of silica particles synthesized with Mode B in the presence of ionic compounds at 10^{-4} M concentration (after 24 h of production).

CHAPTER 5

USING SEED PARTICLES TO DISTINGUISH NUCLEATION AND GROWTH

Seed addition to the Classical Stöber method results in particles having mono-sized to multi-sized distributions related to the seed concentration and TEOS addition mode. TEOS in form of active silicic acid can be precipitated on the surface of seeds to increase their diameter or precipitated as new nuclei. According to these knowledge, the mechanisms of colloidal silica formation in high seed concentrations were discussed here.

In seeded growth experiments, changed parameters were various TEOS/NH₃ and seed amounts combined to different TEOS feeding rates.

5.1. NH₃ Concentrations on Growth Solution

The seed particles of this part of the study was obtained from the Stöber synthesis conducted for 4 min (SP1). The SEM image of these particles (4 min, SP1) together with the image of particles after 24 h (SP2) of the reaction were presented in Figure 5.1. It is seen that the size of seed particles was around ~300 nm after 4 min. However, if these particles were allowed to grow in solution for 24 h, they could reach a size nearly 650 nm (SP2).

According to the procedure explained in the section 3.2.3.1, the seed particles after 4 min of the synthesis (SP1) were added into two fresh Stöber solutions (without TEOS), one with standard NH₃ concentration (1.09 M) and the other one with no NH₃ and stirred for 24 hours (GP1) to ensure that unreacted reagents were consumed in the system. Then, additional TEOS (0, 0.025 and 0.25 M; GP1, GP2, GP3, respectively) was introduced to this solution and the system was stirred another 2 hours and characterized. SEM images of these particles (GP1, GP2, GP3) are presented in Figure 5.2 and Figure 5.3 for 1.09 M and 0 M NH₃ concentrations, respectively.

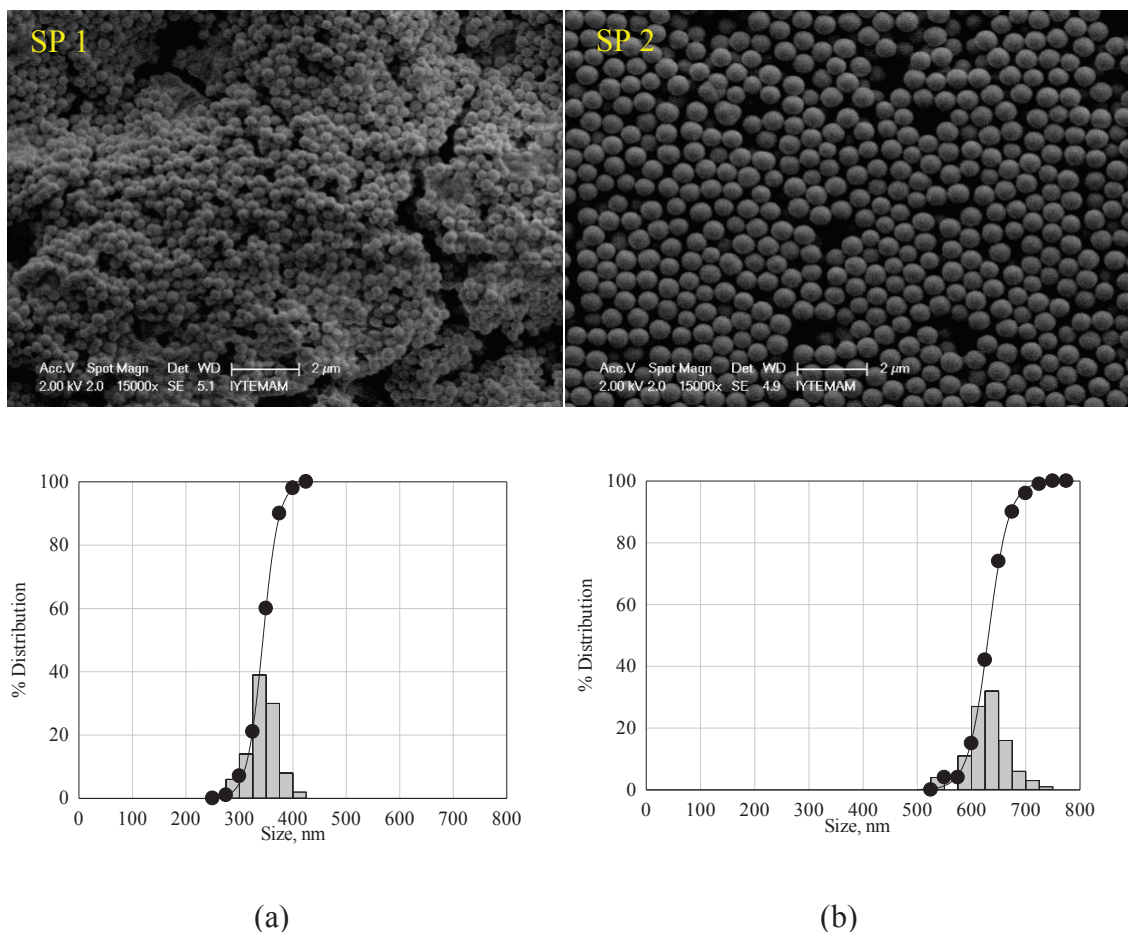
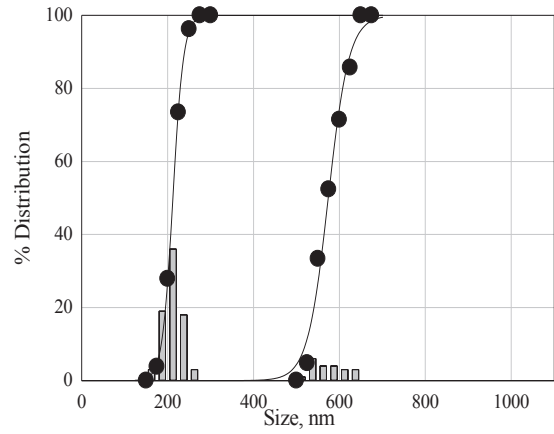
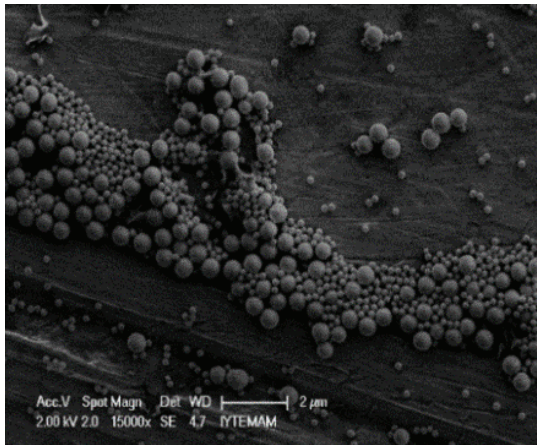


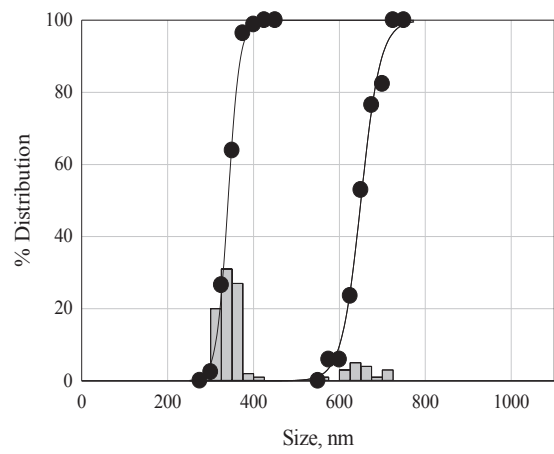
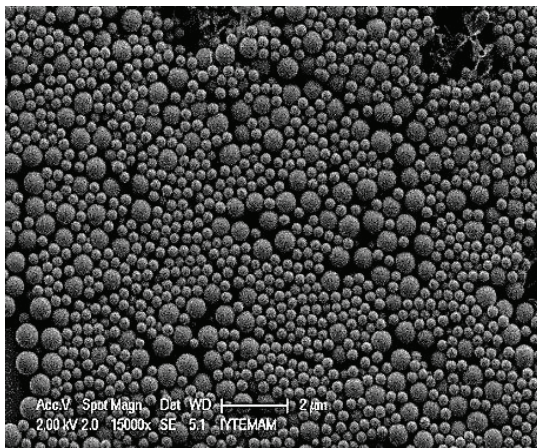
Figure 5.1. SEM images and size distributions for seed particles obtained by Stöber method after; a) 4 min, SP1 and b) 24 h, SP2.

As seen from the Figure 5.2 that there is a bimodal size distribution due to the production of new nucleation centers (*secondary SNPs*). Even the system contains no additional TEOS, the residual TEOS in the seed solution (very small compared to the original concentration) created new nucleation sites (Figure 5.2-a). With addition of TEOS, both fresh nuclei and older seeds grown to a bigger sizes. However, the seed particles (SP1) were still be able to distinguished among the newly formed particles (GP1) with slightly larger sizes which were comparable to the ones (SP2) stayed in the original system for 24 hours.

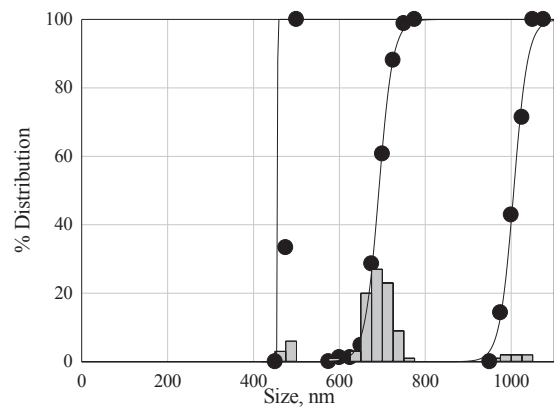
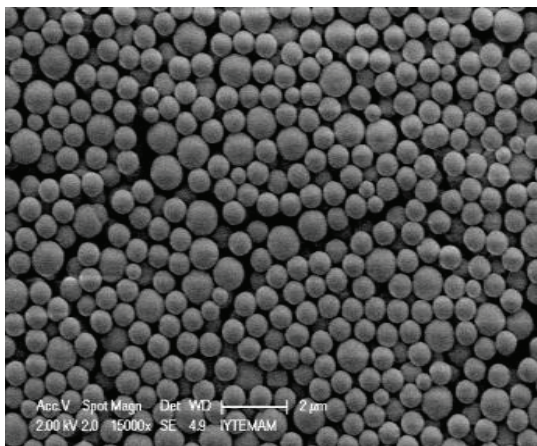
The size of new generated particles changed depending on the amount of silica source (TEOS) added. If the amount of TEOS added in the seeding process was same as the original Stöber concentration (0.25 M), the size of new generated particles was almost comparable to the seed particles after 24 h (SP2).



(a) TEOS = 0 M (GP1)

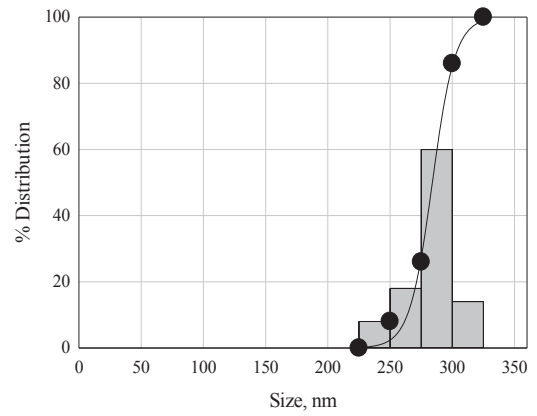
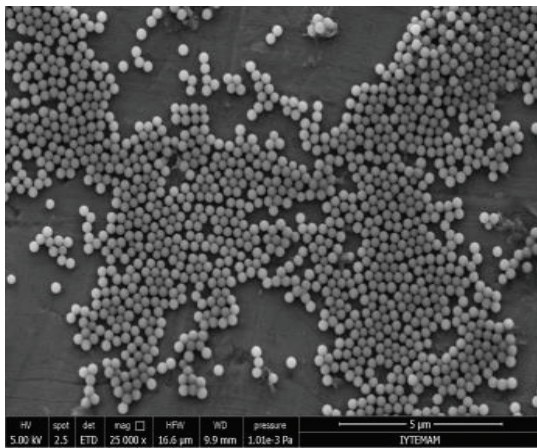


(b) TEOS = 0.025 M (GP2)

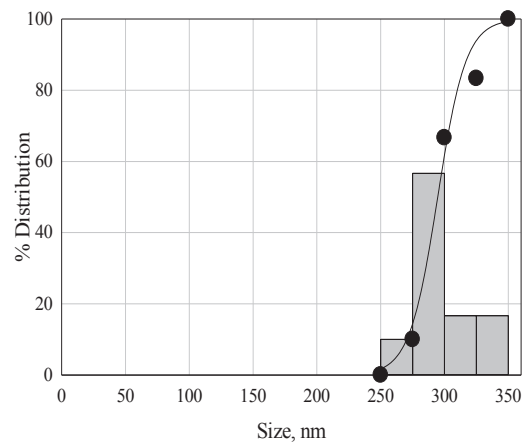
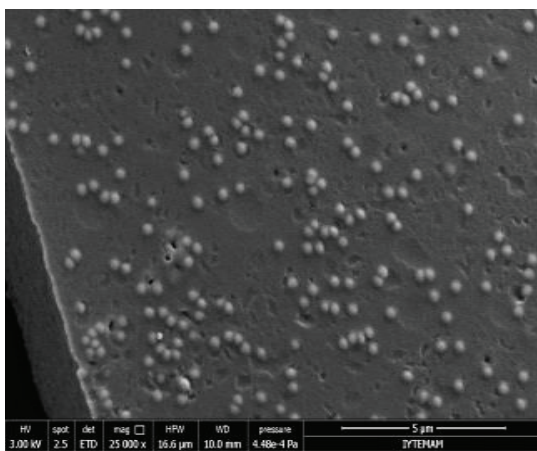


(c) TEOS = 0.25 M (GP3)

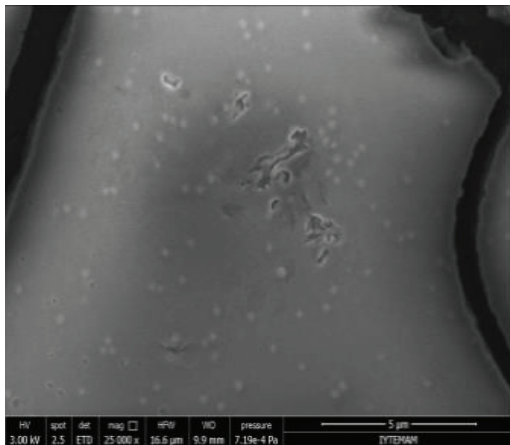
Figure 5.2. SEM images of GP particles in 1.09 M NH₃.



(a) TEOS= 0 M (GP1)



(b) TEOS = 0.025 M (GP2)



(c) TEOS = 0.25 M (GP3)

Couldn't be obtained

Figure 5.3. SEM images of GP particles in the absence of NH_3 (0 M) in growth solution.

If TEOS was not added to this system, there were still newly generated particles (GP1) and a bimodal size distribution obtained due to the production of new nucleation

centers and growth in the new solution with the leftover silica source (Figure 5.2). That is the generation of nucleation sites seems to depend on the solution content (most probably the NH_3 amount) not the silica source. The growth of particles, on the other hand, seems to depend on the silica source. However, if there was no new NH_3 in the solution (Figure 5.3) the supplement of new silica source (whatever the concentration is) did not produce new nucleation sites and there was also no particle growth. As a conclusion, NH_3 seems to be responsible both from the production of nucleation sites and the growth of particles. The silica source, on the other hand, seems to be responsible only from the growth of generated particles. As long as the solution content has not changed, the presence of silica content do not produce new nucleation sites and produce a narrow size distribution.

5.2. Effect of Seed Amounts and TEOS Feeding Rates

In order to determine quantitatively how much of the TEOS will form fresh nuclei which will grow into a new population of particles (*secondary SNPs*) or will be consumed to grow the seed particles (*seed SNPs or seeds*) which already exist in the solution and the seed concentrations, TEOS amount and addition rate were changed. 0.125 M and 0.250 M TEOS were added into Stöber solutions containing 25, 50, 75, 100, 150, 200 and 300 mg seed particles. The experiments were repeated for 0.02 mL/min, 0.10 mL/min and pulse TEOS addition rates.

The SEM photograph and size distribution of seed particles are shown in Figure 5.4-a and b. It is seen that the size of seed particles was around 435 nm with monosized distribution within a time period of 24 h. The representative SEM photographs of the final SNPs obtained after 24 h in the presence of seed particles (shown in Figure 5.4) are presented in Figure 5.5 for demonstration purposes for the pulse addition of 0.125 M and 0.250 M TEOS. The photographs display that the SNPs developed distinct bi-modal distributions: the ones with the larger mode are clearly the seed particles which have grown in size due to condensation of TEOS on their surfaces whereas those with the smaller mode are the freshly formed secondary SNPs. Note that both groups are nearly mono-sized with very narrow size distributions.

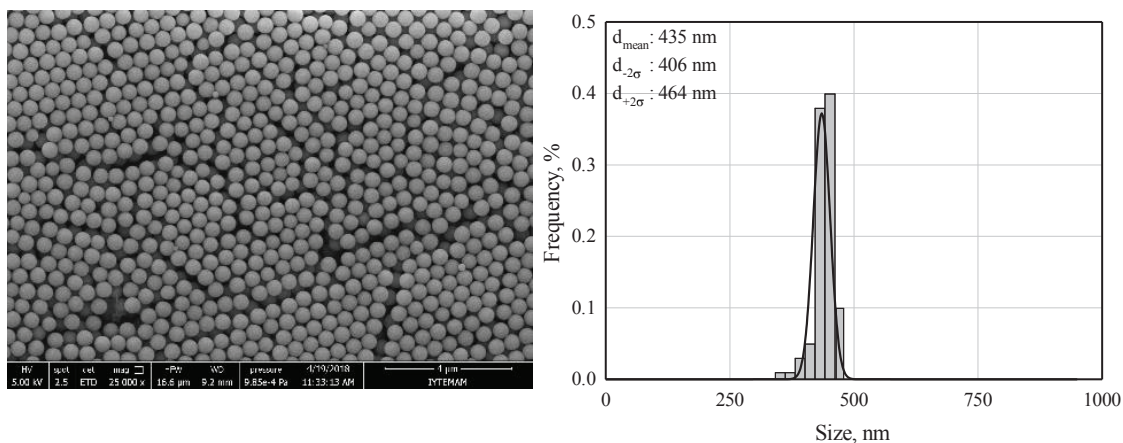


Figure 5.4. a) A representative SEM image of the seeds after 24 h of synthesis; b) number frequency size distribution obtained from the SEM image. $d_{-2\sigma}$ and $d_{+2\sigma}$ represent the nominal lower and upper size bounds of the distribution which contain 95.4% of the population.

The measured mean sizes together with the nominal 95.4% lower and upper sizes for the seed and the secondary SNPs are presented in Figure 5.6 as a function of the initial seed surface area for different TEOS addition rates and total TEOS amounts. The Figure 5.6 shows that the final mean sizes of the seeds are always greater than the mean size of the initial seed particles (435 nm), validating the growth of the seed particles due to TEOS condensation. The increase in the seed particle size at the very small seed surface areas is due to the smaller number of seed particles acquiring more TEOS condensing on their surfaces on a per particle base. However, the mean sizes of the seed SNPs display a general decrease with increasing seed surface area. This should be expected since less TEOS will be available in the system for each seed particle as the seed amount, hence the number of seed particles, increase in the system. Actually, the mean sizes of the seed SNPs approach each other for all TEOS addition scenarios as the seed surface area becomes larger. Another important observation is the fact that the initial mono-sized seed particles preserve their narrow size distribution, indicating that each seed particle acquires a similar amount of TEOS during growth.

The secondary SNPs also show a decrease in size as the seed surface area increases since more TEOS condensing on the seed particles with increasing seed surface area leaves a progressively smaller amount of TEOS available for secondary particle growth.

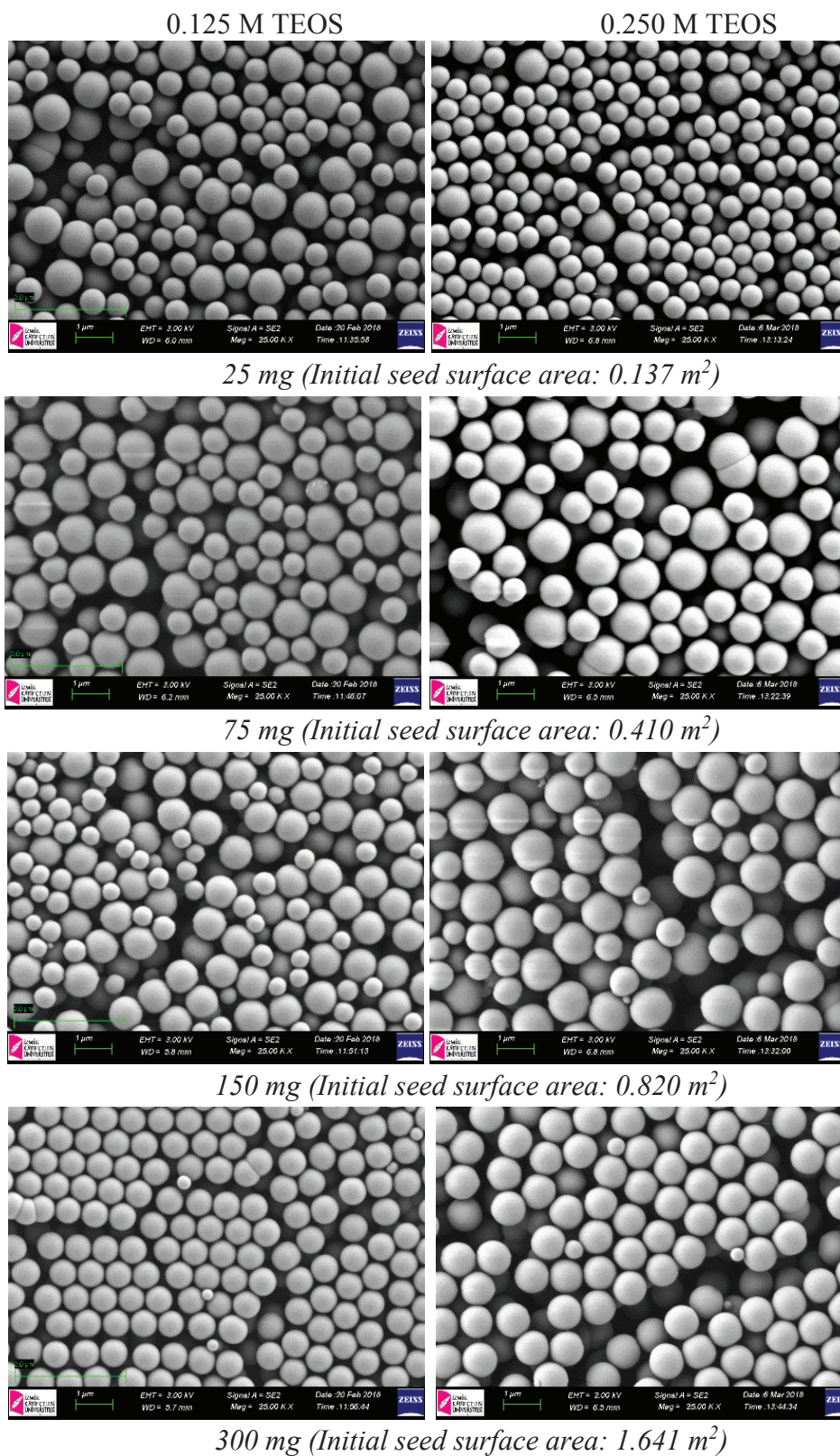


Figure 5.5. SEM images of the SNPs after 24 hours of synthesis in the presence of selected seed amounts for 0.125 M and 0.250 M total TEOS amounts for *pulse addition case*.

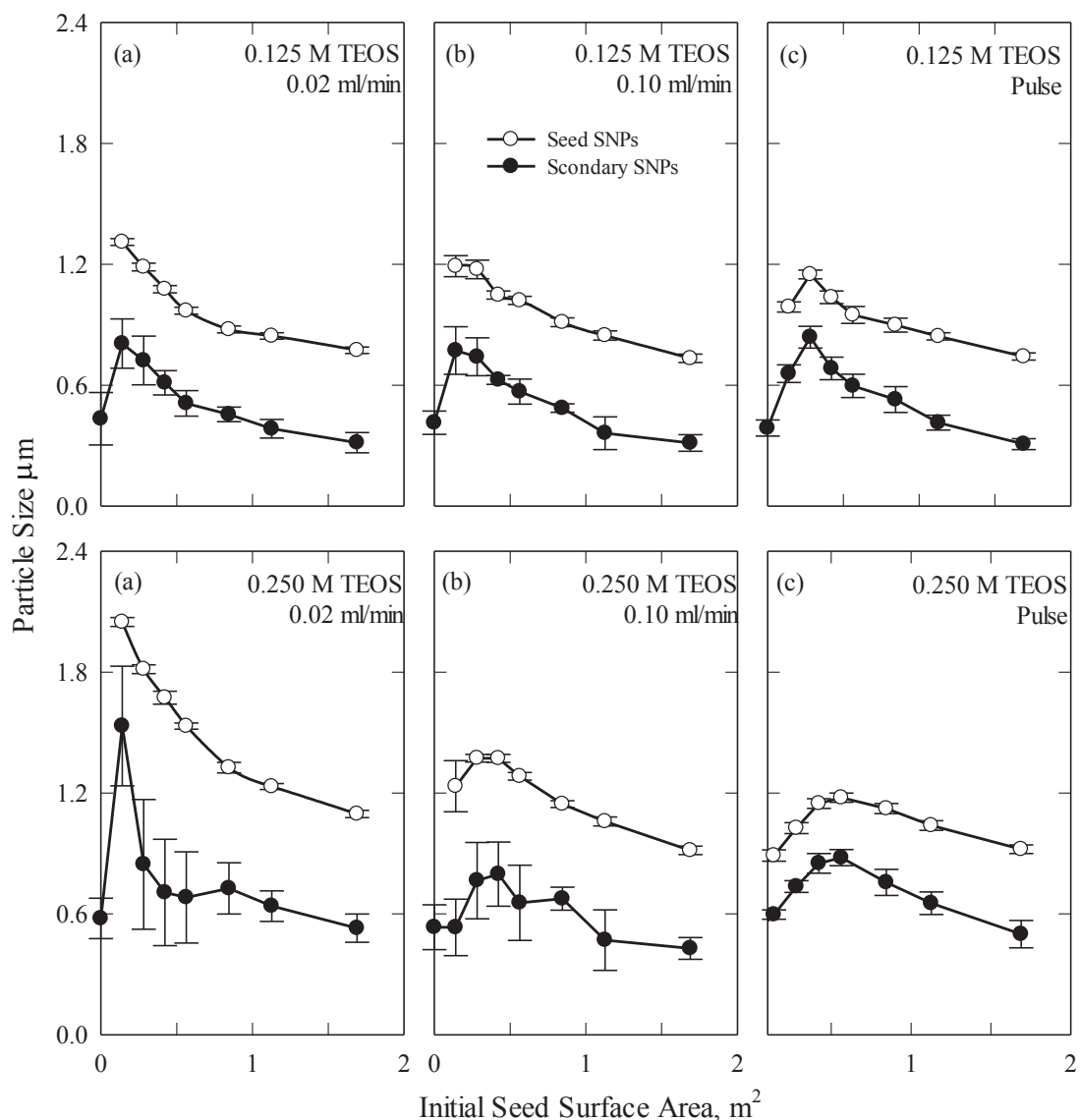


Figure 5.6. Sizes of the SNPs after 24 hours of synthesis carried out in the presence of different amounts of seeds for the case of 0.125 and 0.250 M total TEOS additions for 0.02 mL/min, 0.10 mL/min and pulse TEOS additions.

The initial increase in the secondary SNP sizes at low seed surface areas, especially at high TEOS addition rates, is due to having relatively more TEOS available in the system for secondary particle formation. Also, it is important to note that the secondary SNPs displayed much broader size distributions compared to the grown seed SNPs, especially at lower TEOS addition rates. This implies that the formation of new nuclei which grow into the secondary particles continue for longer times into the synthesis for slow TEOS addition rates and lead to broader size distributions as should be expected.

The total amount of TEOS condensed on the seeds (calculated through the final and the initial mean sizes of the seed SNPs) is presented in Figure 5.7 for 0.125 M and 0.250 M *pulse* TEOS additions as a function of the initial seed surface area. The amount of TEOS condensed on the primary seed particles was calculated from the mass difference using the sizes of the re-grown and the primary seed particles. Similarly, the amount of TEOS condensed as secondary particles was calculated by deducting the amount of TEOS condensed on the seed particles from the total amount of TEOS added into solution which corresponded to 2.715 grams of silica for 0.250 M TEOS and 1.357 grams silica for 0.125 M TEOS assuming complete conversion. It can be seen that the amount of TEOS condensed on the seed particles displays an exponential increase with the seed surface area, eventually reaching the total TEOS amount in the system in both cases (the dashed line in the graphs corresponding to 1.35 and 2.70 grams). This implies that all TEOS in the system would condense on the seed surfaces provided that there is a sufficient seed surface area. The graphs show that the amount of TEOS condensed on the primary seed particles reaches the total available amount of TEOS in the system at a varied seed amount, implies that formation of new nuclei, hence the secondary particles, will cease when the primary seed concentration is above this critical value.

The Figure 5.7 displays that the critical surface area for this case is around 2.0 m² for 0.125 M TEOS and 1.25 m² for 0.250 M TEOS. As the surface area of the seeds in the system approaches this value, the amount of TEOS forming new nuclei, hence the secondary SNPs, will progressively decrease towards zero as it can be seen from the SEM photographs in Figure 5.5. This is displayed quantitatively in Figure 5.7 where the number of secondary SNPs (calculated from the amount of TEOS forming secondary SNPs and the mean secondary particle size) decreases to zero as the seed surface areas reach the critical values.

It is apparent that as the amount of TEOS available for secondary particle formation decreases, the probability for forming new nuclei decreases precipitously. This observation suggests that mono-sized and mono-modal SNPs with the desired size can be obtained by the addition of sufficient amount of seeds (surface area) into the system as has been often observed with the seed experiments (Chen et al., 1996).

Figure 5.8 displays the amount of TEOS condensed on seed particles for all TEOS addition scenarios. The data show that the amount of TEOS condensed on the seed particles increase and reach the total TEOS in the system for all cases. It can also be seen

that the seed surface area required for all TEOS condensing on the seed particles becomes lower as the TEOS addition rate is reduced. In other words, the formation of the secondary particles will be suppressed at lower seed surface areas at lower TEOS addition rates.

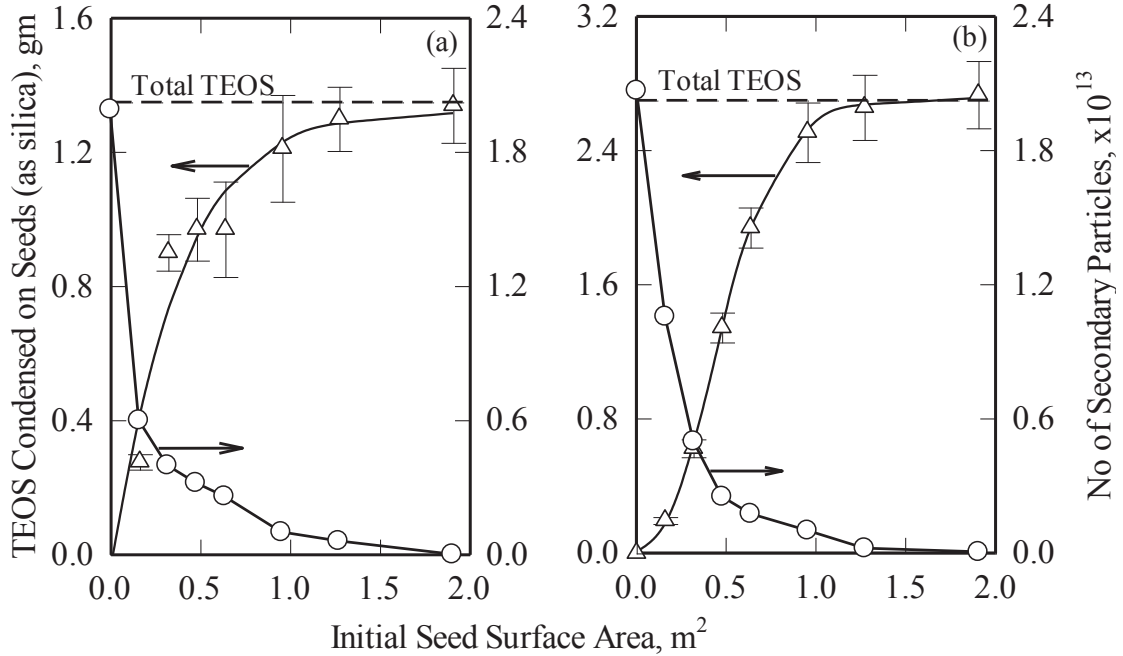


Figure 5.7. Amount of TEOS condensed on seed SNPs and the number of secondary SNPs formed for (a) 0.125 M and (b) for 0.250 M pulse TEOS addition in the presence of different seed amounts. The dashed line represents the total TEOS in the system.

Critical seed surface areas for changing TEOS addition rates and concentrations were tabulated in Table 5.1. For 0.25 M TEOS concentration and lower TEOS addition rate (0.02 mL/min), critical seed surface was decreased, meaning that TEOS preferred to precipitate around the seed particles and system tend to be mono-modal.

Table 5.1. Critical seed surface areas for changing TEOS addition rates and concentrations

TEOS Concentration, M	TEOS Addition rate		
	Pulse	0.1 mL/min	0.02 mL/min
0.125	2.00	1.50	1.25
0.250	1.25	1.00	0.50

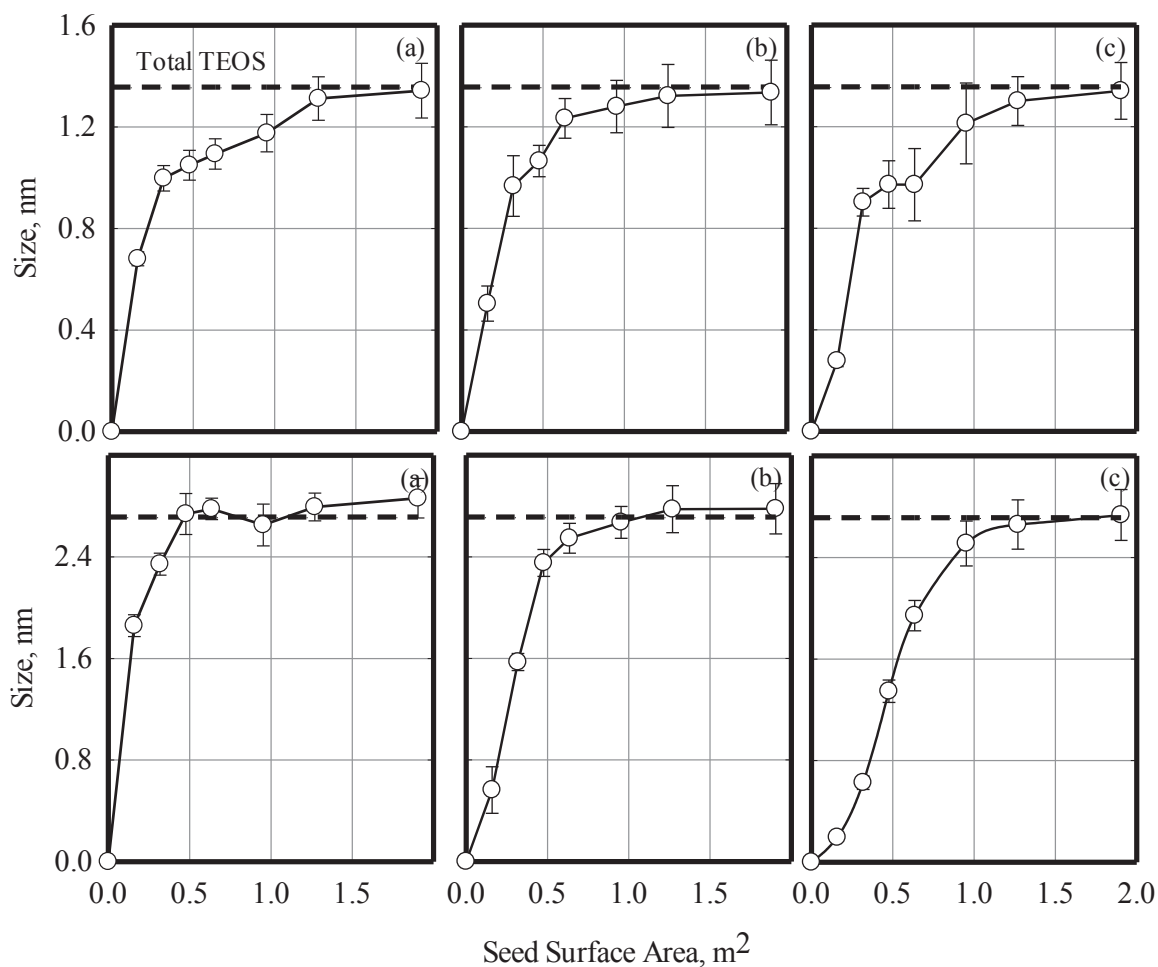


Figure 5.8. Amount of TEOS condensed on seeds after 24 hours of synthesis carried out in the presence of different amounts of seeds for the case of 0.125 (top row graphs) and 0.250 M (bottom row graphs) total TEOS additions; a) 0.02 mL/min, b) 0.10 mL/min and c) Pulse TEOS additions.

Figure 5.9 gives the kinetic observation of the system. The first row of photos gives the state of the system on the 10th minute of the synthesis where only a small fraction of the total TEOS (10% of 0.250 M) has been delivered into the system. It can be seen that practically all the TEOS added up to this point in synthesis is consumed by the seeds for the 150 mg case. On the other hand, a significant amount of residual TEOS could be clearly seen as a gel-like formation around the seeds for the 25 mg and 75 mg seed additions. Careful inspection reveals that the gel contains a number of initial nuclei which will eventually grow into secondary particles. The fact that TEOS has apparently formed fresh nuclei early in the synthesis when only one-tenth of the TEOS is in the system

supports the hypothesis suggested in Chapter 5.1 and 5.2 that oversaturation is not necessary for condensation of TEOS into fresh nuclei.

The second row of photos represent the 30th minute in the synthesis where 30% of the total TEOS has been added to the system. The photographs for the 25 and 75 mg cases clearly display the growth of the initial nuclei observed above into secondary SNPs. Though formation of a very few secondary particles is observed for the 150 mg seed addition, their number density is much smaller compared to the 25 and 75 mg seed additions. Also, the 25 mg case already starts to display a broad size distribution with some quite large secondary SNPs. This trend basically continues as the synthesis progresses to yield the size distributions presented in the bottom row figures in Figure 5.9. It is apparent that while condensation on the seeds is favored at larger seed surface area, the formation of secondary SNPs is favored at the lower end. For higher seed amounts, the seed surface area is sufficient to consume the available TEOS early in the synthesis, suppressing the formation of the secondary SNPs. Nucleation into secondary SNPs is favored early in the process at lower seed amounts and continue late into the synthesis, which leads to the formation of secondary SNPs with larger mean sizes and broader size distributions. Since the formation of the secondary SNPs initiates early, the size distributions are even broader for the low seed concentrations; largest for the case of no seeds in the system. Also, since the available TEOS has to be shared among a larger number of seed particles, the final size of the grown seed particles becomes smaller with increasing seed amount.

Seeded growth studies were also tested with the whole system used as seed directly after washing the particles or unwashed particles. For this, classical Stöber solution were conducted (EtOH: 12.14 M, H₂O: 11.67 M, NH₃: 1.09 M, TEOS: 0.25 M) and after 24h, for one set of experiment, particles were washed with water three times and redispersed in Stöber solution. For another set of experiment, particles were not washed stayed in the reaction solution. 0.25 M additional TEOS were added to both of these systems and stirred for another 4 h. The SEM results are given in Figure 5.10. When whole silica particles unwashed after synthesis used as seed particles, additional TEOS precipitated around these particles but resulted in smaller mean sized compared to washed seed particles. This may be due to the residual NH₃/H₂O/EtOH present in the system created new nuclei small in number after the addition of TEOS. This new nuclei formation consumed a portion of TEOS, and residual TEOS precipitated around seed particles

resulted in increasing size. However, if seed particles washed and purified from residual components, TEOS solely preferred to growth seed particles resulting in higher sizes compared to unwashed samples. Monosized distribution was achieved in both systems with different mean sizes.

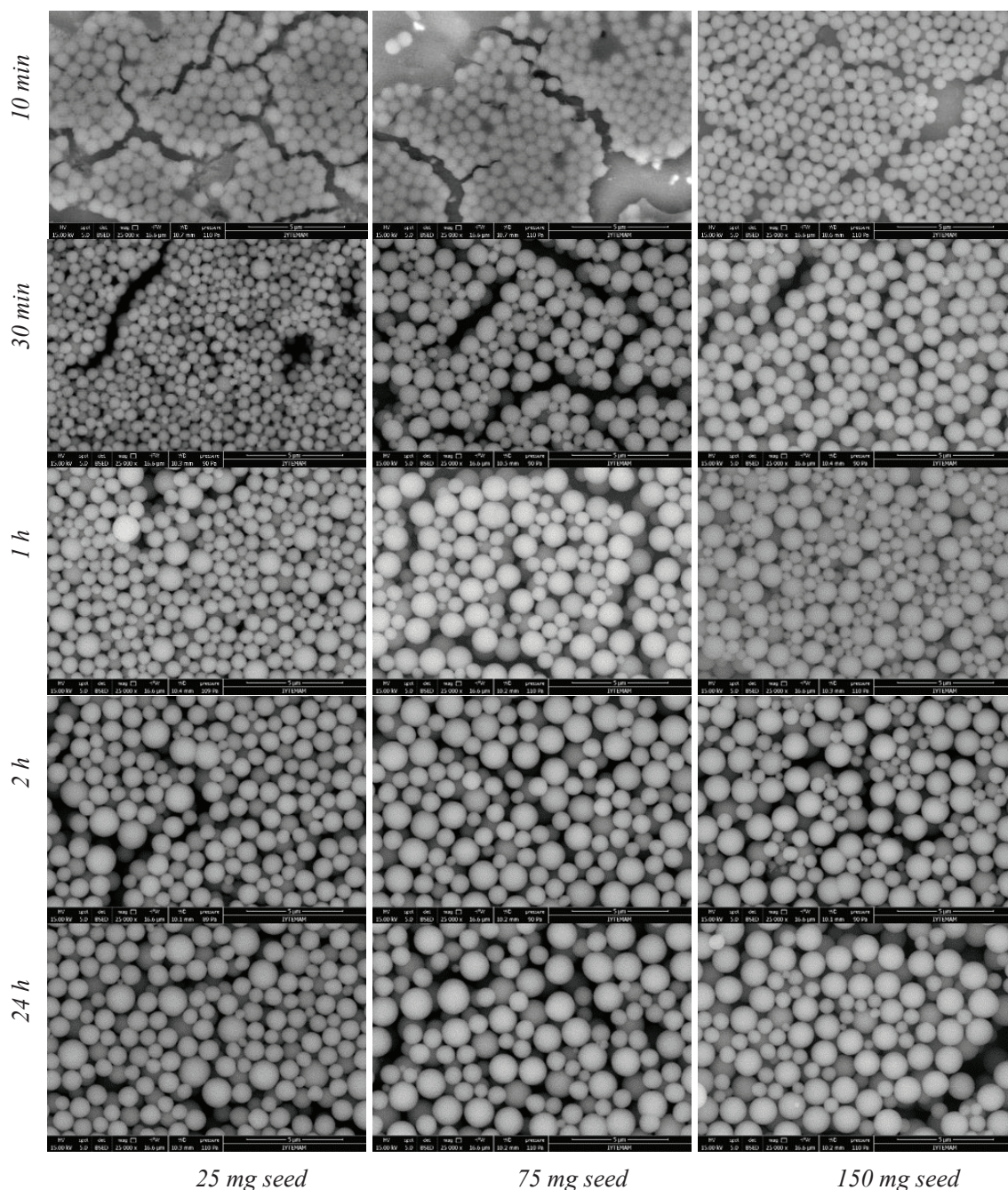


Figure 5.9. Representative SEM images of the SNPs sampled at different synthesis times in the presence of different amount of seeds for continuous TEOS addition case (0.1 mL/min) (*the scale is the same in all photos*).

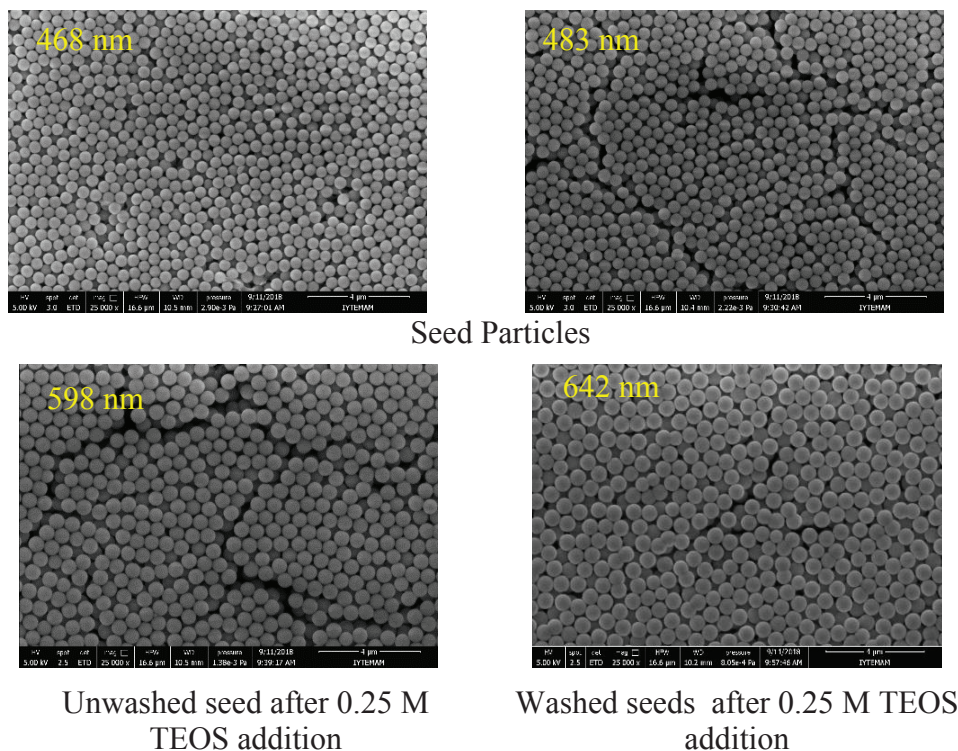
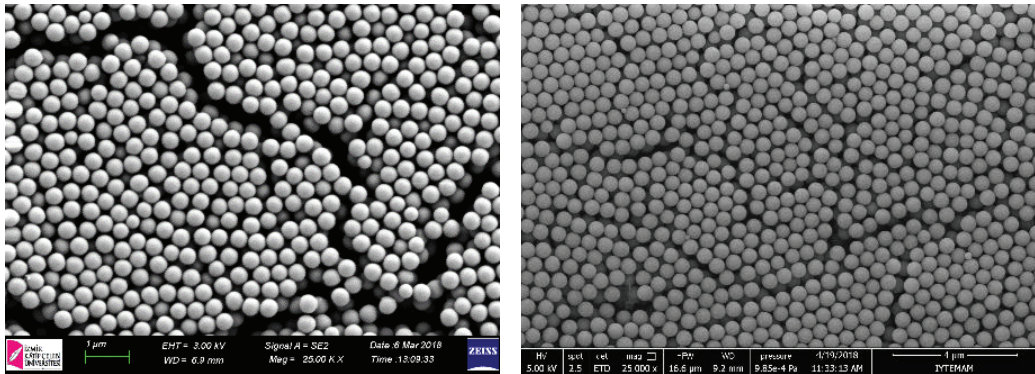


Figure 5.10. SEM images of seeded growth method agitation conditions vs solute size.

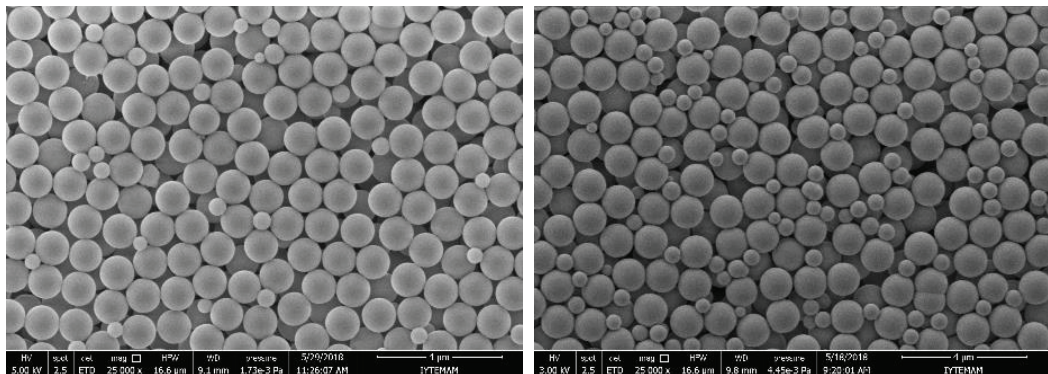
As a conclusion, when no seed particles are present, all the TEOS creates fresh nuclei which grow into SNPs whose final size and distribution depend on the amount and the rate of TEOS addition (see Figure 4.17). When a specific amount of seed particles are added to the system, a certain fraction of TEOS condenses on the seed surfaces while the remaining amount will form new nuclei. Condensation on the seed particles will cause the growth of the seed SNPs whereas formation of new nuclei will lead to the creation and growth of secondary SNPs (see Figure 5.6). At a critical seed surface area, all the TEOS in the system will be consumed by the seed particles, creating a mono-sized, but larger SNPs. The mean size of the system can be adjusted by varying the amount, addition rate of TEOS. In between these two extremes which lead to a mono-sized distribution, a bi-modal distribution, one mode belonging to the grown seeds and the other to the newly formed secondary SNPs should be expected and the resulted SEM images are given in Figure 5.11. The location of the modes and the breadth of these two distributions can be controlled as desired by varying the seed amount or TEOS addition conditions in the system.

Mono-sized



Different seed particles

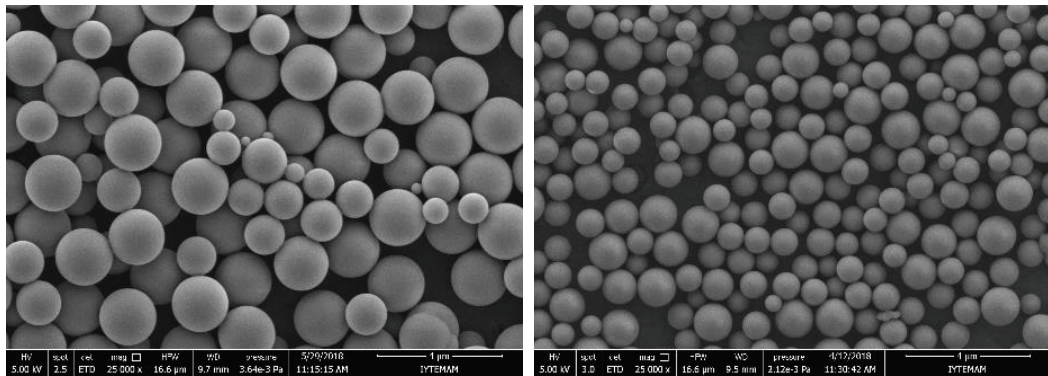
Bimodal



300 mg seed 10 mL TEOS
0.02mL/min

300 mg seed 10 mL TEOS
0.04mL/min

Multimodal



25 mg seed 5 mL TEOS
0.04 mL/min

25 mg seed 5 mL TEOS
0.1mL/min

Figure 5.11. SEM images of the size distribution of silica particles with different modalities obtained from seeding studies.

5.3. Seed Addition in the Presence of Electrolytes

Silica synthesis in the presence of seed particles were also performed with Stöber solutions that contain 4×10^{-2} M electrolyte solutions. For this purpose, known aliquots from the seed stock solution (seed amounts of 25, 50, 75, 100, 150, 200 and 300 mg) were transferred into TEOS free Stöber solutions that contain 4×10^{-2} M NaCl, CaCl₂ and AlCl₃. SEM images related to this part were given in Figure 5.12, Figure 5.13 and Figure 5.14 for NaCl, CaCl₂ and AlCl₃, respectively.

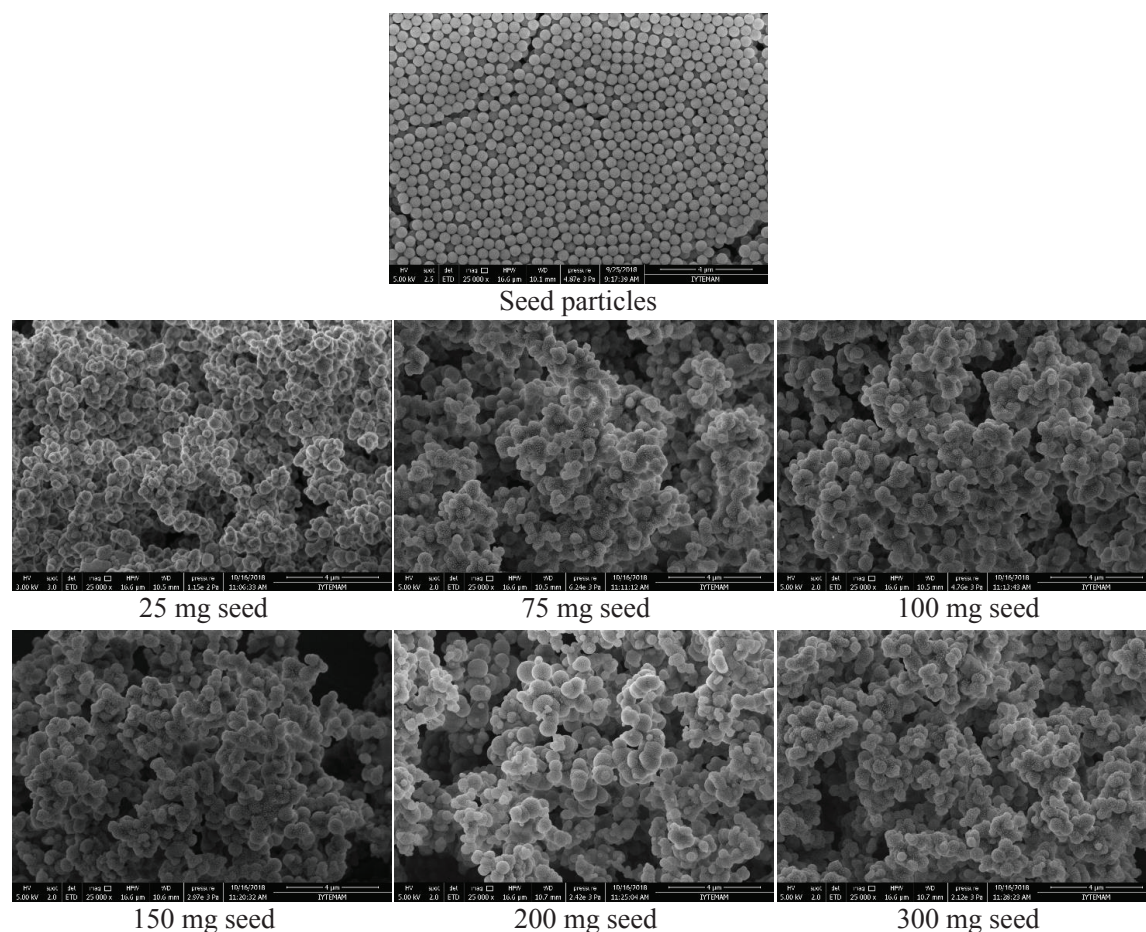


Figure 5.12. SEM images of the silica particles with seed particles in the presence of 4×10^{-2} M NaCl in growth solution.

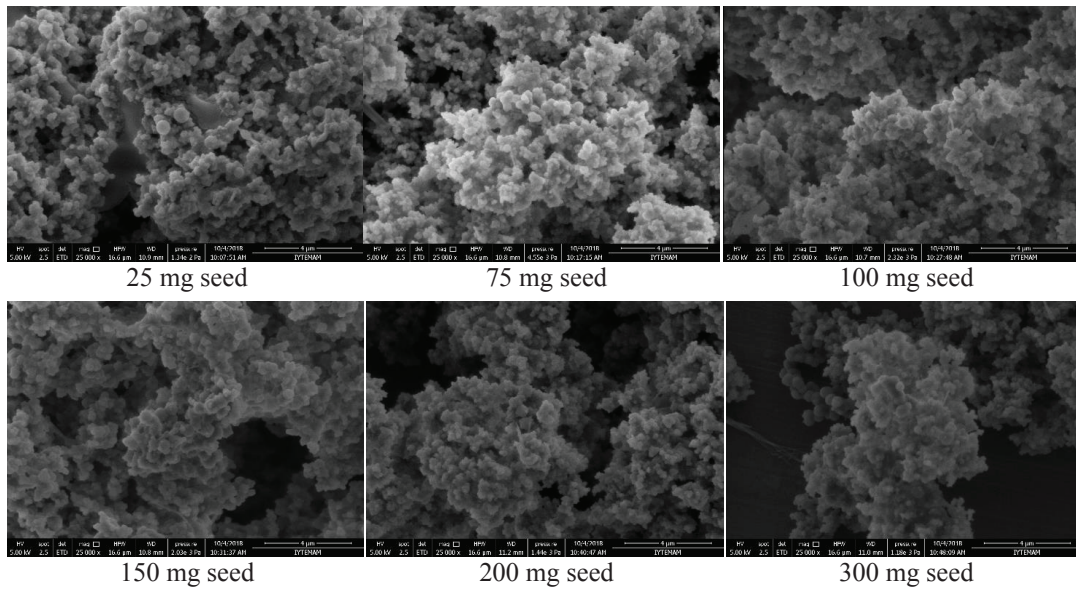


Figure 5.13. SEM images of the silica particles with seed particles in the presence of 4×10^{-2} M CaCl_2 in growth solution.

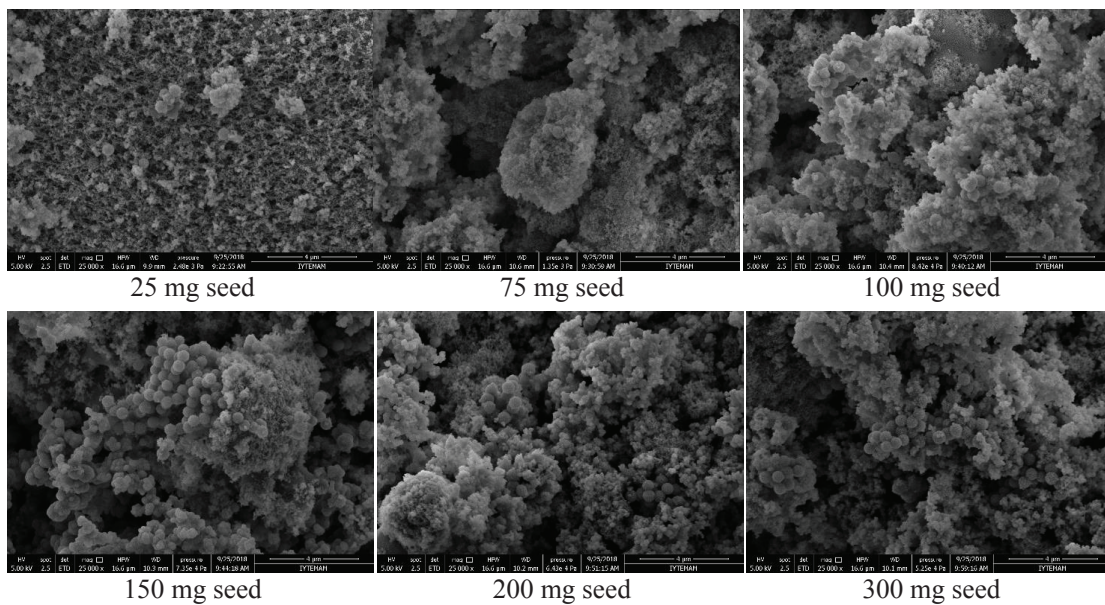


Figure 5.14. SEM images of the silica particles with seed particles in the presence of 4×10^{-2} M AlCl_3 in growth solution.

New nucleation occurred in the presence of electrolytes however, growth of seeds were hindered as can be seen from Figure 5.12, Figure 5.13 and Figure 5.14. Addition of

TEOS preferred to create new nucleation and presence of electrolytes in growth solution promoted secondary particles to be agglomerated. This results were compatible with the results that obtained in Section 4.2.2. The size of these secondary particles decreased as the valence of electrolytes increased (smaller in AlCl_3 , bigger in NaCl) whereas number of secondary particles increased.

CHAPTER 6

DEVELOPMENT OF A MODEL FOR PARTICLE GROWTH

Since the particle growth mechanism is seriously important, this chapter includes the development of a model for SNP growth. Firstly the concept of the model is given and following that equations are given in detail.

6.1. Concept of the Model

Before moving into the concept description of the model suggested in this study, it is useful to define the terms employed to describe the various species referred to in the model. These are listed above.

- i) *Monomers*: Monomers are the single Si-containing species of different degree of hydrolysis such as Si(OR)_4 , $\text{Si(OR)}_3\text{OH}$, $\text{Si(OR)}_2(\text{OH})_2$, Si(OR)(OH)_3 and Si(OH)_4 . Si(OR)_4 is the unhydrolyzed TEOS molecule and its initial number concentration in solution is n_T . The total number of monomers n_m is equal to the sum of the number concentration of the above 5 species. In the absence of any condensation reactions, n_m is equal to n_T . However, in the presence of condensation, n_m is a function of time and decreases with time from the initial value n_T towards zero. The radii of the all monomer species have been assumed to be equal to the radius R_T of the TEOS molecule and is around 0.360 nm (see discussion below).
- ii) *Oligomers*: Oligomers of radii R_o form from condensation of individual monomers of different degree of hydrolysis through water (OH-OH) or alcohol (OH-OR) condensation. Note that R_o changes with time from the initial value of R_T . The number of oligomeric species is n_o and varies with time.

iii) *Nuclei*: Oligomers grow to larger oligomeric structures (nuclei) with radii R_a again condensing through water (OH-OH) or alcohol (OH-OR) condensation. Similar to R_o , R_a increases with time from an initial value of R_o . The number of nuclei species is n_a . There is no clear distinction between an oligomer and a nucleus since the transformation is gradual. However, in this thesis a loose definition which depends on the following will be employed to distinguish between oligomers and nuclei: If the condensed species are still small enough to be better described by the number of monomers condensed on the structure, they will be defined as oligomers. If the condensed species are large enough to be better described by their radii, they will be defined as nuclei.

The concept of the model is based some assumptions and these are listed above.

- i. Hydrolysis of TEOS into hydrolyzed monomers, condensation of hydrolyzed monomers into oligomers and oligomer aggregation to form nuclei is assumed to take place by diffusional transport. The validation of a diffusion dominated system will be presented in the following paragraphs using Peclet number analysis and calculation of Kolmogorov microscale of turbulence.
- ii. Monomers diffuse towards a random central monomer in an infinitely small volume v_o to form a central oligomer R_o , which grows by further monomer (or oligomer) addition.
- iii. Oligomers with radius R_o which grow in their own infinitely small volumes also diffuse towards a central oligomer (or nucleus) in a micro volume v_a ($v_a \gg v_o$) and condense to form nuclei R_a . The nuclei R_a grow by both monomer and oligomer condensation to final particles of number n_a . Each micro volume is assumed to yield a single final particle. In other words, micro volumes can be likened to batch micro reactors, each of which generating a single final particle. It follows that, the number of these micro volumes can be estimated from the number of final particles.

The schematic description of the conceptual model is presented in Figure 6.1. Each squares show an infinitely small microvolumes v_o and v_a . In the schematic representation, K_1 is the hydrolysis rate constant and K_2 is the condensation rate constant.

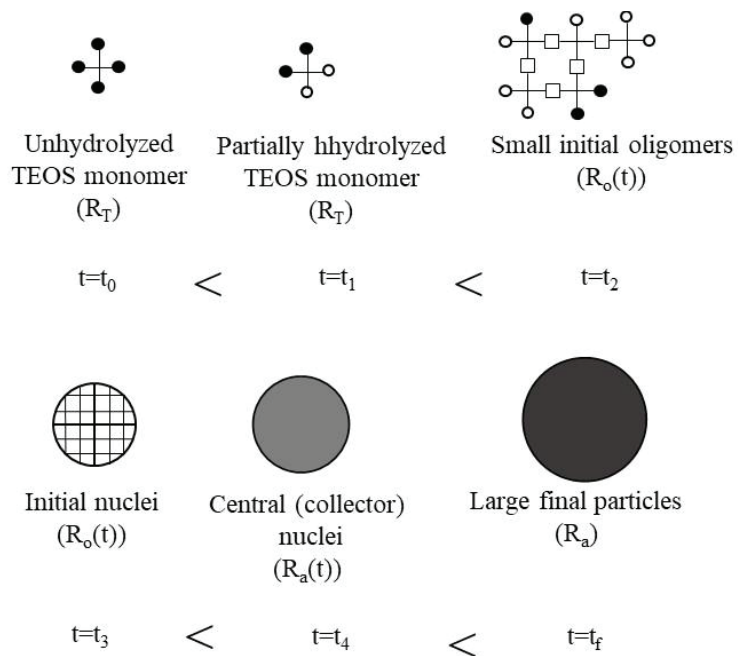
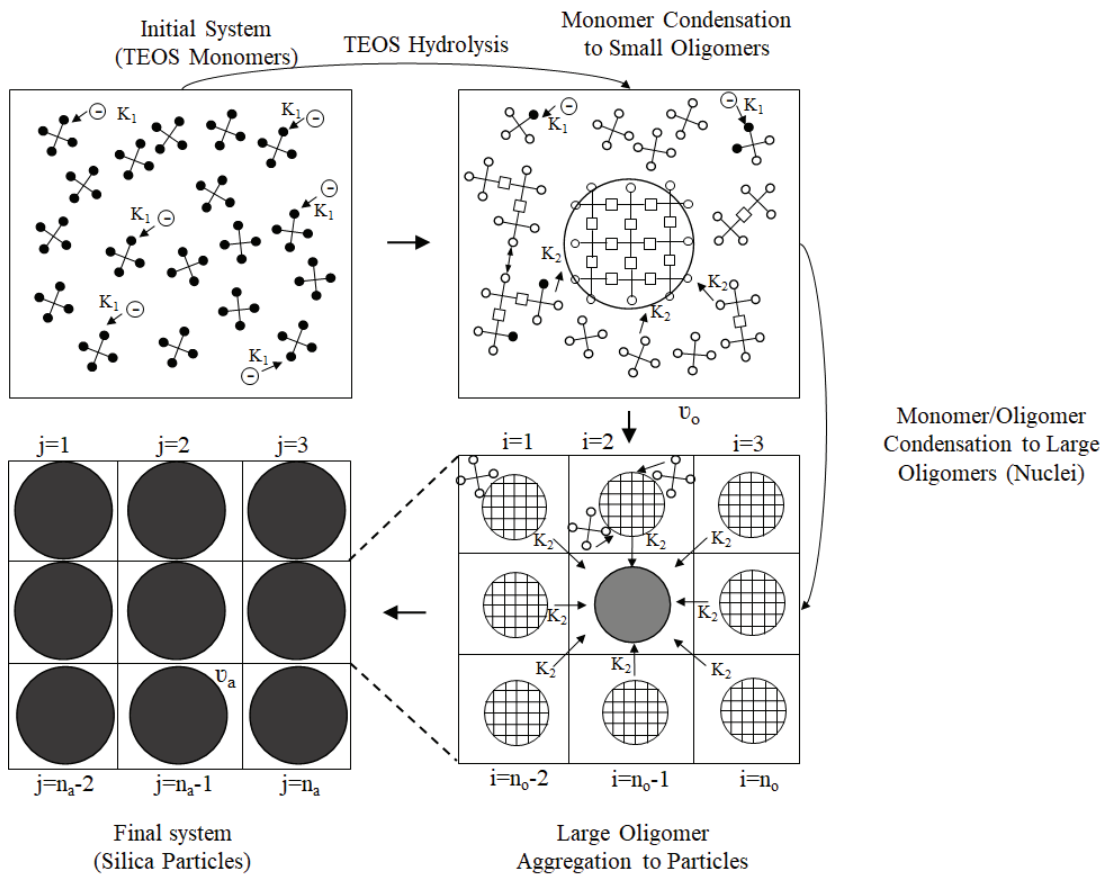


Figure 6.1. Schematics of the idea under the particle growth process.

The above concept that the monomers form oligomers and later monomers and oligomers form nuclei and final particles in isolated volumes similar to micro reactors suggests that the particle growth should take place by diffusion only. This can be substantiated by comparing the Kolmogorov microscale of turbulence to the size of the micro volumes. The Kolmogorov microscale of turbulence can be calculated from the power input into the standard cell as follows:

$$P = N_p D^5 N^3 \rho \quad (6.1)$$

where P is the mixing power imparted into the standard cell in watts. D is the impeller diameter (2.5 cm), N is the mixing speed in revolutions per minute (250 1/min) and ρ is the density of the medium (0.82 gm/cm³). N_p is the Power Number which is approximately equal to 4 for the standard cell configuration given in Figure 1 (Tatterson, 1991). Under these conditions, the power input into the cell comes out to be 2.32 mW.

The dissipation rate, ε , in the cell which is given by:

$$\varepsilon = \frac{P}{m} \quad (6.2)$$

and calculated to be $5.54 \times 10^{-3} \text{ m}^2/\text{s}^3$ where m is the mass of the fluid in the tank (137 gm). The Kolmogorov microscale of turbulence is calculated from:

$$\lambda_0 = \left(\frac{\nu^3}{\varepsilon}\right)^{0.25} \quad (6.3)$$

Where ν is the kinematic viscosity in m²/s. The Kolmogorov microscale of turbulence comes out to be 111 μm for the alcohol-water kinematic viscosity of $0.95 \times 10^{-6} \text{ m}^2/\text{sec}$.

Glasgow and Hsu, 1985 suggest that the probability of shearing a volume in a standard cell is a function of the size of the micro eddies. Since the length of the micro eddies in the mixing cell (111 μm) is 50 times larger than the length of the micro volumes (which vary between 2 and 2.4 μm), it can be safely assumed that the micro volumes are unaffected by the turbulence in the flow; that is, diffusive effects are dominant within the micro volumes.

This can be further demonstrated by the data given in Figure 4.20 where the SNP synthesis for pulse addition of TEOS (0.25 M) was repeated at different mixing regimes

(250 rpm, 810 rpm and 250 rpm mixed only for the first minute of the synthesis). The data show qualitatively that the final particle size was independent of the mixing regime. This is not surprising since the associated hydrodynamic Peclet number (Pe) is much smaller than unity for both the 250 and 810 rpm mixing speeds shown in Figure 4.21. The Peclet number compares the relative influence of shearing (convective) effects in the cell with the diffusive effects. Molecular diffusion coefficients were calculated for the dominant species in our systems so as to cover diameters ranging from TEOS molecules (about 4 Å) to full grown SNPs (about 400 nm) for the two mixing speeds of 250 rpm (4.16 Hz) and 810 rpm (13.50 Hz). These speeds which correspond to respective Reynolds numbers of 1.96×10^3 and 6.36×10^3 fall in the turbulent region for the standard cell employed in our tests. It can be seen that almost all the particles in the system are under diffusive effects for the mixing speeds calculated, supporting the findings from the Kolmogorov microscale of turbulence. These results are also consistent with the study of Nozawa et al., 2005 and Liang et al., 2016 who demonstrated that stirring rates has no significant impact on the average size of SNPs.

The model presented above for nuclei formation and growth during Stöber synthesis suggests that the TEOS added into the synthesis solution forms nuclei as soon as it comes into contact with the reaction solution. The intermediate species (hydrolyzed monomers, oligomers or early nuclei) move under diffusive effects towards a central collector nucleus in micro volumes which mimic isolated micro reactors each of which yielding a single final SNP. That is, there is no need for the concept of over saturation which was repeatedly suggested in the literature (Chang et al., 2005).

6.2. Rate of Collision and Aggregation under Diffusion

Collision and aggregation kinetics can be modelled considering two particles that are apart from each other with a distance r and the aggregation rate $\left(\frac{dn_1(r)}{dt}\right)$ using Fick's first and second laws. The schematic of this idea is given in Figure 6.2. Radii of particles are equal to each other at initial, than can change.

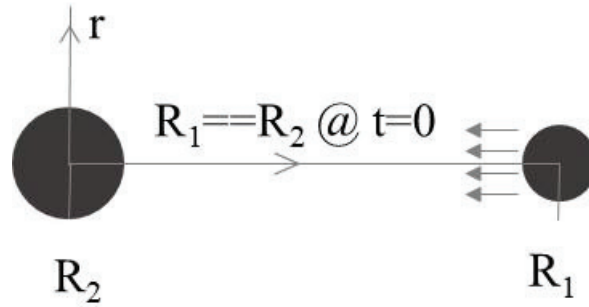


Figure 6.2. Aggregation of two particles apart from each other with a distance r .

If a particle of radius R_1 diffused towards a random particle R_2 , the number of particles 1 crossing a unit area towards particle 2 can be given by Fick's first law of diffusion which relates the diffusive flux to the number concentration in spherical coordinates.

$$\frac{dn_1(r)}{dt} = -D_1 \frac{dn_1(r)}{dr} = J(r) \quad (6.4)$$

Where $J(r)$ is the aggregation flux of particles 1 towards particle 2,

D is the diffusion coefficient (m^2/s),

$n_1(r)$ is the number concentration of "1" particles

Fick's second law of diffusion predicts how diffusion causes the concentration to change with time. This law can be applied for the number concentration change of particles with time and given in spherical coordinates as;

$$\frac{dn_1(r)}{dt} = -D_1 \frac{1}{r^2} \frac{d}{dr} \left[r^2 \frac{dn_1(r)}{dr} \right] \quad (6.5)$$

The diffusion coefficient of particle 1 towards particle 2 is given by the Stokes-Einstein equation as;

$$D_1 = \frac{kT}{6\pi\mu R_1} \quad (6.6)$$

Where k is the Boltzmann constant (J/K), T is the temperature (K), μ is the dynamic viscosity (Pa s), R_l is the particle radius (m).

Note that if particle 2 is also diffusing towards particle 1:

$$D_2 = \frac{kT}{6\pi\mu R_2} \quad (6.7)$$

Then the overall diffusion coefficient D_{12} can be approximated by adding the two diffusion coefficients:

$$D_{12} = \frac{kT}{6\pi\mu R_1} + \frac{kT}{6\pi\mu R_2} = \frac{kT}{6\pi\mu} \left(\frac{1}{R_1} + \frac{1}{R_2} \right) \quad (6.8)$$

The equation 6.8 shows that for $R_1=R_2$ (then $D_1=D_2$), the overall diffusion coefficient will be $D_{12}=2D_1$. On the other extreme, where $R_1 \ll R_2$, the overall diffusion coefficient will be $D_{12} \approx D_1$. This is what should be the case since only R_1 will be diffusing towards R_2 hence $D_{12} \approx D_1$.

Assuming steady-state diffusion such that;

$$\frac{dn_1(r)}{dt} = 0 \quad (6.9)$$

Equation 6.5 becomes;

$$\frac{d}{dr} \left[r^2 \frac{dn_1(r)}{dr} \right] = 0 \quad (6.10)$$

$$r^2 \frac{dn_1(r)}{dr} = C_1 \quad (6.11)$$

$$\frac{dn_1(r)}{dr} = \frac{C_1}{r^2} \quad (6.12)$$

$$n_1(r) = -\frac{C_1}{r} + C_2 \quad (6.13)$$

C_1 and C_2 are the integration constants.

To determine these integration constants, boundary conditions should be put forward. These are;

- When r equals to infinity;

$$n_1(\infty) = n_1$$

- When r equals to R_1+R_2 ;

$$n_1(R_1+R_2)=0$$

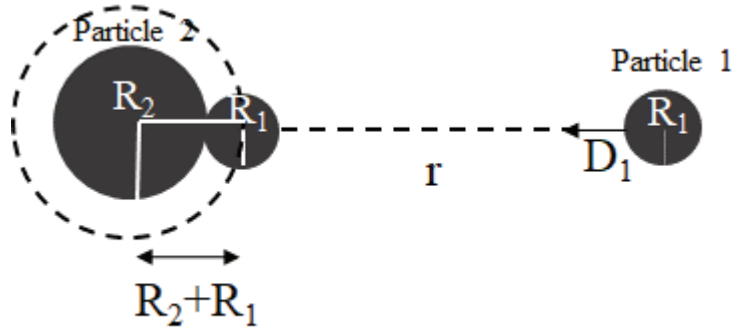


Figure 6.3. Diffusion of particle 1 towards particle 2.

Substituting these data into the general equation gives;

$$C_2 = n_1 \quad (6.14)$$

$$C_1 = n_1(R_1 + R_2) \quad (6.15)$$

Using integration constants, the general equation becomes;

$$n_1(r) = n_1 - \frac{n_1(R_1 + R_2)}{r} \quad (6.16)$$

Taking derivation of this equation according to the r gives;

$$\frac{dn_1(r)}{dr} = \frac{n_1(R_1 + R_2)}{r^2} \quad (6.17)$$

Substituting this equation into the Fick's 1st law Equation (6.4) yields;

$$J(r) = -D_1 \frac{n_1(R_1 + R_2)}{r^2} \quad (6.18)$$

When two particles having diameter of R_1 and R_2 come closer with a distance of R_1+R_2 (at contact point), the flux becomes as;

$$J(R_1 + R_2) = -D_1 \frac{n_1(R_1 + R_2)}{(R_1 + R_2)^2} \quad (6.19)$$

$$J(R_1 + R_2) = -D_1 \frac{n_1}{(R_1 + R_2)} \quad (6.20)$$

The negative sign indicates that particles 1 are transported towards particle 2.

The collision rate of particles 1 with a single stationary particles 2 at a distance of R_1+R_2 surface can be written as;

$$Z_1 = |J(R_1 + R_2)|4\pi(R_1 + R_2)^2 \quad (6.21)$$

$$Z_1 = 4\pi D_1 n_1(R_1 + R_2) \quad (6.22)$$

If the collisions are taking place with n_2 number of particles 2 who may also diffuse towards particles 1, Equation 6.22 becomes as;

$$Z_{12} = 4\pi D_{12} (R_1 + R_2)n_1 n_2 \quad (6.23)$$

Equation 6.23 gives the number of n_1 particles colliding with n_2 particles per second.

If the true probability of every collision producing an aggregate of particles 1 and 2, then the rate of reduction of the number of particles 1 per time is given as;

$$\frac{dn_1(t)}{dt} = -KZ_{12} \quad (6.24)$$

$$\frac{dn_1(t)}{dt} = -4\pi K D_{12} (R_1 + R_2)n_1 n_2 \quad (6.25)$$

Replacing the effective diffusion coefficient D_{12} in the rate equation gives;

$$\frac{dn_1(t)}{dt} = -4\pi K \frac{kT}{6\pi\mu} \left(\frac{1}{R_1} + \frac{1}{R_2}\right)(R_1 + R_2)n_1 n_2 \quad (6.26)$$

$$\frac{dn_1(t)}{dt} = -K \frac{2kT}{3\mu} \frac{(R_1 + R_2)^2}{R_1 R_2} n_1 n_2 \quad (6.27)$$

If R_2 reasonably larger than R_1 ($R_2 \gg R_1$), equation 6.27 can be safely approximated to;

$$\frac{dn_1(t)}{dt} = -K \frac{2kT}{3\mu} \left(2 + \frac{R_2}{R_1}\right) n_1 n_2 \quad (6.28)$$

Where

n_1 : Number concentration ($1/m^3$)

n_2 : Number concentration ($1/m^3$)

K : True probability of each collision yielding a reaction

kT : Thermal energy at temperature T (Joule)

- μ : Viscosity of the medium where collisions take place (kg/m sec)
- R_1 : Radius of particles 1 (m)
- R_2 : Radius of particles 2 (m)

Justification of approximating $\frac{(R_1+R_2)^2}{R_1R_2}$ with $\left(2 + \frac{R_2}{R_1}\right)$ is presented in Figure 6.4.

It can be seen that the two equations become nearly equal when R_2 becomes even slightly larger than R_1 .

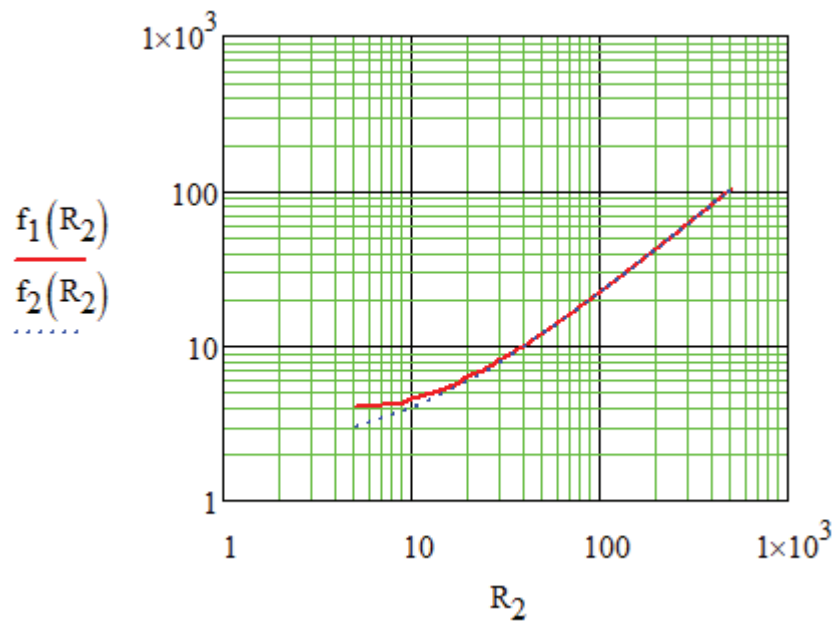


Figure 6.4. Approximation of $\frac{(R_1+R_2)^2}{R_1R_2}$ ($f_1(R_2)$) and $\left(2 + \frac{R_2}{R_1}\right)$ ($f_2(R_2)$) for different radii.

Equation 6.28 gives a general rate expression for the reduction in the number of R_1 in bulk with collisions of particles of R_2 such that each collision produces an aggregate according to a true probability constant K under diffusion.

6.3. Hydrolysis of TEOS with No Condensation and No Aggregation

The rate of TEOS hydrolysis can be modeled by the collisions of the free OH^- ions with the TEOS monomers such that each collision has the true probability K_1 to produce

a hydrolyzed arm in monomeric species. Then, using Equation 6.28, it can be written for the unhydrolyzed TEOS species that;

$$\frac{dn_{T0}}{dt} = -K_1 \frac{2kT}{3\mu} \left(2 + \frac{R_T}{R_{OH}} \right) n_{T0} n_{OH} \quad (6.29)$$

Where;

n_{T0} : Number concentration of unhydrolyzed TEOS monomers in solution (1/m³)

R_T : Radius of unhydrolyzed TEOS monomer (0.360 nm)

R_{OH} : Radius of free OH⁻ ion (0.110 nm) (Marcus, 2012)

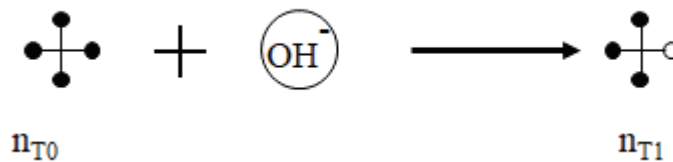
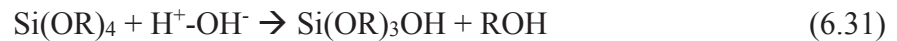
n_{OH} : Number concentration of free OH⁻ ions in solution (1/m³)

The radius R_T is given in literature (Dixit et al., 2016) as 0.475 nm from silanization models. The radius can also be estimated from;

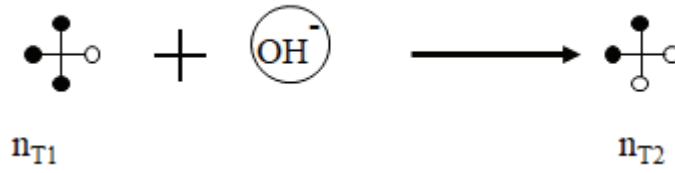
$$R_T = \frac{1}{2} \left(\frac{\rho_T N_{av}}{M_{wT}} \right)^{-1/3} = 3.6 \times 10^{-10} m \quad (6.30)$$

Where ρ_T is the bulk density of TEOS (933 kg/m³), M_{wT} is the molecular weight of TEOS (208 g/mol).

Note that the unhydrolyzed TEOS species, n_{T0} , hydrolyze by free OH⁻ ions through reaction given in 6.31 to produce TEOS monomers n_{T1} . By definition n_{T0} is not generated but only consumed during hydrolysis reactions.



The n_{T1} species created by reaction 6.31 are also consumed by hydrolysis through free OH⁻ in the system to produce n_{T2} such that;

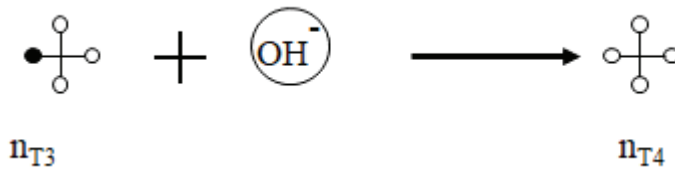
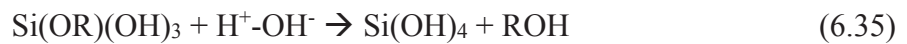
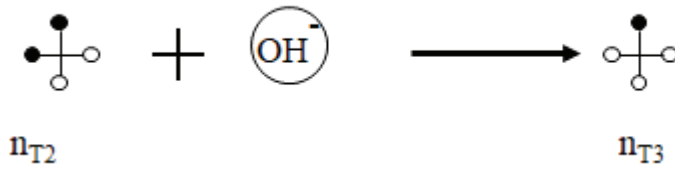


The rate reaction for the hydrolysis of n_{T1} can be given as;

$$\frac{dn_{T1}}{dt} = +K_1 \frac{2kT}{3\mu} \left(2 + \frac{R_T}{R_{OH}}\right) n_{T0} n_{OH} - K_1 \left(\frac{3}{4}\right) \frac{2kT}{3\mu} \left(2 + \frac{R_{T1}}{R_{OH}}\right) n_{T1} n_{OH} \quad (6.33)$$

The factor $\frac{3}{4}$ comes because the monomer n_{T1} has only three OR which can be hydrolyzed out of the four possible hydrolysis sites on the TEOS molecule.

Similar hydrolysis expressions can be written for TEOS monomers n_{T2} , n_{T3} and n_{T4} such that;



Where n_{T4} is a completely hydrolyzed TEOS monomer. The rate expressions for n_{T2} , n_{T3} and n_{T4} are;

$$\frac{dn_{T2}}{dt} = +K_1 \left(\frac{3}{4}\right) \frac{2kT}{3\mu} \left(2 + \frac{R_{T1}}{R_{OH}}\right) n_{T1} n_{OH} - K_1 \left(\frac{2}{4}\right) \frac{2kT}{3\mu} \left(2 + \frac{R_{T2}}{R_{OH}}\right) n_{T2} n_{OH} \quad (6.36)$$

$$\frac{dn_{T3}}{dt} = +K_1 \left(\frac{2}{4}\right) \frac{2kT}{3\mu} \left(2 + \frac{R_{T2}}{R_{OH}}\right) n_{T2} n_{OH} - K_1 \left(\frac{1}{4}\right) \frac{2kT}{3\mu} \left(2 + \frac{R_{T3}}{R_{OH}}\right) n_{T3} n_{OH} \quad (6.37)$$

$$\frac{dn_{T4}}{dt} = +K_1 \left(\frac{1}{4}\right) \frac{2kT}{3\mu} \left(2 + \frac{R_{T3}}{R_{OH}}\right) n_{T3} n_{OH} \quad (6.38)$$

Note that n_{T4} species only appear in the system in this case since no condensation between the hydrolyzed monomers is allowed.

Since above equations only deal with hydrolysis of TEOS monomers and no condensation is allowed, through the number of individual monomers change, total number of monomers in solution, n_m remains equal to the initial number of TEOS molecules in solution, n_T such that:

$$n_m = n_T = n_{T0} + n_{T1} + n_{T2} + n_{T3} + n_{T4} \quad (6.39)$$

It is also true that assuming steady-state approximation as;

$$\frac{d}{dt} (n_{T0} + n_{T1} + n_{T2} + n_{T3} + n_{T4}) = \frac{dn_T}{dt} = 0 \quad (6.40)$$

For hydrolysis of TEOS, assuming no other reactions such as condensation into oligomers or aggregation of oligomers into nuclei take place and for constant n_{OH} in solution, Equation 6.29 can be written as;

$$\frac{dn_{T0}}{dt} = - \left[K_1 \frac{2kT}{3\mu} \left(2 + \frac{R_T}{R_{OH}}\right) n_{OH} \right] n_{T0} \quad (6.41)$$

If it is assumed that the radii of all the monomeric species are approximately the same and constant ($R_T \sim R_{T1} \sim R_{T2} \sim R_{T3} \sim R_{T4} = \text{constant}$), the term $\left[K_1 \frac{2kT}{3\mu} \left(2 + \frac{R_T}{R_{OH}}\right) n_{OH} \right]$ also becomes a constant. If it is named as the rate constant κ , it follows that the disappearance of the n_{T0} species follows a first-order rate equation;

$$\frac{dn_{T0}}{n_{T0}} = -\kappa dt \quad (6.42)$$

$$\ln(n_{T0}) = -\kappa t + C_1 \quad (6.43)$$

n_{T0} should equal to n_T initially at time=0. So the integral constant C_1 is $\ln(n_T)$ and the equation become as;

$$n_{T0} = n_T e^{-\kappa t} \quad (6.44)$$

Here, n_T is the initial TEOs monomer concentration in solution in the beginning of synthesis.

Similarly, placing the functional form of n_{T0} in Equation 6.44 into equation 6.33 allows for a solution for n_{T1} . Continuing this procedure allows that the system be solved for n_{T1} , n_{T2} , n_{T3} and n_{T4} with following expressions using the boundary condition that n_{T1} , n_{T2} , n_{T3} and n_{T4} are all equal to zero initially at time $t=0$;

$$n_{T1} = 4n_T e^{-\kappa t} \left(e^{\frac{\kappa t}{4}} - 1 \right) \quad (6.45)$$

$$n_{T2} = 6n_T e^{-\kappa t} \left(e^{\frac{\kappa t}{4}} - 1 \right)^2 \quad (6.46)$$

$$n_{T3} = 4n_T e^{-\kappa t} \left(e^{\frac{\kappa t}{4}} - 1 \right)^3 \quad (6.47)$$

$$n_{T4} = n_T e^{-\kappa t} \left(e^{\frac{\kappa t}{4}} - 1 \right)^4 \quad (6.48)$$

where κ is a true rate constant with units 1/sec such that:

$$\kappa = K_1 \frac{2kT}{3\mu} \left(2 + \frac{R_T}{R_{OH}} \right) n_{OH} \quad (6.49)$$

Note that the sum of all monomeric species should be constant and equal to the initial TEOS concentration such that;

$$n_{T0} + n_{T1} + n_{T2} + n_{T3} + n_{T4} = n_T \quad (6.50)$$

The Mathcad solution of these equations are given in Appendix B and the change in the number of monomeric species is shown in Figure 6.5 for the absence of any condensation reactions. It can be seen that all the n_{T0} monomers which are initially at a concentration n_T convert to n_{T4} monomers at the end of the reaction period where n_{T1} , n_{T2} and n_{T3} are intermediate species which are eventually consumed in the hydrolysis

reactions. It should be noted that assigning different molecular radii for the monomeric species n_{T0} , n_{T1} , n_{T2} , n_{T3} , and n_{T4} with different degrees of hydrolysis did not cause any appreciable change in the behavior of these species.

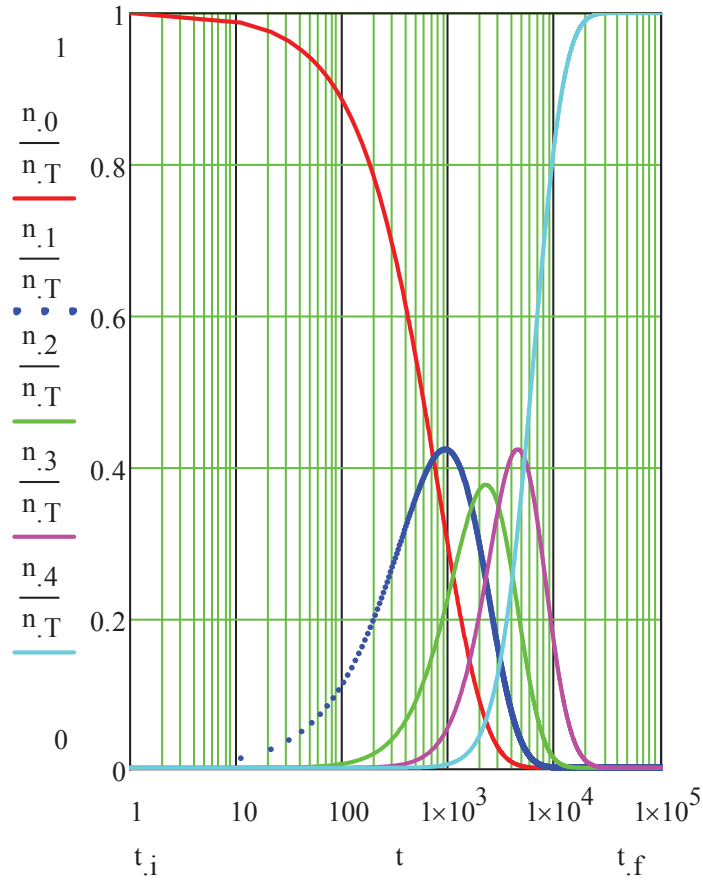


Figure 6.5. Changes in the number of monomers as a function of time.

Equations 6.41 and 6.42 show that the hydrolysis of TEOS (in the absence of any condensation reactions) is a first order reaction such that κ is a rate constant with unit of 1/sec. From the literature, the rate of disappearance of unhydrolyzed TEOS (n_{T0}) is given as 0.0754 (1/min) (Chen et al., 1996). This information allows us to calculate the true probability constant K_1 for the above system for any specific ammonia concentration such that;

$$\kappa = 0.0754 \left(\frac{1}{min} \right) = K_1 \frac{2kT}{3\mu} \left(2 + \frac{R_T}{R_{OH}} \right) n_{OH}$$

For an ammonia concentration of 1.00 mol/L, $K_1 = 1.453 \times 10^{-13} \text{ s}^{-1}$.

6.4. Hydrolysis of TEOS with Condensation to Form Oligomers and No Aggregation of Oligomers

Assume that the solution is divided into n_0 number of infinitely small volumes v_0 where hydrolyzed monomers (R_T) diffuse towards and condense with a central oligomer (R_o) in each volume through OH-OH interaction. Note that the oligomer radius R_o varies with time and can grow to a specific size enforced by the number n_0 of the infinite-small volumes. Assuming for the time being that the oligomers formed in each volume v_0 , do not interact, that is, the extremely small volumes in which the central oligomer grows to a specific size can be considered as discrete micro reactors. Further note that, monomers condense into the central monomer singly, or after forming quasi oligomers; it is assumed that both condensation mechanism are similar and do not affect the overall rate of growth of the central oligomer. If the probability of actual condensation taking place for each monomer-oligomer collision through OH-OH interactions is K_2 , the rate equations for the appearance and disappearance of the monomer species R_T along with the oligomers R_o can be given as;

$$\frac{dn_{T0}}{dt} = -K_1 \frac{2kT}{3\mu} \left(2 + \frac{R_T}{R_{OH}}\right) n_{T0} n_{OH} \quad (6.51)$$

$$\frac{dn_{T1}}{dt} = -K_1 \frac{2kT}{3\mu} \left(2 + \frac{R_T}{R_{OH}}\right) n_{OH} \left[\frac{3}{4} n_{T1} - n_{T0}\right] + K_2 \left(2 + \frac{R_o}{R_T}\right) \left(\frac{1}{4} n_{T1}\right) n_o \quad (6.52)$$

$$\begin{aligned} \frac{dn_{T2}}{dt} = & -K_1 \frac{2kT}{3\mu} \left(2 + \frac{R_T}{R_{OH}}\right) n_{OH} \left[\frac{2}{4} n_{T2} - \frac{3}{4} n_{T1}\right] \\ & + K_2 \left(2 + \frac{R_o}{R_T}\right) \left(\frac{2}{4} n_{T2}\right) n_o \end{aligned} \quad (6.53)$$

$$\begin{aligned} \frac{dn_{T3}}{dt} = & -K_1 \frac{2kT}{3\mu} \left(2 + \frac{R_T}{R_{OH}}\right) n_{OH} \left[\frac{1}{4} n_{T3} - \frac{2}{4} n_{T2}\right] \\ & + K_2 \left(2 + \frac{R_o}{R_T}\right) \left(\frac{3}{4} n_{T3}\right) n_o \end{aligned} \quad (6.54)$$

$$\frac{dn_{T4}}{dt} = +K_1 \frac{2kT}{3\mu} \left(2 + \frac{R_T}{R_{OH}}\right) n_{OH} \left[\frac{1}{4} n_{T3}\right] + K_2 \left(2 + \frac{R_o}{R_T}\right) (n_{T4}) n_o \quad (6.55)$$

where R_o is the size of the central oligomer at time t , n_o is the number of oligomers. The parameter n_o is taken constant in this part since each extremely small volume eventually yields only one full grown oligomer through condensation; in other words, each oligomer grows in its own small volume and the number of oligomers n_o is the time-independent. The dimensionless constant K_2 is the probability of condensation of a monomer R_T onto a growing central oligomer R_o through water condensation alone such that;

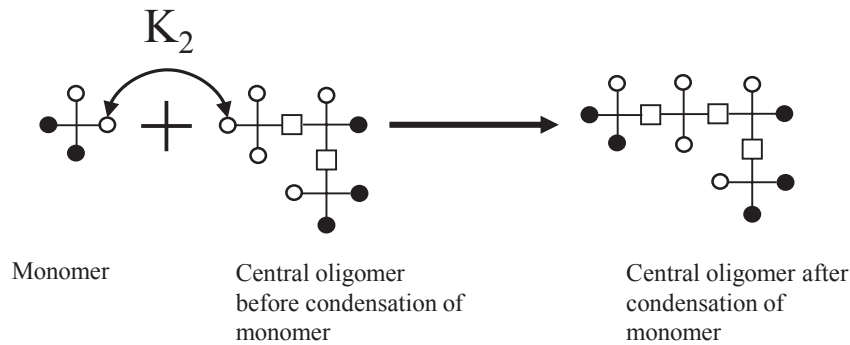


Figure 6.6. Condensation of monomers to form oligomers.

Note that alcohol condensation is ignored since it has been stated in literature that it proceeds at much slower rates than water condensation (Brinker, 1990).

The above equations 6.51 to 6.55 cannot be solved analytically, hence, numerical methods need to be employed. Also, these equations are not sufficient for solution since there are six unknowns (n_{T0} , n_{T1} , n_{T2} , n_{T3} , n_{T4} and R_o) but five equations. Therefore, one more equation needs to be set up for the oligomeric R_o species for proper solution.

If the central oligomer with the mass μ_o in each small volume collides through diffusion with a monomer of mass μ_m , its mass will increase with each successful collision by μ_m such that;

$$\frac{d\mu_o}{dt} = K_2 \frac{2kT}{3\mu} \left(2 + \frac{R_o}{R_T} \right) \left[\frac{1}{4} n_{T1} + \frac{2}{4} n_{T2} + \frac{3}{4} n_{T3} + n_{T4} \right] \mu_m \quad (6.56)$$

Equation 6.56 gives the rate at which each central oligomer grows in its own discrete volume through collisions which yield water condensation by the probability

constant K_2 . Note that various monomeric TEOS species are assumed to have the same radii R_T . The multiplication factors in front of the numbers of the monomer species denote the fraction of the OH arms which are ripe for water condensation. It is also assumed in the above equations that any left-over OR sites on the oligomers hydrolyze much faster through oligomer-free OH ions collisions compared to the monomer-oligomer condensation reactions. In other words, it is assumed that any left-over OR sites on the oligomers hydrolyze very quickly to have only OH bonds on the oligomer surfaces.

Also, it is inherent that R_o denotes an average hydrodynamic radius for the oligomers. Then, the radius R_o , the oligomer mass can be expressed as;

$$\mu_o = \frac{4}{3}\pi\rho R_o^3 \quad (6.57)$$

where ρ is the density of amorphous silica since the monomers should eventually position themselves in the oligomers to yield a final amorphous silica structure after water condensation reactions.

By similar reasoning the colliding monomers add mass μ_m to the oligomer after a successful collision such that;

$$\mu_m = 8\rho R_m^3 \quad (6.58)$$

where R_m is the radius of a TEOS monomer would occupy in the amorphous silica structure after condensation. It is assumed that the silica in monomeric form will assume a cubic shape consistent with the lattice symmetry after condensation. It can be shown that R_m would be equal to;

$$R_m = \frac{1}{2} \left(\frac{\rho N_{av}}{M_{wSiO_2}} \right)^{-1/3} = 1.81 \times 10^{-10} \text{ (nm)} \quad (6.59)$$

where ρ is the density of amorphous silica (2196 g/m³), M_{wSiO_2} is the molecular weight of amorphous silica (60 g/mole).

Combining Equation 6.56 with equations 6.57 and 6.58 gives;

$$\begin{aligned} \frac{d\mu_o}{dt} &= \frac{4}{3}\pi\rho \frac{d}{dt}(R_o^3) \\ &= K_2 \frac{2kT}{3\mu} \left(2 + \frac{R_o}{R_T} \right) \left[\frac{1}{4}n_{T1} + \frac{2}{4}n_{T2} + \frac{3}{4}n_{T3} + n_{T4} \right] 8\rho R_m^3 \end{aligned} \quad (6.60)$$

$$\frac{\pi}{3} 3R_o^2 \frac{dR_o}{dt} = K_2 \frac{2kT}{3\mu} \left(2 + \frac{R_o}{R_T} \right) \left[\frac{1}{4}n_{T1} + \frac{2}{4}n_{T2} + \frac{3}{4}n_{T3} + n_{T4} \right] 2R_m^3 \quad (6.61)$$

$$\frac{dR_o}{dt} = K_2 \frac{2kT}{3\mu} \left(\frac{2R_m^3}{\pi R_T R_o} \right) \left[\frac{1}{4} n_{T1} + \frac{2}{4} n_{T2} + \frac{3}{4} n_{T3} + n_{T4} \right] \quad (6.62)$$

Note that R_T is neglected as against R_o in the numerator of the Equation 6.62. An example solution for the equations 6.51 to 6.55 and 6.62 is given below for $K_1=1.453 \times 10^{-13}$ and $K_2=5 \times 10^{-8} \text{ s}^{-1}$ assuming that number of oligomers forming at the end of the synthesis was $2 \times 10^{-6} n_T$ ($n_T=1.505 \times 10^{26} \text{ \#/mol}$ for $C_T=0.25 \text{ M}$). The Mathcad solution is also given in Appendix C and the resulted graphs are given in Figure 6.7, Figure 6.8 and Figure 6.9.

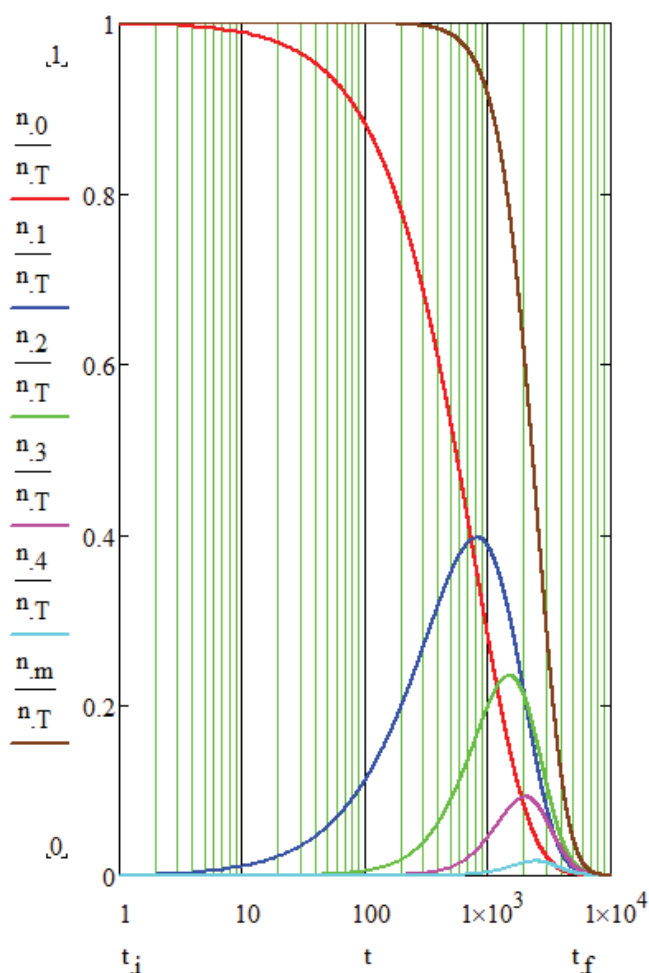


Figure 6.7. Change in the number of monomeric species with considering condensation into oligomers.

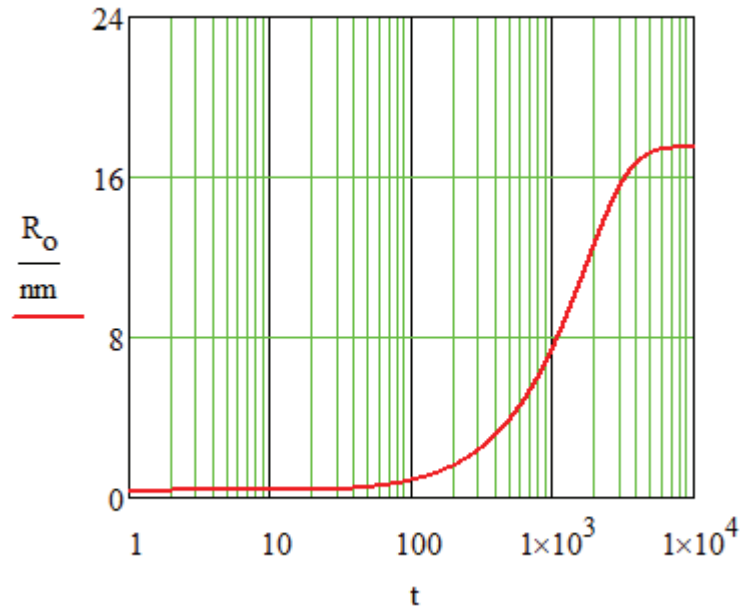


Figure 6.8. Change in the oligomer radius as a function of time when oligomers do not interact with each other.

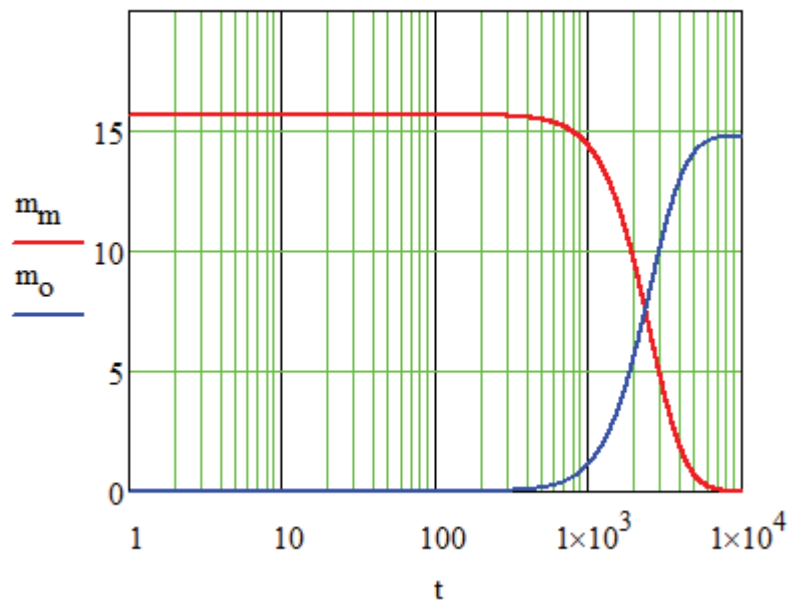


Figure 6.9. Change in the mass of monomers and oligomers with respect to time.

It can be seen that the oligomer size grows to about 18 nm and 3.01×10^{20} (#/m³) oligomers are generated at the end of the synthesis. It should be noted that the oligomer in each infinite small discrete volume do not interact with each other but only collect the

hydrolyzing monomers through diffusion. Interaction of the oligomers through OH-OH condensation (water condensation) which leads to formation of nuclei and to eventual final particles will be discussed in the next section.

6.5. Hydrolysis of TEOS with Condensation to Form Oligomers and Aggregation of Oligomers to Form Final Particles

In the previous section, it was assumed that hydrolyzed monomers can condense through OH-OH interactions into a central oligomer in discrete infinite small volumes. The oligomers were not allowed to interact with each other such that each infinite small volume acted as a discrete reactor yielding a single mature oligomer.

However, this is an over simplification since oligomers forming may interact with other oligomers and aggregate forming nuclei which grow into particles by collecting other oligomers and monomer existing in solution. To model such system, it can be assumed that the oligomers, R_o , forming as explained in the previous section in infinite small volumes, v_o , may also diffuse towards a central oligomer in a microvolume v_a such that $v_a \gg v_o$ and aggregate to form a single nuclei which grows into a final particle in each v_a .

The microvolume v_a must be much larger than volumes v_o but should be small enough for diffusional transport. This is the same as dividing the total solution volume into n_a number of microvolumes such that each microvolume, which consist of large number of infinite small oligomer-forming volumes, v_o , produces a single final particle. In other words, n_a is also the number of the final particles after synthesis and is experimentally determinable value such that $n_a = V/v_a$. The conceptual representation of such system and the description of the species pertinent to this concept were described Section 6.1 and in Figure 6.1.

It must be noted that while v_o is an arbitrary, experimentally determined parameter, v_a is determined by the number n_a of the final particle population such that $n_a = V/v_a$ which can be easily obtained by observation.

Since n_a , hence, v_a are determined by the product characteristics and each v_a produces a single final particle, R_a , the model enforces that R_a particles do not aggregate.

Each R_a grows from a central oligomer by monomer addition plus oligomer aggregation but R_a particles themselves are not allowed to aggregate. This is a reasonable assumption considering the fact that the energy barrier grows exponentially with particle size as was shown in Figure 4.23.

The rate equations for the TEOS monomers modified to include the oligomer aggregation take the following forms:

$$\frac{dn_{T0}}{dt} = -K_1 \frac{2kT}{3\mu} \left(2 + \frac{R_T}{R_{OH}}\right) n_{T0} n_{OH} \quad (6.63)$$

$$\begin{aligned} \frac{dn_{T1}}{dt} = & -K_1 \frac{2kT}{3\mu} \left(2 + \frac{R_T}{R_{OH}}\right) n_{OH} \left[\frac{3}{4} n_{T1} - n_{T0}\right] \\ & + K_2 \left(\frac{1}{4} n_{T1}\right) \left[\left(2 + \frac{R_o}{R_T}\right) n_o + \left(2 + \frac{R_a}{R_T}\right) n_a\right] \end{aligned} \quad (6.64)$$

$$\begin{aligned} \frac{dn_{T2}}{dt} = & -K_1 \frac{2kT}{3\mu} \left(2 + \frac{R_T}{R_{OH}}\right) n_{OH} \left[\frac{2}{4} n_{T2} - \frac{3}{4} n_{T1}\right] \\ & + K_2 \left(\frac{2}{4} n_{T2}\right) \left[\left(2 + \frac{R_o}{R_T}\right) n_o + \left(2 + \frac{R_a}{R_T}\right) n_a\right] \end{aligned} \quad (6.65)$$

$$\begin{aligned} \frac{dn_{T3}}{dt} = & -K_1 \frac{2kT}{3\mu} \left(2 + \frac{R_T}{R_{OH}}\right) n_{OH} \left[\frac{1}{4} n_{T3} - \frac{2}{4} n_{T2}\right] \\ & + K_2 \left(\frac{3}{4} n_{T3}\right) \left[\left(2 + \frac{R_o}{R_T}\right) n_o + \left(2 + \frac{R_a}{R_T}\right) n_a\right] \end{aligned} \quad (6.66)$$

$$\begin{aligned} \frac{dn_{T4}}{dt} = & +K_1 \frac{2kT}{3\mu} \left(2 + \frac{R_T}{R_{OH}}\right) n_{OH} \left[\frac{1}{4} n_{T3}\right] \\ & + K_2 n_{T4} \left[\left(2 + \frac{R_o}{R_T}\right) n_o + \left(2 + \frac{R_a}{R_T}\right) n_a\right] \end{aligned} \quad (6.67)$$

It can be seen that there are five differential equations for the five monomer species. However, the above equations also include terms for R_o and R_a species (R_o , R_a , n_o , n_a). The model assumes that n_a is known. Also, if we know m_a , we can calculate m_o from the mass balance using the known (calculated) mass of the monomeric species m_m at each time. Calculating m_o will allow an estimation of R_o if n_o is known. Therefore, writing two new equations for m_a and n_o would suffice.

The number of oligomers is determined by v_o and maximum at the beginning of the synthesis and only decreases due to aggregation of the oligomers to the central

oligomer in v_a to form the nuclei which grow into particles. Note that monomer condensation to enlarge the R_o oligomers do not change their number. In short, n_o decreases with time only due to diffusion of the oligomers to the central oligomer in v_a and following aggregation. Then it can be written that,

$$\frac{dn_o}{dt} = -\alpha K_2 \left(1 + \frac{R_a}{R_o}\right) n_o n_a \quad (6.68)$$

Where R_a is the nucleus (or the central oligomer) in each v_a growing into a R_a particle with time with aggregation of R_o oligomers. The probability of aggregation in this case is given as K_2 since the aggregation should take place due to OH-OH bonding.

The other rate equation can be written for the rate of change of mass of the R_a particles such that;

$$\frac{dm_a}{dt} = \alpha K_2 \left[\left(1 + \frac{R_a}{R_o}\right) n_o \mu_o n_a + \left(1 + \frac{R_a}{R_T}\right) \mu_m n_a \left[\frac{1}{4} n_{T1} + \frac{2}{4} n_{T2} + \frac{3}{4} n_{T3} + n_{T4} \right] \right] \quad (6.69)$$

Note that $\mu_m = 8\rho R_m^3$ and $\mu_o = 4/3\pi\rho R_o^3$ and each collision of R_o oligomer with R_a adds a mass of μ_o to mass m_a and each collision of R_T oligomer add a mass of μ_m to mass m_a .

An example solution of the above equations is presented below assuming stability factor $w=1$ for the time being and the detailed solution was given in Appendix D and in Figure 6.10 and Figure 6.11.

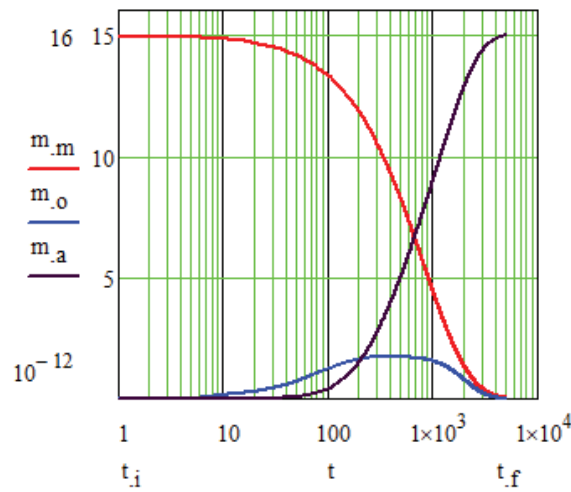


Figure 6.10. Change in the mass of monomers, oligomers and aggregated particles with time.

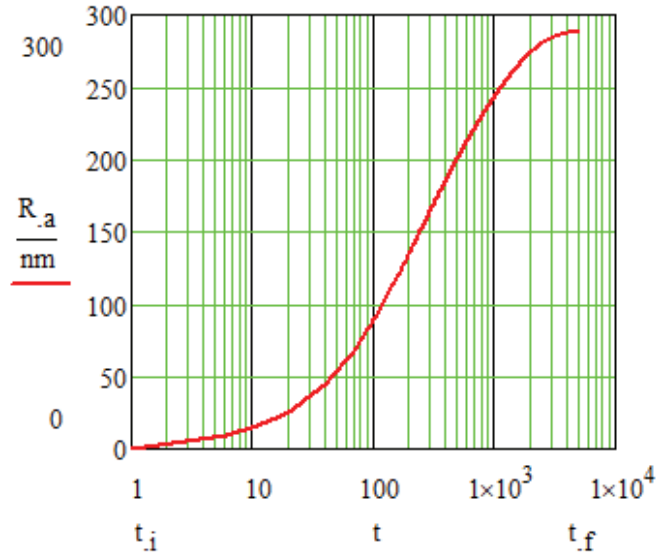


Figure 6.11. Change in the final particle radius with time

Since K_1 is known from the literature, the parameters n_0 and K_2 should be adjusted to fit the experimental data. In short, the above model requires only two parameters to be determined experimentally. In the figure below (Figure 6.12), the change in the size of the particles observed during the synthesis (symbols) carried out with (0.25 M TEOS, 11.67 M H_2O , 12.14 M EtOH, 1.09 M NH_3) are shown. The fitted curve gives $n_0 = 3.01 \times 10^{21}$ ($2 \times 10^{-5} n_T$) and $K_2 = 1.9 \times 10^{-3} \text{ s}^{-1}$ for the test conditions mentioned.

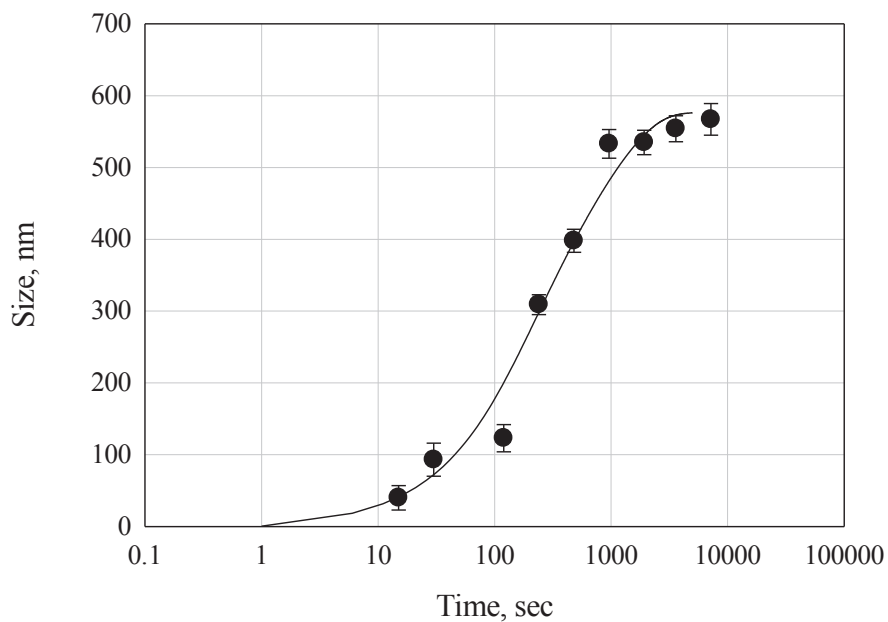


Figure 6.12. Comparison of experimental data with the model.

The TEM picture taken from the 2 mins of the reaction is shown in Figure 6.13. According to the results, it can be clearly seen that final particles consist of smaller components (termed as the R_o particles, large oligomers or initial nuclei in the model). This kind of structure was observed in all the particles which reached maturation. The TEM pictures show that the R_o particles have sizes around 10 nm in diameter. The R_o particles aggregate to form R_a particles while the monomer condensation on both R_o and R_a continues along with the monomers on final nuclei contributing particle growth. The TEM results can be inserted in the model to calculate the initial number of R_o particles n_{o0} . In other words, the parameters n_{o0} is an experimentally determined number. The calculations show that n_{o0} for our experimental conditions comes out to be $2 \times 10^{-5} n_T$. The calculation given on the previous paragraphs have used this number as input for n_{o0} .

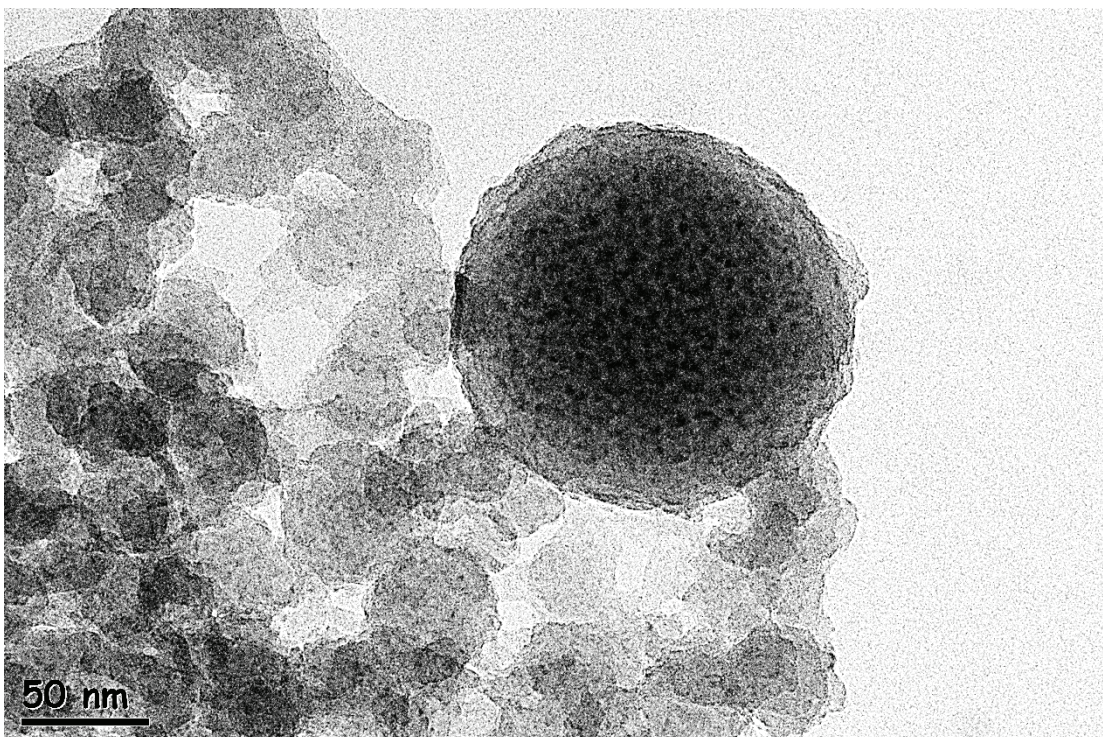


Figure 6.13. TEM images of SNPs after 2 mins of the synthesis

As can be seen, our model works properly. According to our model, monomers are diffuse into the oligomers and oligomers are aggregated to form aggregated particles which will further grow by oligomer or monomer addition. Here, aggregated particles are behave as collector nuclei which gather monomers and oligomers in critical

microvolumes. Based on the DLVO theory, it is reasonable to assume aggregated particles cannot come together because of the surface charge they carry as shown in Figure 6.14. The theory predicts that the activation barrier to aggregation increases linearly with the size of two equal particles. Smaller particles however, will aggregate with larger ones at a much higher rate (Hench, 1998). In the above case only a limited number of nuclei can grow and pick up other nuclei while preys. Then, at the end the number of particles (or number of collector nuclei) with a certain size depends on experimental conditions. This concept is thought to be fits all our results and quite different in principle than other pathway suggested in literature.

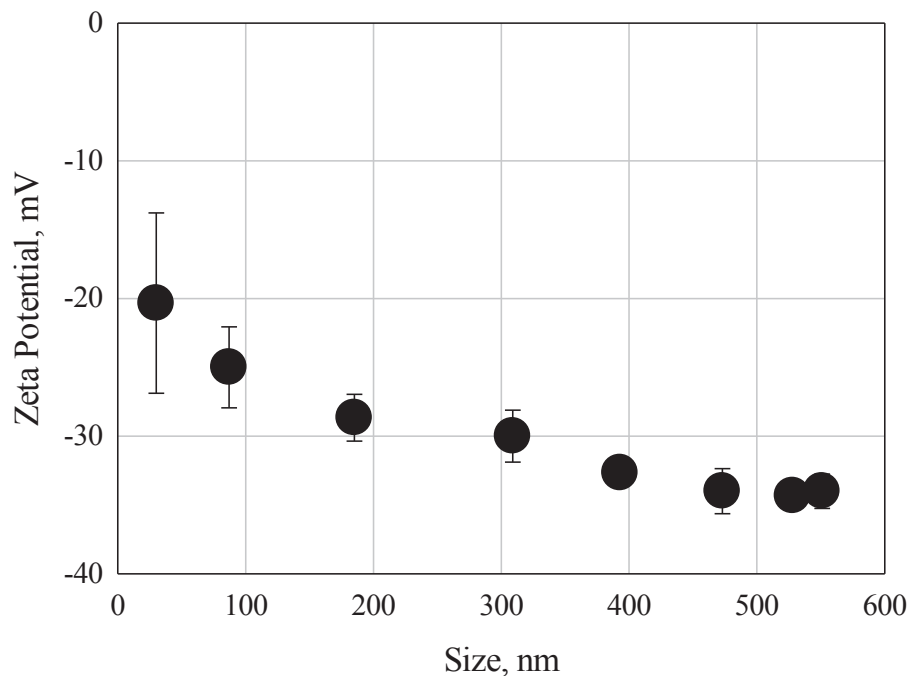


Figure 6.14. Zeta potential of particles as a function of size.

CHAPTER 7

SUMMARY AND CONCLUSIONS

In this thesis, SNPs were synthesized via Stöber method under well controlled conditions and the effect of experimental parameters on size and growth of particles has been studied in detail. It is clear that by controlling the process parameters such as TEOS concentration and addition rate, water amount or H₂O/Si molar ratio and concentration of catalyst, it is possible to vary the structure and properties of sol-gel SNPs over wide ranges. However, there has not been a general agreement on the processes responsible for the silica particle formation and growth. Most models depend on whether silica growth occurred through either monomer addition or aggregation of nuclei/sub particles. The nucleation period was also a contentious subject among the models, some of them suggested nuclei formed continuously throughout the reaction while others proposed significant nucleation only occurred for a short period after reaction initiation. Overall, current understanding of process suggests that reaction conditions are the deciding factor as to which model best represents particle formation for a particular system.

In this study, it has been shown that by controlling the process parameters such as TEOS concentration, and rate of TEOS addition, the amount of water, concentration of catalyst as well as the agitation intensity, it is possible to vary the size and distribution of Stöber SNPs over wide ranges. According to the findings of the study;

1. Solid silica particles of desired mean particle size and size distribution can be obtained through variation of process parameters and electrolytes. The final particle size characteristics were influenced by;
 - *NH₃ concentration* because its increase facilitated hydrolysis and condensation reactions that provide reduced induction period which results in fewer and larger particles.
 - *TEOS concentration* since increasing TEOS concentration does not change the number of final aggregated particle, but increased the final size of SNPs because the amount of TEOS is collected by collector or central nuclei is much in the case of high TEOS concentration.

- *TEOS addition rate* since the rate of TEOS addition influenced the number of nuclei formed which potentially grow into final particles. Direct addition of TEOS created smaller particles with narrow size distribution, whereas continuous addition created larger particles with wide size distribution.
 - *Addition of electrolytes* since the presence of an electrolyte led to enhanced particle aggregation because of the depression of electrical double layer. *Addition of seed particles* such that with increasing seed concentration secondary nucleation can be depressed and system forced to have mono-size distribution. Therefore, the seed amount not only influences the final mean particle size but also the size distributions of final particles. At lower seed concentration multi-sized solid particles will be obtained, however at high seed concentration distribution changed to mono-sized.
2. A mathematical model was developed to describe the time-change of the particle size during synthesis which can shed light on particle nucleation and growth mechanisms. According to the concept of the model, hydrolyzed monomers diffuse and condense with a central oligomer through condensation and oligomers aggregate with each other forming central nuclei which grow into final particles in isolated micro volumes by collecting other oligomers or monomers present in the solution. The model quite smoothly predicts the growth of SNPs compared to experimental findings. In the model, hydrolysis rate of TEOS is obtained from the literature for similar experimental conditions, allowing the condensation rate, which is lacking in the literature, to be determined by fitting the model to experimental data.

REFERENCES

- Abdelaal, H. M.; Zawrah, M. F.; Harbrecht, B. Facile one-pot fabrication of hollow porous silica nanoparticles. *Chem-A Eur. J.* **2014**, *20* (3), 673–677. <https://doi.org/10.1002/chem.201303656>.
- Bailey, J. K., & Mecartney, M. L. Formation of colloidal silica particles from alkoxides. *Colloids and Surf.* 1992, *63*(1-2), 151-161. [https://doi.org/10.1016/0166-6622\(92\)80081-C](https://doi.org/10.1016/0166-6622(92)80081-C).
- Barrabino, A. Synthesis of mesoporous silica particles with control of both pore diameter and particle size. *Master of Science Thesis in Materials and Nanotechnology Program, Chalmers University of Technology, Sweden* **2011**, 1–63.
- Beganskienė, A.; Sirutkaitis, V.; Kurtinaitienė, M.; Juškėnas, R.; Kareiva, A. FTIR, TEM and NMR investigations of Stöber silica nanoparticles. *Mater. Sci.* **2004**, *10* (4), 287–290.
- Bergna, H. E., Bergna, W. O. R., Roberts, W. O. Colloidal silica: fundamentals and applications. *Int. J. Numer. Methods Fluids.* **2003**, *41* (1), 1–1. <https://doi.org/10.1002/fld.463>.
- Bogush, G. H., Tracy, M.A., Zukoski, C. F. Preparation of monodisperse silica particles: control of size and mass fraction. *J. Non. Cryst. Solids* **1988**, *104*, 95–106. [https://doi.org/10.1016/0022-3093\(88\)90187-1](https://doi.org/10.1016/0022-3093(88)90187-1).
- Bogush, G. H.; Zukoski IV, C. F. Studies of the kinetics of the precipitation of uniform silica particles through the hydrolysis and condensation of silicon alkoxides. *J. Colloid Interface Sci.* **1991**, *142* (1), 1–18. [https://doi.org/10.1016/0021-9797\(91\)90029-8](https://doi.org/10.1016/0021-9797(91)90029-8).
- Bogush, G. H.; Zukoski IV, C. F. Uniform silica particle precipitation: an aggregative growth model. *J. Colloid Interface Sci.* **1991**, *142* (1), 19–34. [https://doi.org/10.1016/0021-9797\(91\)90030-C](https://doi.org/10.1016/0021-9797(91)90030-C).
- Bonacchi, S.; Genovese, D.; Juris, R.; Montalti, M.; Prodi, L.; Rampazzo, E.; Zaccheroni, N. Luminescent silica nanoparticles: extending the frontiers of brightness. *Angew. Chemie - Int. Ed.* **2011**, *50* (18), 4056–4066. <https://doi.org/10.1002/anie.201004996>.

- Branda, F.; Silvestri, B.; Luciani, G.; Costantini, A. The effect of mixing alkoxides on the stöber particles size. *Colloids Surfaces A Physicochem. Eng. Asp.* **2007**, *299* (1–3), 252–255. <https://doi.org/10.1016/j.colsurfa.2006.11.048>.
- Brinker, C.J.; Hydrolysis and condensation of silicates: effects on structure. *J. Non-Cryst. Solids* **1988**, *100* (c), 31–50. [https://doi.org/10.1016/0022-3093\(88\)90005-1](https://doi.org/10.1016/0022-3093(88)90005-1).
- Brinker, C.J.; Scherer, G.W. Sol-Gel Science: The physics and chemistry of sol-gel processing. *Academic Press*. **1990**, p 462. <https://doi.org/10.1186/1471-2105-8-444>.
- Buining, P.; Liz-Marzan, L. M.; Philipse, A. P. A Simple preparation of small, smooth silica spheres. *J. Colloid Interface Sci.* **1996**, *179* (179), 318–321. <https://doi.org/10.1006/jcis.1996.0220>.
- Buyukserin, F.; Altuntas, S.; Aslim, B. Fabrication and modification of composite silica nano test tubes for targeted drug delivery. *RSC Adv.* **2014**, *4* (45), 23535–23539. <https://doi.org/10.1039/c4ra00871e>.
- Carcouët, C. C. M. C.; Van De Put, M. W. P.; Mezari, B.; Magusin, P. C. M. M.; Laven, J.; Bomans, P. H. H.; Friedrich, H.; Esteves, A. C. C.; Sommerdijk, N. A. J. M.; Van Benthem, R. A. T. M.; et al. Nucleation and growth of monodisperse silica nanoparticles. *Nano Lett.* **2014**, *14* (3), 1433–1438. <https://doi.org/10.1021/nl404550d>.
- Chang, M. S.; Lee, M.; Kim, W. S. Preparation of large monodispersed spherical silica particles using seed particle growth. *J. Colloid Interface Sci.* **2005**, *286* (2), 536–542. <https://doi.org/10.1016/j.jcis.2005.01.059>.
- Chen, S.L.; Dong, P.; Yang, G.-H.; Yang, J.-J. Characteristic aspects of formation of new particles during the growth of monosize silica seeds. *J. Colloid Interface Sci.* **1996**, *180* (1), 237–241. <https://doi.org/10.1006/jcis.1996.0295>.
- Chen, S. L.; Dong, P.; Yang, G. H.; Yang, J. J. Kinetics of formation of monodisperse colloidal silica particles through the hydrolysis and condensation of tetraethylorthosilicate. *Ind. Eng. Chem. Res.* **1996**, *35* (12), 4487–4493. <https://doi.org/10.1021/ie9602217>.
- Chen, Q.; Friman, M.; Vilonen, K.; Hannula, S. The control of size and surface morphology of silica microspheres by sol-gel emulsion. *Suranaree J. Sci. Technol.* **2013**, *20* (2), 89–98.

- Chieruzzi, M.; Miliozzi, A.; Crescenzi, T.; Torre, L.; Kenny, J. M. A new phase change material based on potassium nitrate with silica and alumina nanoparticles for thermal energy storage. *Nanoscale Res. Lett.* **2015**, *10* (1).
<https://doi.org/10.1186/s11671-015-0984-2>.
- Cho, K.; Chang, H.; Kil, D. S.; Park, J.; Jang, H. D.; Sohn, H. Y. Mechanisms of the formation of silica particles from precursors with different volatilities by flame spray pyrolysis. *Aerosol Sci. Technol.* **2009**, *43* (9), 911–920.
<https://doi.org/10.1016/j.apsusc.2012.03.102>.
- Chou, K. Sen; Chen, C. C. The critical conditions for secondary nucleation of silica colloids in a batch Stöber growth process. *Ceram. Int.* **2008**, *34* (7), 1623–1627.
<https://doi.org/10.1016/j.ceramint.2007.07.009>.
- Ciriminna, R.; Sciortino, M.; Alonzo, G.; De Schrijver, A.; Pagliaro, M. From molecules to systems: sol-gel microencapsulation in silica-based materials. *Chem. Rev.* **2011**, *111* (2), 765–789. <https://doi.org/10.1021/cr100161x>.
- Dabbaghian, M. A.; Babalou, A. A.; Hadi, P.; Jannatdoust, E. A parametric study of the synthesis of silica nanoparticles via sol-gel precipitation method. *Int. J. Nanosci. Nanotechnol.* **2010**, *6* (2), 104–113.
- Dam, B.; Pal, A. K.; Gupta, A. Nano-Fe₃O₄@silica sulfuric acid as a reusable and magnetically separable potent solid acid catalyst in biginelli-type reaction for the one-pot multicomponent synthesis of fused dihydropyrimidine derivatives: a greener nose and sfric approach. *Synth. Commun.* **2016**, *46* (3), 275–286.
<https://doi.org/10.1080/00397911.2015.1135955>.
- Dixit, C. K.; Bhakta, S.; Kumar, A.; Suib, S. L.; Rusling, J. F. Fast nucleation for silica nanoparticle synthesis using a sol-gel method. *Nanoscale* **2016**, *8* (47), 19662–19667. <https://doi.org/10.1039/C6NR07568A>.
- Dubey, R. S.; Rajesh, Y. B. R. D.; More, M. A. Synthesis and characterization of sio₂nanoparticles via sol-gel method for industrial applications. *Mater. Today Proc.* **2015**, *2* (4–5), 3575–3579. <https://doi.org/10.1016/j.matpr.2015.07.098>.
- Finnie, K. S.; Bartlett, J. R.; Barbé, C. J. A.; Kong, L. Formation of silica nanoparticles in microemulsions. *Langmuir* **2007**, *23* (6), 3017–3024.
<https://doi.org/10.1021/la0624283>.
- Fouilloux, S.; Daillant, J.; Thill, A. Single step synthesis of 5-30 nm monodisperse silica nanoparticles: important experimental parameters and modeling. *Colloids Surfaces A Physicochem. Eng. Asp.* **2012**, *393*, 122–127.
<https://doi.org/10.1016/j.colsurfa.2011.11.009>.

- Giesche, H. Synthesis of monodispersed silica powders I. particle properties and reaction kinetics. *J. Eur. Ceram. Soc.* **1994**, *14* (3), 189–204. [https://doi.org/10.1016/0955-2219\(94\)90087-6](https://doi.org/10.1016/0955-2219(94)90087-6).
- Glasgow, L. A., and J. P. Hsu. Flocculation sedimentation and consolidation, b. m. moudgil and p. somasundaran, eds., Proceedings of the Engineering Foundation Conference, Sea Island, GA. 1985
- Gorji, B, Allahgholi Ghasri, M,R, Fazaeli, R., Niksirat, N. Synthesis and characterizations of silica nanoparticles by a new sol-gel method. *J. Appl. Chem. Res.* **2012**, *6* (3), 22–26.
- Greasley, S. L.; Page, S. J.; Sirovica, S.; Chen, S.; Martin, R. A.; Riveiro, A.; Hanna, J. V.; Porter, A. E.; Jones, J. R. Controlling particle size in the stober process and incorporation of calcium. *J. Colloid Interface Sci.* **2016**, *469*, 213–223. <https://doi.org/10.1016/j.jcis.2016.01.065>.
- Green, D. L.; Jayasundara, S.; Lam, Y. F.; Harris, M. T. Chemical reaction kinetics leading to the first stober silica nanoparticles - NMR and SAXS investigation. *J. Non. Cryst. Solids* **2003**, *315* (1–2), 166–179. [https://doi.org/10.1016/S0022-3093\(02\)01577-6](https://doi.org/10.1016/S0022-3093(02)01577-6).
- Green, D. L.; Lin, J. S.; Lam, Y. F.; Hu, M. Z. C.; Schaefer, D. W.; Harris, M. T. Size, volume fraction, and nucleation of Stöber silica nanoparticles. *J. Colloid Interface Sci.* **2003**, *266* (2), 346–358. [https://doi.org/10.1016/S0021-9797\(03\)00610-6](https://doi.org/10.1016/S0021-9797(03)00610-6).
- Gustafsson, H.; Isaksson, S.; Altskär, A.; Holmberg, K. Mesoporous silica nanoparticles with controllable morphology prepared from oil-in-water emulsions. *J. Colloid Interface Sci.* **2016**, *467*, 253–260. <https://doi.org/10.1016/j.jcis.2016.01.026>.
- Habibi, D.; Vakili, S. Nano-sized silica supported FeCl₃ as an efficient heterogeneous catalyst for the synthesis of 1,2,4-triazine derivatives. *Cuihua Xuebao/Chinese J. Catal.* **2015**, *36* (4), 620–625. [https://doi.org/10.1016/S1872-2067\(15\)60829-4](https://doi.org/10.1016/S1872-2067(15)60829-4).
- Hakeem, A.; Duan, R.; Zahid, F.; Dong, C.; Wang, B.; Hong, F.; Ou, X.; Jia, Y.; Lou, X.; Xia, F. Dual stimuli-responsive nano-vehicles for controlled drug delivery: mesoporous silica nanoparticles end-capped with natural chitosan. *Chem. Commun.* **2014**, *50* (87), 13268–13271. <https://doi.org/10.1039/C4CC04383A>.
- Han, Y.; Lu, Z.; Teng, Z.; Liang, J.; Guo, Z.; Wang, D.; Han, M. Y.; Yang, W. Unraveling the growth mechanism of silica particles in the Stöber method: in situ seeded growth model. *Langmuir* **2017**, *33* (23), 5879–5890. <https://doi.org/10.1021/acs.langmuir.7b01140>.

- Harris, M. T.; Brunson, R. R.; Byers, C. H. The base-catalyzed hydrolysis and condensation reactions of dilute and concentrated TEOS solutions. *J. Non. Cryst. Solids* **1990**, *121* (1–3), 397–403. [https://doi.org/10.1016/0022-3093\(90\)90165-I](https://doi.org/10.1016/0022-3093(90)90165-I).
- He, Q.; Gao, Y.; Zhang, L.; Bu, W.; Chen, H.; Li, Y.; Shi, J. One-pot self-assembly of mesoporous silica nanoparticle-based ph-responsive anti-cancer nano drug delivery system. *J. Mater. Chem.* **2011**, *21* (39), 15190–15192. <https://doi.org/10.1039/c1jm13598h>.
- He, Q.; Shi, J. Mesoporous silica nanoparticle based nano drug delivery systems: synthesis, controlled drug release and delivery, pharmacokinetics and biocompatibility. *J. Mater. Chem.* **2011**, *21* (16), 5845. <https://doi.org/10.1039/c0jm03851b>.
- Hench, L. L. Sol-gel silica: properties, processing and technology transfer. 1st *William Andrew.1998*
- Hiemenz, P. C. Principles of colloid and surface chemistry, 3rd edition. **1986**. (Vol. 188). New York: M. Dekker.
- Huang, Y.; Pemberton, J. E. Synthesis of uniform, spherical sub-100 nm silica particles using a conceptual modification of the classic Lamer model. *Colloids Surfaces A Physicochem. Eng. Asp.* **2010**, *360* (1–3), 175–183. <https://doi.org/10.1016/j.colsurfa.2010.02.031>.
- Hyde, E. D. E. R.; Seyfaee, A.; Neville, F.; Moreno-Atanasio, R. Colloidal silica particle synthesis and future industrial manufacturing pathways: a Review. *Ind. Eng. Chem. Res.* **2016**, *55* (33), 8891–8913. <https://doi.org/10.1021/acs.iecr.6b01839>.
- Ibrahim, I. a. M.; Zikry, a. a. F.; Sharaf, M. a. Preparation of spherical silica nanoparticles: Stöber silica. *J. Am. Sci.* **2010**, *6* (11), 985–989. <https://doi.org/10.7537/marsjas061110.133>.
- Iler, R. K. The Chemistry of Silica. solubility, polymerization, colloid and surface properties, and biochemistry. John Wiley and Sons, Chichester, XXIV, 886 S., *geb, Angewandte Chemie.* **1980**, *92*(4), 328–328. <https://doi.org/10.1002/ange.19800920433>
- Innocenzi, P. The sol to gel transition e-book. *Springer.* **2016**. ISBN 978-3-319-39718-4. <https://doi.org/10.1007/978-3-319-39718-4>.

- Jarzębski, M.; Śliwa, T.; Jarzębska, M.; Szutkowski, K. Fabrication of size-tunable silica particles during seed-growth process. *Curr. Top. Biophys.* **2015**, *37* (1), 35–41. <https://doi.org/10.2478/ctb-2014-0072>.
- Jiang, X.; Tang, X.; Tang, L.; Zhang, B.; Mao, H. Synthesis and formation mechanism of amorphous silica particles via sol–gel process with tetraethylorthosilicate. *Ceram. Int.* **2019**, *45* (6), 7673–7680. <https://doi.org/10.1016/j.ceramint.2019.01.067>.
- Jin, Y.; Li, A.; Hazelton, S. G.; Liang, S.; John, C. L.; Selid, P. D.; Pierce, D. T.; Zhao, J. X. Amorphous silica nanohybrids: synthesis, properties and applications. *Coord. Chem. Rev.* **2009**, *253* (23–24), 2998–3014. <https://doi.org/10.1016/j.ccr.2009.06.005>.
- Kim, K. D.; Kim, H. T. Formation of silica nanoparticles by hydrolysis of TEOS using a mixed semi-batch/batch method. *J. Sol-Gel Sci. Technol.* **2002**, *25* (3), 183–189. <https://doi.org/10.1023/A:1020217105290>.
- Kim, S. S.; Kim, H. S.; Kim, S. G.; Kim, W. S. Effect of electrolyte additives on sol-precipitated nano silica particles. *Ceram. Int.* **2004**, *30* (2), 171–175. [https://doi.org/10.1016/S0272-8842\(03\)00085-3](https://doi.org/10.1016/S0272-8842(03)00085-3).
- Kim, T. G.; An, G. S.; Han, J. S.; Hur, J. U.; Park, B. G.; Choi, S. Communication synthesis of size controlled spherical silica nanoparticles via sol-gel process within hydrophilic solvent. **2017**, *54* (1), 49–54. <https://doi.org/10.4191/kcers.2017.54.1.10>.
- Kim, J. Y., Park, J. H., Kim, M., Jeong, H., Hong, J., Chuck, R. S., & Park, C. Y. Safety of nonporous silica nanoparticles in human corneal endothelial cells. *Scientific reports.* **2017**, *7*(1), 14566. <https://doi.org/10.1038/s41598-017-15247-2>.
- Krutovertsev, S., Tarasova, A., Ivanova, O., & Krutovertseva, L. Nanostructured doped silica films application as sensitive layers for chemical sensors. *In Adv. Mat. Res.* **2013**, *684*, 7-11. Trans Tech Publications. <https://doi.org/10.4028/www.scientific.net/AMR.684.7>.
- LaMer, V. K.; Dinegar, R. H. Theory, production and mechanism of formation of monodispersed hydrosols. *J. Am. Chem. Soc.* **1950**, *72* (11), 4847–4854. <https://doi.org/10.1021/ja01167a001>.
- Leach, W. T., Zhu, J. H., & Ekerdt, J. G. Thermal desorption effects in chemical vapor deposition of silicon nanoparticles. *J. of Cryst. Growth.* **2002**, *243*(1), 30-40. [https://doi.org/10.1016/S0022-0248\(02\)01472-0](https://doi.org/10.1016/S0022-0248(02)01472-0).

- Lee, K.; Look, J.; Harris, M.; McCormick, A. Assessing extreme models of the stober synthesis using transients under a range of initial composition. *J. Colloid Interface Sci.* **1997**, *194* (1), 78–88. <https://doi.org/10.1006/jcis.1997.5089>.
- Lee, K., Sathyagal, A. N., McCormick, A. V. A closer look at an aggregation model of the Stöber process. *Colloids and Surfaces A: Physicochemical and Engineering Aspects.* **1998**, *144*(1), 115-125. [https://doi.org/10.1016/S0927-7757\(98\)00566-4](https://doi.org/10.1016/S0927-7757(98)00566-4).
- Li, J.; Chen, L. X.; Zhang, Z. M.; Jiao, C. Bin. Synthesis and size control of monodisperse silica sol nanospheres via a modified stöber method. *Adv. Mater. Res.* **2012**, *560–561*, 462–468. <https://doi.org/10.4028/www.scientific.net/AMR.560-561.462>.
- Liang, X., Lian, L., Liu, Y., Kong, Q., & Wang, L. Controlled synthesis of monodisperse silica particles. *Micro & Nano Let.* **2016**, *11*(9), 532-534. <https://doi.org/10.1049/mnl.2016.0189>.
- Liberman, A., Mendez, N., Trogler, W. C., & Kummel, A. C. Synthesis and surface functionalization of silica nanoparticles for nanomedicine. *Surf. Sci. Reports.* **2014**, *69*(2-3), 132-158. . <https://doi.org/10.1016/j.surfrep.2014.07.001>.
- Lim, J.; Ha, S. W.; Lee, J. K. Precise size-control of silica nanoparticles via alkoxy exchange equilibrium of tetraethyl orthosilicate (TEOS) in the mixed alcohol solution. *Bull. Korean Chem. Soc.* **2012**, *33* (3), 1067–1070. <https://doi.org/10.5012/bkcs.2012.33.3.1067>.
- Lin, C.-H.; Chang, J.-H.; Yeh, Y.-Q.; Wu, S.-H.; Liu, Y.-H.; Mou, C.-Y. Formation of hollow silica nanospheres by reverse microemulsion. *Nanoscale* **2015**, *7* (21), 9614–9626. <https://doi.org/10.1039/C5NR01395J>.
- Liu, Y., Lou, C., Yang, H., Shi, M., & Miyoshi, H. Silica nanoparticles as promising drug/gene delivery carriers and fluorescent nano-probes: recent advances. *Cur. Can. Drug Tar..* **2011**, *11*(2), 156-163. <https://doi.org/10.2174/156800911794328411>.
- Liu, R. L., Xu, Y., Li, Z. H., Wu, D., Sun, Y. H., Gao, H. C., ... & Deng, F. Liquid-state Si-29 NMR study on the chemical kinetics of Stober synthesis. **2004**.
- Ma, J., Xu, Q., Zhou, J., Zhang, J., Zhang, L., Tang, H., & Chen, L. Synthesis and biological response of casein-based silica nano-composite film for drug delivery system. *Colloids and Surfaces B: Biointerfaces.* **2013**, *111*, 257-263. <https://doi.org/10.1016/j.colsurfb.2013.06.011>.

- Malay, O.; Yilgor, I.; Menciloglu, Y. Z. Effects of solvent on TEOS hydrolysis kinetics and silica particle size under basic conditions. *J. Sol-Gel Sci. Technol.* **2013**, *67* (2), 351–361. <https://doi.org/10.1007/s10971-013-3088-4>.
- Marcus, Y. Volumes of aqueous hydrogen and hydroxide ions at 0 to 200 C. *The Journal of Chem. Phys.* **2012**, *137*(15), 154501. <https://doi.org/10.1063/1.4758071>
- Masalov, V. M.; Sukhinina, N. S.; Kudrenko, E. a; Emelchenko, G. a. Mechanism of formation and nanostructure of Stöber silica particles. *Nanotechnology* **2011**, *22* (27), 275718. <https://doi.org/10.1088/0957-4484/22/27/275718>.
- Masalov, V. M., Kudrenko, E. A., Grigoryeva, N. A., Ezdakova, K. V., Roddatis, V. V., Sukhinina, N. S., ... & Emelchenko, G. A. Direct observation of the shell-like structure of SiO₂ particles synthesized by the multistage Stöber method. *Nano*, **2013**, *8*(04), 1350036. <https://doi.org/10.1142/S1793292013500367>.
- Matsoukas, T.; Gulari, E. Dynamics of growth of silica particles from ammonia-catalyzed hydrolysis of tetra-ethyl-orthosilicate. *J. Colloid Interface Sci.* **1988**, *124* (1), 252–261. [https://doi.org/10.1016/0021-9797\(88\)90346-3](https://doi.org/10.1016/0021-9797(88)90346-3).
- Matsoukas, T.; Gulari, E. Monomer-addition growth with a slow initiation step: a growth model for silica particles from alkoxides. *J. Colloid Interface Sci.* **1989**, *132* (1), 13–21. [https://doi.org/10.1016/0021-9797\(89\)90210-5](https://doi.org/10.1016/0021-9797(89)90210-5).
- Matsoukas, T.; Gulari, E. Self-sharpening distributions revisited-polydispersity in growth by monomer addition. *J. Colloid Interface Sci.* **1991**, *145* (2), 557–562. [https://doi.org/10.1016/0021-9797\(91\)90385-L](https://doi.org/10.1016/0021-9797(91)90385-L).
- Membreno, D., Smith, L., & Dunn, B. Silica sol–gel chemistry: creating materials and architectures for energy generation and storage. *J. Sol-Gel Sci. Tech.* **2014**, *70*(2), 203-215. <https://doi.org/10.1007/s10971-014-3299-3>.
- Mine, E.; Nagao, D.; Kobayashi, Y.; Konno, M. Solvent Effects on Particle Formation in Hydrolysis of Tetraethyl Orthosilicate. *J Sol-Gel Sci Technol*, **2005**, *35*(3), 197–201. <https://doi.org/10.1007/s10971-005-2289-x>.
- Mumper, R. J., Cui, Z., & Oyewumi, M. O. Nanotemplate engineering of cell specific nanoparticles. *J. Dis. Sci. Tech*, **2003**, *24*(3-4), 569-588. <https://doi.org/10.1081/DIS-120021814>.
- Nagao, D.; Satoh, T.; Konno, M. A generalized model for describing particle formation in the synthesis of monodisperse oxide particles based on the hydrolysis and condensation of tetraethyl orthosilicate. **2000**, *110*, 102–110. <https://doi.org/10.1006/jcis.2000.7195>.

- Nagao, D., Kon, Y., Satoh, T., & Konno, M. Electrostatic interactions in formation of particles from tetraethyl orthosilicate. *J. Chem. Eng. Japan*, **2000**, *33*(3), 468-473. <https://doi.org/10.1252/jcej.33.468>.
- Nakabayashi, H.; Yamada, A.; Noba, M.; Kobayashi, Y.; Konno, M.; Nagao, D. Electrolyte-added one-pot synthesis for producing monodisperse, micrometer-sized silica particles up to 7 μM . **2010**, *26* (16), 7512–7515. <https://doi.org/10.1021/la904316f>.
- Nogueira, L. S., Ribeiro, S., Granadeiro, C. M., Pereira, E., Feio, G., Cunha-Silva, L., & Balula, S. S. Novel polyoxometalate silica nano-sized spheres: efficient catalysts for olefin oxidation and the deep desulfurization process. *Dalton Trans.* **2014**, *43*(25), 9518-9528. <https://doi.org/10.1039/C3DT53444H>.
- Norazmi, F. S., Chaudhary, K. T., Mazalan, E., Hader, Z., & Ali, J. Effect of various amount of ammonium hydroxide on morphology of silica nanoparticles grown by sol-gel. *Mal. J. Fund. App. Sci.* **2018**, *14*, 482-484. <https://doi.org/10.11113/mjfas.v14n0.1278>.
- Nozawa, K.; Gailhanou, H.; Raison, L.; Panizza, P.; Ushiki, H.; Sellier, E.; Delville, J. P.; Delville, M. H. Smart control of monodisperse Stöber silica particles: effect of reactant addition rate on growth process. *Langmuir*. **2005**, *21* (4), 1516–1523. <https://doi.org/10.1021/la048569r>.
- Okudera, H., & Hozumi, A. The formation and growth mechanisms of silica thin film and spherical particles through the Stöber process. *Thin Solid Films*. **2003**, *434*(1), 62-68. [https://doi.org/10.1016/S0040-6090\(03\)00535-2](https://doi.org/10.1016/S0040-6090(03)00535-2).
- Ono, H., Takahashi, K. Preparation of silica microcapsules by sol-gel method in w/o emulsion, *J. Chem. Eng. Japan*. **1998**, *31*(5):808-812. <https://doi.org/10.1252/jcej.31.808>.
- Owens, G. J.; Singh, R. K.; Foroutan, F.; Alqaysi, M.; Han, C. M.; Mahapatra, C.; Kim, H. W.; Knowles, J. C. Sol-gel based materials for biomedical applications. *Prog. Mater. Sci.* **2016**, *77*, 1–79. <https://doi.org/10.1016/j.pmatsci.2015.12.001>.
- Pahlevanneshan, Z., Moghadam, M., Mirkhani, V., Tangestaninejad, S., Mohammadpoor-Baltork, I., & Loghmani-Khouzani, H. A new N-heterocyclic carbene palladium complex immobilized on nano silica: An efficient and recyclable catalyst for Suzuki–Miyaura C C coupling reaction. *J. Organomet. Chem.* **2016**, *809*, 31-37. <https://doi.org/10.1016/j.jorganchem.2016.02.019>.
- Park, J.; Hah, H.; Koo, S.; Lee, Y. Effect of alcohol chain length on particle growth in a mixed solvent system. *J. Ceram. Process. Res.* **2006**, *7* (1), 83–89.

- Pordal, H. S.; Matice, C. J. Multi-tiered solution technique for design, analysis and scale-up of mixing processes. *Chem. Process. Mag.* **2003**, 1–9.
- Rahman, I. A.; Vejayakumaran, P.; Sipaut, C. S.; Ismail, J.; Abu Bakar, M.; Adnan, R.; Chee, C. K. Effect of anion electrolytes on the formation of silica nanoparticles via the sol-gel process. *Ceram. Int.* **2006**, *32* (6), 691–699.
<https://doi.org/10.1016/j.ceramint.2005.05.004>.
- Rahman, I. A.; Vejayakumaran, P.; Sipaut, C. S.; Ismail, J.; Bakar, M. A.; Adnan, R.; Chee, C. K. An optimized sol-gel synthesis of stable primary equivalent silica particles. *Colloids Surfaces A Physicochem. Eng. Asp.* **2007**, *294* (1–3), 102–110. <https://doi.org/10.1016/j.colsurfa.2006.08.001>.
- Rahman, I. A.; Padavettan, V. Synthesis of silica nanoparticles by sol-gel: size-dependent properties, surface modification, and applications in silica-polymer nanocomposites a review. *J. Nanomater.* **2012**, *2012*.
<https://doi.org/10.1155/2012/132424>.
- Roca, M., and Haes, A. J. Silica– void– gold nanoparticles: temporally stable surface-enhanced raman scattering substrates. *J. Am. Chem. Soc.* **2008**, *130*(43), 14273–14279. <https://doi.org/10.1021/ja8059039>.
- Samuel, J., Raccurt, O., Poncelet, O., Auger, A., Ling, W. L., Chems, P., ... & Tillement, O. Surface characterizations of fluorescent-functionalized silica nanoparticles: from the macroscale to the nanoscale. *J. Nano. Res.* **2010**, *12*(6), 2255–2265. <https://doi.org/10.1007/s11051-009-9792-x>.
- Sato-Berrú, R.; Saniger, J. M.; Flores-Flores, J.; Sanchez-Espíndola, M. simple method for the controlled growth of SiO₂ spheres. *J. Mater. Sci. Eng. A* **2013**, *3* (4), 237–242.
- Schubert, U. and Hüsing, N. Synthesis of inorganic materials, 3rd edn, *VCH-Wiley Verlag GmbH, Weinheim*, **2012**, ISBN 3-527-32714-1.
- Shin, Y.; Lee, D.; Lee, K.; Ahn, K. H.; Kim, B. Surface properties of silica nanoparticles modified with polymers for polymer nanocomposite applications. *J. Ind. Eng. Chem.* **2008**, *14* (4), 515–519.
<https://doi.org/10.1016/j.jiec.2008.02.002>.
- Shirshahi, V.; Soltani, M. Solid silica nanoparticles: applications in molecular imaging. *Contrast Media Mol. Imaging* **2015**, *10* (1), 1–17.
<https://doi.org/10.1002/cmmi.1611>.

- Singh, R. K.; Garg, A.; Bandyopadhyaya, R.; Mishra, B. K. Density fractionated hollow silica microspheres with high-yield by non-polymeric sol-gel/emulsion route. *Colloids Surfaces A Physicochem. Eng. Asp.* **2007**, *310* (1–3), 39–45. <https://doi.org/10.1016/j.colsurfa.2007.05.064>.
- Singh, L. P.; Agarwal, S. K.; Bhattacharyya, S. K.; Sharma, U.; Ahalawat, S. Preparation of silica nanoparticles and its beneficial role in cementitious materials. *Nanomater. nanotechnol.* **2011**, *1* (1), 44–51. <https://doi.org/10.5772/50950>.
- Specialty silica market size, share & trends analysis report by product (precipitated, silica gel, colloidal, fumed), by application (rubber, paints & coatings, food), and segment forecasts, 2019 – 2025. Accessed date 19 March 2019. <https://www.grandviewresearch.com/industry-analysis/specialty-silica-market>
- Somasundaran, P. Encyclopedia of surface and colloid science, 2nd edition. **2004**, volume 8, USA, ISBN: 0-8247-2154-3,817-818.
- Stöber, W.; Fink, A.; Bohn, E. Controlled growth of monodisperse silica spheres in the micron size range. *J. Colloid Interface Sci.* **1968**, *26* (1), 62–69. [https://doi.org/10.1016/0021-9797\(68\)90272-5](https://doi.org/10.1016/0021-9797(68)90272-5).
- Sun, Z., Li, H., Cui, G., Tian, Y., & Yan, S. Multifunctional magnetic core–shell dendritic mesoporous silica nanospheres decorated with tiny Ag nanoparticles as a highly active heterogeneous catalyst. *App. Surf. Sci.*, **2016**, *360*, 252–262. <https://doi.org/10.1016/j.apsusc.2015.11.013>.
- Tabatabaei, S.; Shukohfar, a; Aghababazadeh, R.; Mirhabibi, a. experimental study of the synthesis and characterisation of silica nanoparticles via the sol-gel method. *J. Phys. Conf. Ser.* **2006**, *26*, 371–374. <https://doi.org/10.1088/1742-6596/26/1/090>.
- Tan, S. Y.; Ang, C. Y.; Li, P.; Yap, Q. M.; Zhao, Y. Drug encapsulation and release by mesoporous silica nanoparticles: the effect of surface functional groups. *Chem. - A Eur. J.* **2014**, *20* (36), 11276–11282. <https://doi.org/10.1002/chem.201403551>.
- Tao, S., Fanguy, J. C., & Xu, L. Sol-gel derived porous silica as a constituent material for designing optical fiber chemical sensors. *In MRS Proceedings.* **2004**, *828*, A1-9. Cambridge University Press. <https://doi.org/10.1557/PROC-828-A1.9>.
- Tatterson, G. B. Fluid mixing and gas dispersion in agitated tanks, *Ž. McGraw-Hill.* **1991**, New York .

- Teng, Z.; Han, Y.; Li, J.; Yan, F.; Yang, W. Preparation of hollow mesoporous silica spheres by a sol-gel/emulsion approach. *Microporous Mesoporous Mater.* **2010**, *127* (1–2), 67–72. <https://doi.org/10.1016/j.micromeso.2009.06.028>.
- Thanh, N. T. K.; Maclean, N.; Mahiddine, S. Mechanisms of nucleation and growth of nanoparticles in solution. *Chem. Rev.* **2014**, *114* (15), 7610–7630. <https://doi.org/10.1021/cr400544s>.
- Tsai, M.; Yang, C.; Huang, P. Effects of seeds concentration on the formation of colloidal silica. **2005**, *123* (3), 238–241. <https://doi.org/10.1016/j.mseb.2005.08.084>.
- Toygun, Ş.; Köçenoğlu, G.; Kalpaklı, Y. General principles of sol – gel. *Sigma.* **2013**, *31*, 456-476.
- Van Blaaderen, A., Van Geest, J., Vrij, A. Monodisperse colloidal silica spheres from tetraalkoxysilanes: particle formation and growth mechanism. *J. Colloid Interface Sci.* **1992**, *154* (2), 481–501. [https://doi.org/10.1016/0021-9797\(92\)90163-G](https://doi.org/10.1016/0021-9797(92)90163-G).
- Wang, J., Sugawara, A., Shimojima, A., & Okubo, T. Preparation of anisotropic silica nanoparticles via controlled assembly of presynthesized spherical seeds. *Langmuir.* **2010a**, *26*(23), 18491-18498. <https://doi.org/10.1021/la103564p>.
- Wang, X. D.; Shen, Z. X.; Sang, T.; Cheng, X. Bin; Li, M. F.; Chen, L. Y.; Wang, Z. S. Preparation of spherical silica particles by stöber process with high concentration of tetra-ethyl-orthosilicate. *J. Colloid Interface Sci.* **2010b**, *341* (1), 23–29. <https://doi.org/10.1016/j.jcis.2009.09.018>.
- Wong, Y. J., Zhu, L., Teo, W. S., Tan, Y. W., Yang, Y., Wang, C., & Chen, H. Revisiting the Stöber method: inhomogeneity in silica shells. *J. Am. Chem. Soc.* **2011**, *133*(30), 11422-11425. <https://doi.org/10.1021/ja203316q>.
- Xiao-Hong, H., Cui-Miao, Z., Xiao-Long, L., Xing-Jie, L., Guang, J., & Jin-Chao, Z. Recent advances of mesoporous silica based multifunctional nano drug delivery systems. *Prog. Biochem. Biophys.* **2013**, *40*(10), 1014-1022.
- Yang, W., Lopez, P. J., & Rosengarten, G. Diatoms: self assembled silica nanostructures, and templates for bio/chemical sensors and biomimetic membranes. *Analyst.* **2011**, *136*(1), 42-53. <https://doi.org/10.1039/c0an00602e>.
- Yoo, W. C.; Stein, A. Solvent effects on morphologies of mesoporous silica spheres prepared by pseudomorphic transformations. *Chem. Mater.* **2011**, *23* (7), 1761–1767. <https://doi.org/10.1021/cm102829m>.

- Yue, R., Meng, D., Ni, Y., Jia, Y., Liu, G., Yang, J., ... & Chen, Y. One-step flame synthesis of hydrophobic silica nanoparticles. *Pow. Tech.* **2013**, 235, 909-913. <https://doi.org/10.1016/j.powtec.2012.10.021>.
- Zainal, N. A.; Rizal, S.; Shukor, A.; Azwana, H.; Wab, A.; Razak, K. A. Study on the effect of synthesis parameters of silica nanoparticles entrapped with rifampicin. *The Italian Assoc. of Chem. Eng.* **2013**, 11, 431-440. <https://doi.org/10.3303/ACOS1311044>.
- Zare, A., Merajoddin, M., Moosavi-Zare, A. R., Zarei, M., Beyzavi, M. H., & Zolfigol, M. A. Design and characterization of nano-silica-bonded 3-n-propyl-1-sulfonic acid imidazolium chloride {nano-SB-[PSIM] Cl} as a novel, heterogeneous and reusable catalyst for the condensation of arylaldehydes with β -naphthol and alkyl carbamates. *Res. Chem. Int.* **2016**, 42(3), 2365-2378. <https://doi.org/10.1007/s11164-015-2154-7>.
- Zeng, D., Zhang, H., Wang, B., Sang, K., & Yang, J. Effect of ammonia concentration on silica spheres morphology and solution hydroxyl concentration in Stöber process. *J. nanosci. and nanotech.* **2015**, 15(9), 7407-7411. <https://doi.org/10.1166/jnn.2015.10595>.
- Zhang, J. H.; Zhan, P.; Wang, Z. L.; Zhang, W. Y.; Ming, N. B. Preparation of monodisperse silica particles with controllable size and shape. *J. Mater. Res.* **2003**, 18 (03), 649-653. <https://doi.org/10.1557/JMR.2003.0085>.
- Zhang, H.; Wu, J.; Zhou, L.; Zhang, D.; Qi, L. Facile synthesis of monodisperse microspheres and gigantic hollow shells of mesoporous silica in mixed water-ethanol solvents. *Langmuir.* **2007**, 23(3), 1107-1113. <https://doi.org/10.1021/la062542l>.
- Zhang, Y., Cao, M., Yao, Z., Wang, Z., Song, Z., Ullah, A., ... & Liu, H. Effects of silica coating on the microstructures and energy storage properties of BaTiO₃ ceramics. *Mat. Res. Bull.* **2015**, 67, 70-76. <https://doi.org/10.1016/j.materresbull.2015.01.056>.
- Zhao, S.; Xu, D.; Ma, H.; Sun, Z.; Guan, J. Controllable preparation and formation mechanism of monodispersed silica particles with binary sizes. *J. Colloid Interface Sci.* **2012**, 388, 40-46. <https://doi.org/10.1016/j.jcis.2012.08.012>.

APPENDIX A

ELECTROSTATIC INTERACTIONS

The general solution for the solution expressing the interaction between the electrical double layers surrounding any dissimilar colloidal particles is given below.

$$V_{el}(h) = \frac{\pi\epsilon\epsilon_0 d_1 d_2}{2(d_1 + d_2)} \left[2\varphi_1 \varphi_2 \ln \left(\frac{1 + e^{-\kappa h}}{1 - e^{-\kappa h}} \right) + (\varphi_1^2 + \varphi_2^2) \ln(1 - e^{-2\kappa h}) \right]$$

For spherical particles van der Waals attraction can be given as:

$$V_{vdW}(h) = -\frac{A_H d_1 d_2}{12(d_1 + d_2)h}$$

And total energy becomes as;

$$V_{tot}(h) = V_{el}(h) + V_{vdW}(h)$$

Where;

V_{tot} : Total energy of interaction between macroscopic bodies

V_{vdW} : van der Waals energy of interaction between macroscopic bodies

V_{el} : Electrostatic energy of interaction between macroscopic bodies

ϵ : Relative permittivity of water (78.5)

ϵ_0 : Permittivity of vacuum (8.854×10^{-12} C²/J.m)

h : Particle separation distance (m)

κ : Reciprocal thickness of the double layer or Debye-Hückel parameter (m⁻¹)

φ_{12} : Potential distribution between two macroscopic bodies

$\varphi_{0,i}$: Surface potential of material i (volts)

The values of constants are taken as;

$$A_H = 10^{-10}m$$

$$F = 96484.56 \frac{\text{coul}}{\text{mole}}$$

$$k = 1.380658 \times 10^{-23} \frac{\text{Joule}}{\text{K}}$$

$$R = 8.3144 \frac{\text{Joule}}{\text{molK}}$$

$$\epsilon_0 = 8.85 \times 10^{-12} \frac{\text{coul}^2}{\text{joule m}}$$

$$h = 1 A, 2A \dots 10000A$$

$$\epsilon = 25 \text{ for ethanol}$$

The total interaction energy curve (V_{tot}) is also called the curve of potential interaction energy is the sum of electrostatic and vdW interactions according to the DLVO theory;

$$\frac{V_{el}(100 A)}{kT} + \frac{V_{vdW}(100 A)}{kT} = -50.61$$

This equation is a general solution expressing the interaction between the electrical double layers surrounding any dissimilar colloidal particles.

APPENDIX B

HYDROLYSIS OF TEOS WITH NO CONDENSATION AND NO AGGREGATION

The Mathcad results related to Section 6.3 are given below including both analytical and numerical solutions.

$$\begin{array}{llllll}
 \underline{W}_w := 1 & M_{Ww} := 0.208 & N_{av} := 6.02 \cdot 10^{23} & R_{mT} := .36 \cdot 10^{-9} & R_{OH} := .11 \cdot 10^{-9} & k := 1.380 \cdot 10^{-23} \\
 C_T := 250 & n_T := C_T \cdot M_{Ww} & n_T := C_T \cdot N_{av} & n_T = 1.505 \times 10^{26} & & \mu := 1.074 \cdot 10^{-3} \\
 n_{OH} := 4.36 \cdot n_T & n_{OH} = 6.562 \times 10^{26} & & & & \underline{T}_w := 293 \\
 n_m(t, Y) := Y_0 + Y_1 + Y_2 + Y_3 + Y_4 & & & & & \alpha := \frac{2 \cdot k \cdot T}{3 \mu} \\
 t_i := 1 & t_f := 100000 & num := 10000 & & & K_1 := \frac{0.0757}{60} \\
 & & & & & \alpha \left(2 + \frac{R_{mT}}{R_{OH}} \right) \cdot n_{OH} \\
 & & & & & K_1 = 1.453 \times 10^{-13}
 \end{array}$$

$$D(t, Y) := \begin{bmatrix} \frac{-2 \cdot k \cdot T}{3 \cdot \mu} \cdot K_1 \cdot \left[\left(2 + \frac{R_{mT}}{R_{OH}} \right) \cdot n_{OH} \cdot Y_0 \right] \\ \frac{-2 \cdot k \cdot T}{3 \cdot \mu} \cdot \left[K_1 \cdot \left(2 + \frac{R_{mT}}{R_{OH}} \right) \cdot n_{OH} \cdot \left(\frac{3}{4} Y_1 - Y_0 \right) \right] \\ \frac{-2 \cdot k \cdot T}{3 \cdot \mu} \cdot \left[K_1 \cdot \left(2 + \frac{R_{mT}}{R_{OH}} \right) \cdot n_{OH} \cdot \left(\frac{2}{4} Y_2 - \frac{3}{4} Y_1 \right) \right] \\ \frac{-2 \cdot k \cdot T}{3 \cdot \mu} \cdot \left[K_1 \cdot \left(2 + \frac{R_{mT}}{R_{OH}} \right) \cdot n_{OH} \cdot \left(\frac{1}{4} Y_3 - \frac{2}{4} Y_2 \right) \right] \\ \frac{-2 \cdot k \cdot T}{3 \cdot \mu} \cdot \left[K_1 \cdot \left(2 + \frac{R_{mT}}{R_{OH}} \right) \cdot n_{OH} \cdot \left(\frac{-1}{4} \cdot Y_3 \right) \right] \end{bmatrix} \quad \underline{Y}_0 := \begin{pmatrix} n_T \\ 0.01 \\ .01 \\ .01 \\ .01 \end{pmatrix}$$

$$S1 := \text{Rkadapt}(Y_0, t_i, t_f, num, D)$$

$$t := S1^{(0)} \quad n_0 := S1^{(1)} \quad n_1 := S1^{(2)} \quad n_2 := S1^{(3)} \quad n_3 := S1^{(4)} \quad n_4 := S1^{(5)}$$

$$\underline{n}_{\text{tot}} := n_0 + n_1 + n_2 + n_3 + n_4$$

$t := 0, 1.. 50000$

$$C := K_1 \cdot \alpha \cdot n_{OH} \left(1 + \frac{R_{mT}}{R_{OH}} \right)$$

$$n_{0a}(t) := n_T \cdot \exp(-C \cdot t)$$

$$n_{1a}(t) := 4 \cdot n_T \cdot \exp(-C \cdot t) \cdot \left(\exp\left(\frac{C \cdot t}{4}\right) - 1 \right)$$

$$n_{2a}(t) := 6 \cdot n_T \cdot \exp(-C \cdot t) \cdot \left(\exp\left(\frac{1}{4} C \cdot t\right) - 1 \right)^2$$

$$n_{3a}(t) := 4 \cdot n_T \cdot \exp(-C \cdot t) \cdot \left(\exp\left(\frac{1}{4} C \cdot t\right) - 1 \right)^3$$

$$n_{4a}(t) := n_T \cdot \exp(-C \cdot t) \cdot \left(\exp\left(\frac{1}{4} C \cdot t\right) - 1 \right)^4$$

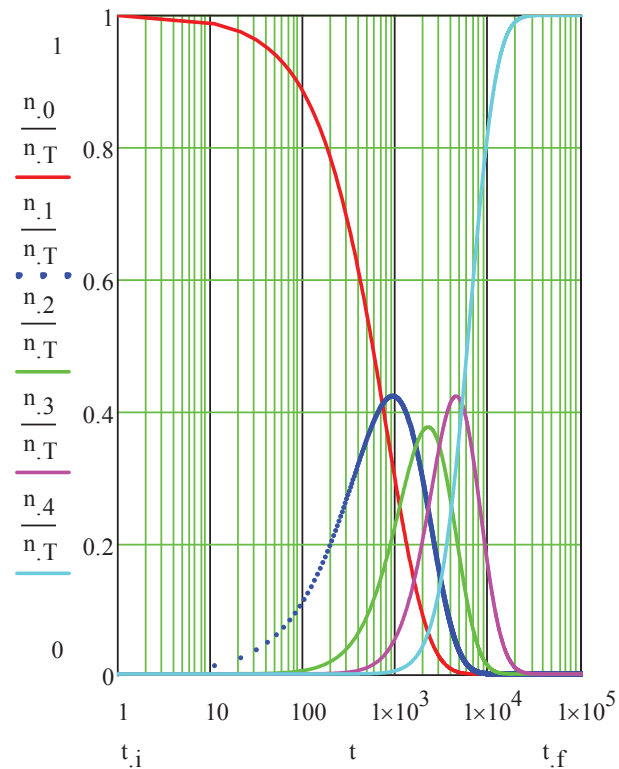


Figure B.1. Numerical solution of the model belongs to hydrolysis of TEOS with no condensation and no aggregation

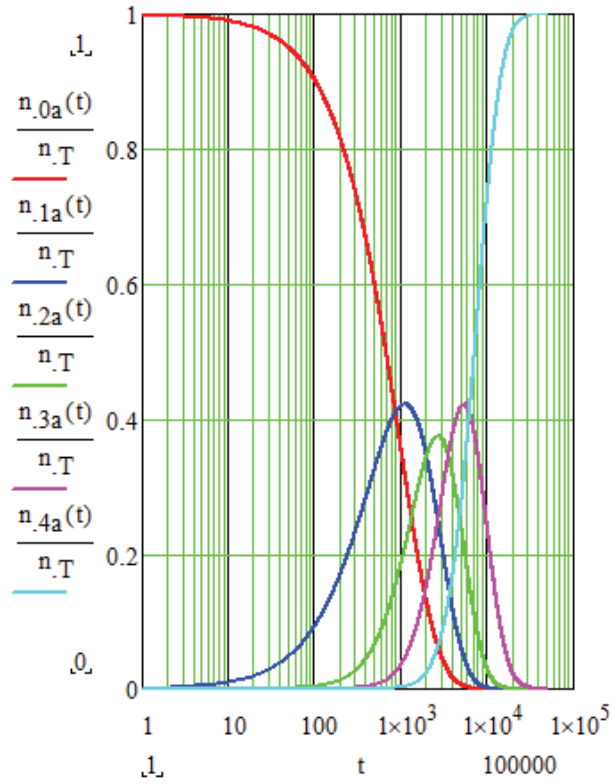


Figure B.2. Analytical solution of the model belongs to hydrolysis of TEOS with no condensation and no aggregation

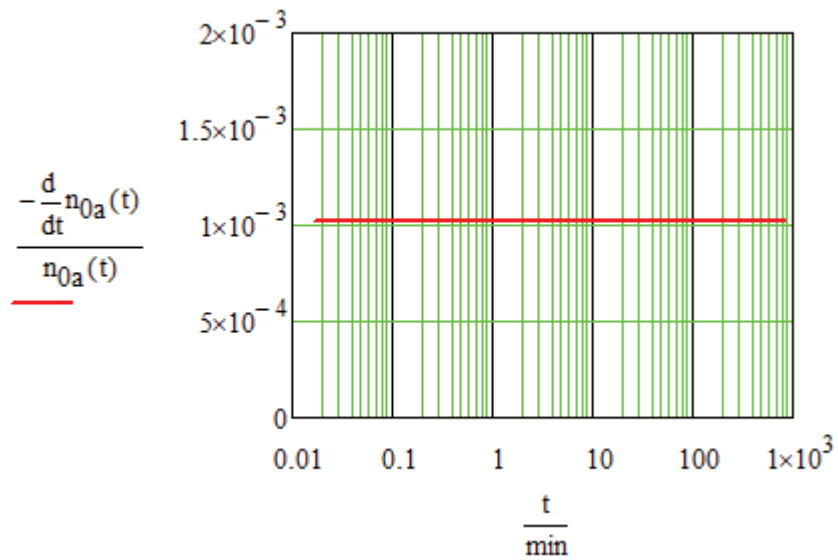


Figure B.3. $-\frac{dn_{0a}(t)}{n_{0a}(t)}$ vs time

APPENDIX C

CONDENSATION OF HYDROLYZED TEOS MONOMERS INTO OLIGOMERS

The results related to Section 6.4 are given below.

$$\begin{aligned}
 K_1 &:= 1.453 \cdot 10^{-13} & K_2 &:= 5 \cdot 10^{-8} & C_T &:= 250 & n_T &:= C_T \cdot N_{av} & \frac{W}{M} &:= 1 \\
 n_{OH} &:= 4.36 n_T & n_o &:= 2 \cdot 10^{-6} \cdot n_T & n_o &:= 3.01 \times 10^{20} & n_T &:= 1.505 \times 10^{26} & R_{OH} &:= .11 \cdot 10^{-9} \\
 \alpha &:= \frac{2 \cdot k \cdot T}{3\mu} & n_m(Y, t) &:= Y_0 + Y_1 + Y_2 + Y_3 + Y_4 & t_f &:= 10000 & t_i &:= 1 & R_m &:= .181 \cdot 10^{-9} \\
 & & & & & & & & R_T &:= .35 \cdot 10^{-9}
 \end{aligned}$$

$$D(t, Y) := \begin{bmatrix}
 -\frac{2 \cdot k \cdot T}{3\mu} \cdot K_1 \cdot \left[\left(2 + \frac{R_T}{R_{OH}} \right) \cdot n_{OH} \cdot Y_0 \right] \\
 -\frac{2 \cdot k \cdot T}{3\mu} \cdot \left[K_1 \cdot \left(2 + \frac{R_T}{R_{OH}} \right) \cdot n_{OH} \cdot \left(\frac{3}{4} \cdot Y_1 - Y_0 \right) + K_2 \cdot \left(2 + \frac{Y_5}{R_T} \right) \cdot \left(\frac{1}{4} \cdot Y_1 \right) \cdot n_o \cdot 1 \right] \\
 -\frac{2 \cdot k \cdot T}{3\mu} \cdot \left[K_1 \cdot \left(2 + \frac{R_T}{R_{OH}} \right) \cdot n_{OH} \cdot \left(\frac{2}{4} \cdot Y_2 - \frac{3}{4} \cdot Y_1 \right) + K_2 \cdot \left(2 + \frac{Y_5}{R_T} \right) \cdot \left(\frac{2}{4} \cdot Y_2 \right) \cdot n_o \cdot 1 \right] \\
 -\frac{2 \cdot k \cdot T}{3\mu} \cdot \left[K_1 \cdot \left(2 + \frac{R_T}{R_{OH}} \right) \cdot n_{OH} \cdot \left(\frac{1}{4} \cdot Y_3 - \frac{2}{4} \cdot Y_2 \right) + K_2 \cdot \left(2 + \frac{Y_5}{R_T} \right) \cdot \left(\frac{3}{4} \cdot Y_3 \right) \cdot n_o \cdot 1 \right] \\
 -\frac{2 \cdot k \cdot T}{3\mu} \cdot \left[K_1 \cdot \left(2 + \frac{R_T}{R_{OH}} \right) \cdot n_{OH} \cdot \left(-\frac{1}{4} \cdot Y_3 \right) + K_2 \cdot \left(2 + \frac{Y_5}{R_T} \right) \cdot \left(Y_4 \right) \cdot n_o \cdot 1 \right] \\
 \frac{2 \cdot k \cdot T}{3\mu} \cdot K_2 \cdot \left[\frac{2 R_m^3 \cdot \left(\frac{1}{4} \cdot Y_1 + \frac{2}{4} \cdot Y_2 + \frac{3}{4} \cdot Y_3 + Y_4 \right)}{\pi \cdot R_T \cdot (Y_i)} \right]
 \end{bmatrix} \cdot \begin{matrix}
 num := 10000 \\
 \begin{matrix}
 n_T \\
 0.01 \\
 .01 \\
 .01 \\
 .01 \\
 R_T
 \end{matrix}
 \end{matrix}$$

$$\begin{aligned}
 t &:= S1^{(0)} & n_0 &:= S1^{(1)} & n_1 &:= S1^{(2)} & n_2 &:= S1^{(3)} & n_3 &:= S1^{(4)} & n_4 &:= S1^{(5)} & R_o &:= S1^{(6)} \\
 \frac{n_m}{M} &:= n_0 + n_1 + n_2 + n_3 + n_4 & m_m &:= 8 \cdot \rho_{SiO_2} \cdot R_m^3 \cdot n_m & m_o &:= \frac{4}{3} \cdot \pi \cdot \rho_{SiO_2} \cdot R_o^3 \cdot n_o
 \end{aligned}$$

APPENDIX D

HYDROLYSIS OF TEOS WITH CONDENSATION TO FORM OLIGOMERS AND AGGREGATION OF OLIGOMERS TO FORM FINAL PARTICLES

The results related to Section 6.5 are given below.

$$C_T := 250 \quad n_{o0} := 2 \cdot 10^{-5} \cdot n_T \quad n_a := 6.80 \cdot 10^{16} \quad n_T := C_T \cdot N_{av}$$

$$n_{OH} := 4.36 \cdot (C_T \cdot N_{av}) \quad m_T := C_T \cdot M_{wSiO2}$$

$$K_1 := 1.453 \times 10^{-13} \quad K_2 := 1.9 \times 10^{-3}$$

$$n_m(t, Y) := Y_0 + Y_1 + Y_2 + Y_3 + Y_4 \quad m_m(t, Y) := 8 \cdot \rho_{SiO2} \cdot R_m^3 \cdot n_m(t, Y) \quad m_o(t, Y) := m_T - m_m(t, Y) - Y_6$$

$$R_a(t, Y) := \sqrt[3]{\frac{3 \cdot Y_6}{4 \cdot \pi \cdot n_a \cdot \rho_{SiO2}}}$$

$$R_o(t, Y) := \sqrt[3]{\frac{3 \cdot m_o(t, Y)}{4 \cdot \pi \cdot Y_5 \cdot \rho_{SiO2}}}$$

$$\mu_o(t, Y) := \frac{4}{3} \cdot \pi \cdot \rho_{SiO2} \cdot R_o(t, Y)^3$$

$$\mu_m(t, Y) := 8 \cdot \rho_{SiO2} \cdot R_m^3$$

$$D(t, Y) := \begin{bmatrix} -\alpha \cdot K_1 \cdot \left[\left(2 + \frac{R_{mT}}{R_{OH}} \right) \cdot n_{OH} \cdot Y_0 \right] \\ -\alpha \cdot \left[K_1 \cdot \left(2 + \frac{R_{mT}}{R_{OH}} \right) \cdot n_{OH} \cdot \left(\frac{3}{4} \cdot Y_1 - Y_0 \right) + K_2 \cdot \left(\frac{1}{4} \cdot Y_1 \right) \cdot \left[\left(2 + \frac{R_o(t, Y)}{R_{mT}} \right) \cdot Y_5 + \left(2 + \frac{R_a(t, Y)}{R_{mT}} \right) \cdot n_a \right] \right] \\ -\alpha \cdot \left[K_1 \cdot \left(2 + \frac{R_{mT}}{R_{OH}} \right) \cdot n_{OH} \cdot \left(\frac{2}{4} \cdot Y_2 - \frac{3}{4} \cdot Y_1 \right) + K_2 \cdot \left(\frac{2}{4} \cdot Y_2 \right) \cdot \left[\left(2 + \frac{R_o(t, Y)}{R_{mT}} \right) \cdot Y_5 + \left(2 + \frac{R_a(t, Y)}{R_{mT}} \right) \cdot n_a \right] \right] \\ -\alpha \cdot \left[K_1 \cdot \left(2 + \frac{R_{mT}}{R_{OH}} \right) \cdot n_{OH} \cdot \left(\frac{1}{4} \cdot Y_3 - \frac{2}{4} \cdot Y_2 \right) + K_2 \cdot \left(\frac{3}{4} \cdot Y_3 \right) \cdot \left[\left(2 + \frac{R_o(t, Y)}{R_{mT}} \right) \cdot Y_5 + \left(2 + \frac{R_a(t, Y)}{R_{mT}} \right) \cdot n_a \right] \right] \\ -\alpha \cdot \left[K_1 \cdot \left(2 + \frac{R_{mT}}{R_{OH}} \right) \cdot n_{OH} \cdot \left(-\frac{1}{4} \cdot Y_3 \right) + K_2 \cdot (Y_4) \cdot \left[\left(2 + \frac{R_o(t, Y)}{R_{mT}} \right) \cdot Y_5 + \left(2 + \frac{R_a(t, Y)}{R_{mT}} \right) \cdot n_a \right] \right] \\ -\alpha \cdot \frac{K_2}{W} \cdot \left(2 + \frac{R_a(t, Y)}{R_o(t, Y)} \right) \cdot Y_5 \cdot n_a \\ \alpha \cdot K_2 \cdot \left[\frac{1}{W} \cdot \left(2 + \frac{R_a(t, Y)}{R_o(t, Y)} \right) \cdot Y_5 \cdot \mu_o(t, Y) \cdot n_a + \left(2 + \frac{R_a(t, Y)}{R_{mT}} \right) \cdot \left(\frac{1}{4} \cdot Y_1 + \frac{2}{4} \cdot Y_2 + \frac{3}{4} \cdot Y_3 + Y_4 \right) \cdot \mu_m(t, Y) \cdot n_a \right] \end{bmatrix}$$

$$t_i := 1 \quad t_f := 5000 \quad \text{num} := 1000$$

$$Y0 := \begin{pmatrix} n_T \\ .01 \\ .01 \\ .01 \\ .01 \\ n_{o0} \\ R_{o\max} \end{pmatrix} \quad S1 := \text{Rkadapt}(Y0, t_i, t_f, \text{num}, D)$$

$$t := S1^{(0)} \quad n_0 := S1^{(1)} \quad n_1 := S1^{(2)} \quad n_2 := S1^{(3)}$$

$$n_3 := S1^{(4)} \quad n_4 := S1^{(5)} \quad n_o := S1^{(6)} \quad m_a := S1^{(7)}$$

$$n_{\text{mon}} := n_0 + n_1 + n_2 + n_3 + n_4 \quad m_m := 8 \cdot \rho_{\text{SiO}_2} \cdot R_m^3 \cdot n_m \quad R_{a_m} := \sqrt[3]{\frac{3 \cdot m_a}{4 \cdot \pi \cdot n_a \cdot \rho_{\text{SiO}_2}}}$$

$$m_o := m_T - m_m - m_a \quad R_{a_o} := \sqrt[3]{\frac{3 \cdot m_o}{4 \cdot \pi \cdot n_o \cdot \rho_{\text{SiO}_2}}}$$

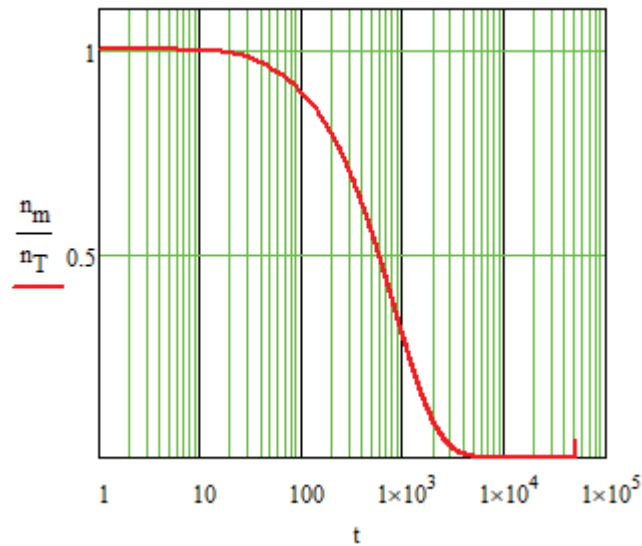


Figure D.1. Change in the number of monomers divided by total TEOS number as a function of time

VITA

PERSONAL INFORMATION

Name: Elif Suna SOP Date of Birth: 15.07.1988 E-mail: sunasop@iyte.edu.tr

EDUCATION

2013-2019 Doctor of Philosophy (Ph. D.)

Izmir Institute of Technology, Department of Chemical Engineering.

Thesis Title: An in-depth study of nucleation and growth processes during
Stöber silica synthesis

2010-2013 Master of Science (M. Sc.)

Hacettepe University, Department of Chemical Engineering.

Thesis title: Hydrogel synthesis as a tissue expander, characterization and
swelling kinetics

2006-2010 Bachelor of Science (B. Sc.)

Gazi University, Department of Chemical Engineering.

WORK and RESEARCH EXPERIENCE

2013-2019 Research and Teaching Assistant,

Izmir Institute of Technology, Department of Chemical Engineering.

2013 August - November 2013 Researcher with scholarship

Project: MARIE CURIE PIRSES-GA-2010-269211, CINDECA UNLP, La
Plata, Argentina

AWARDS:

- 1st of Doctoral Student Category of International R&D Project Market 2017, UTİB-Uludağ Textile Exporters' Association (1st place award)
Title: Bug-Repellent Textiles Coated With Hollow/Mesoporous Nanosilica Particles
- 3th of Best SEM Image Exhibition 2014, İzmir Institute of Technology, Materials Research Center (3th place award)
Title: Nanocosmos Silica

PUBLICATIONS:

- A. E. Demirbaş, E. Kiliç, T. T. Demirtaş, E. S. Sop, A. Alkan & M.Gümüşderelioğlu, "Soft Tissue Expansion With A New Osmotic Tissue Expander Has Delayed Swelling Capability: An Experimental Study In Sheep Mandible", 2017, International Journal of Oral and Maxillofacial Surgery, Volume 46, Supplement 1, 95.
- E. S. Sop, H. Polat & M. Polat." Production of Nano-Sized Silica Particles with Controlled Size Distribution Using Seed Particles", Sözlü Sunum, International Porous&Powder Materials Symposium&Exhibition, September 12-15, 2017, ISBN 978-975-6590-09-6.
- E. S. Sop, G. Palaz, E. Erol, H. Polat & M. Polat, "Manufacturing of Hollow Spherical Silica Nanoparticles with Controlled Morphology by Spontaneous Emulsification", Poster Presentation, International Porous&Powder Materials Symposium&Exhibition, September 15-18, 2015, 978-975-6590-07-2.
- E. S. Sop, M. Schöngut, H. Polat & M. Polat, "Mechanism of Nano-silica Production in a Standard Geometry Cell", Oral Presentation, International Porous&Powder Materials Symposium&Exhibition, September 15-18, 2015, 978-975-6590-07-2.